Nano Research

ISSN 1998-0124 CN 11-5974/O4
https://doi.org/10.26599/NR.2026.94908727

Review Article

Recent advances in structural design and mechanistic studies of Pt-based catalysts toward the reverse water-gas shift reaction

Xiaoyu Hu[1,3], Yingnan Tan[2], Yuanyuan Ma[2], Xiaohan Zhao[2](✉), Bin Wang[1], Tingting Cui[2](✉), Ming Xu[2](✉)

[1] Sinopec (Beijing) Research Institute of Chemical Industry Co., Ltd, Beijing 100013, China

[2] College of Chemistry, Chemical Engineering & Resource Utilization, Center for Innovative Research in Synthetic Chemistry and Resource Utilization, Northeast Forestry University, Harbin 150040, China

[3] State Key Laboratory of Chemical Resource Engineering, Beijing University of Chemical Technology, Beijing 100029, China

Nano Res., **Just Accepted Manuscript** • https://doi.org/10.26599/NR.2026.94908727

https://www.sciopen.com/journal/1998-0124 on Apr. 9, 2026

Just Accepted

TABLE OF CONTENTS (TOC)

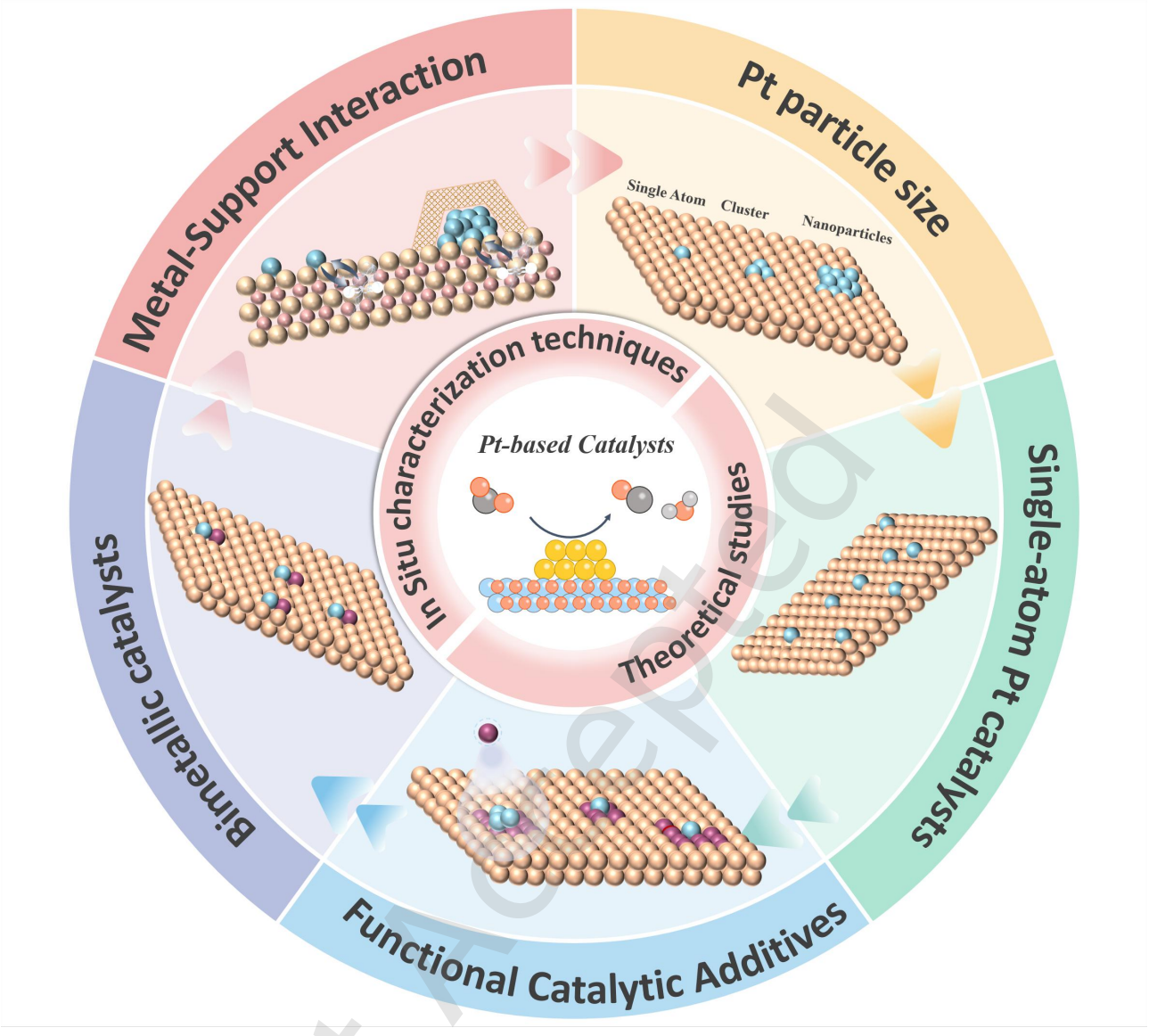

The research progress on Pt-based catalyst structure regulation is comprehensively reviewed, focusing on the catalyst design strategies, active site identification, and reaction mechanism studies.

Nano Research

Open Access

Review Article

Recent advances in structural design and mechanistic studies of Pt-based catalysts toward the reverse water-gas shift reaction

Xiaoyu Hu[1,3], Yingnan Tan[2], Yuanyuan Ma[2], Xiaohan Zhao [2] ✉, Bin Wang[1], Tingting Cui [2] ✉, and Ming Xu [2] ✉

[1] *Sinopec (Beijing) Research Institute of Chemical Industry Co., Ltd, Beijing 100013, China*
[2] *College of Chemistry, Chemical Engineering & Resource Utilization, Center for Innovative Research in Synthetic Chemistry and Resource Utilization, Northeast Forestry University, Harbin 150040, China*
[3] *State Key Laboratory of Chemical Resource Engineering, Beijing University of Chemical Technology, Beijing 100029, China*

Cite this article: *Nano Research*, 2026, 19, 94908727 https://doi.org/10.26599/NR.2026.94908727

ABSTRACT: As a crucial component of the carbon cycle, the reverse water-gas shift (RWGS) reaction enables the conversion of CO_2 and H_2 into CO, serving as a critical feedstock for the production of high-value added chemicals and fuels. However, the practical application of this reaction is severely limited by three primary challenges: the poor CO_2 conversion at the relatively low and moderate temperatures, the occurrence of undesirable side reactions such as methanation, and the high energy consumption at elevated temperatures. Consequently, the development of catalytic systems with high activity and high CO selectivity as well as excellent structure stability is of great importance. Platinum (Pt)-based catalysts have emerged as highly promising candidates for the RWGS reaction owing to their excellent H_2 dissociation capability, effective activation and hydrogenation capability of CO_2, and moderate adsorption strength toward reaction intermediates. In this review, recent advances in Pt-based catalysts for the RWGS reaction are systematically summarized. The innovative structural design of Pt-based catalysts is discussed in detail, followed by an in-depth analysis of the structure-performance relationship and the potential RWGS reaction mechanism via advanced characterization techniques and density functional theory (DFT) calculations. Furthermore, the remaining key scientific challenges and future development directions are highlighted, providing valuable insights for the rational design of highly efficient Pt-based catalysts for the RWGS reaction.

KEYWORDS: CO_2 hydrogenation, reverse water-gas shift (RWGS) reaction, Pt-based catalyst, structure modulation, mechanism studies

1 Introduction

Since the Industrial Revolution, the reliance on fossil fuels have driven a relentless surge in carbon dioxide (CO_2) emissions, exacerbating environmental crises such as global warming, rising sea levels, and increasingly frequent extreme weather events[1-5]. Addressing this challenge, reducing carbon emissions has emerged as a critical priority for sustainable global development[6,7]. Simultaneously, CO_2 presents itself as a vast and untapped carbon resource. From the perspectives of long-term sustainability and environmental friendliness, harnessing renewable carbon sources and ensuring efficient energy supply stand as pivotal strategies to minimize CO_2 emissions[8-11]. Recently, the thermocatalytic CO_2 hydrogenation to high-value added chemicals is a transformative approach, which provide a new avenue to for energy and chemical industry transformation[12-15]. Among the diverse pathways for CO_2 conversion, the reverse water-gas shift (RWGS) reaction occupies a central role in the carbon cycle[16]. This process catalytically transforms CO_2 and hydrogen into CO[17], which serves as a foundational feedstock for downstream synthesis of high-value added chemicals, including alcohols, light hydrocarbons, and liquid fuels[18-21]. It enables the conversion of a global pollutant into a valuable resource, which can be served as a cornerstone of future green chemistry and energy systems[22,23].

The RWGS reaction was discovered by Carl Bosch and Wilhelm Wild in 1914 during the high-temperature water-gas shift (WGS) process for hydrogen production[24]. Since then, it has been extensively studied as an effective method for CO_2 conversion and utilization. As shown in Equation (1), the RWGS reaction is essentially the reverse process of the WGS reaction, and its standard reaction enthalpy indicates an endothermic process at 298 K. From a thermodynamic perspective, increasing the temperature significantly raises the equilibrium constant and shifts the equilibrium toward CO production. However, the equilibrium conversion rate at low to moderate temperatures (e.g., below 500 ℃) remains limited[25]. Additionally, because the total number of gas molecules remains nearly constant before and after the reaction, pressure has a relatively weak effect on the equilibrium position (Figure 1a)[26]. Nevertheless, the partial pressure of hydrogen and the H_2/CO_2 ratio indirectly influence the equilibrium CO yield by altering the chemical potentials of reactants and products. Therefore, high temperature and a high H_2/CO_2 ratio favor the RWGS reaction[27]. However, these conditions may also accelerate metal sintering and support phase transitions, potentially leading to catalyst deactivation[28]. Furthermore, many studies have shown that at low to moderate temperatures,

the strongly exothermic CO_2 methanation reaction (2) and methanol synthesis reaction (3) cause CO to be further hydrogenated into by-products such as CH_4 and CH_3OH, thereby reducing the selectivity for CO[12,13,29,30]. From a kinetic perspective, the actual reaction rate and product distribution of RWGS are not determined solely by equilibrium but also depend on processes such as H_2 activation, CO_2 activation, transformation of surface intermediates, and CO desorption[31,32]. Additionally, gas hourly space velocity (GHSV) is a factor that influences system equilibrium and CO/CH_4 selectivity. While it does not alter the thermodynamic equilibrium position of the RWGS reaction, it affects the extent to which the system approaches equilibrium. The representative reversible power-law (PL) rate expression for the RWGS reaction is shown in Equation (4), where K_{eq} represents the thermodynamic equilibrium constant, and the rate term describes the kinetic dependence of the reaction rate on the partial pressures of the reactants. Under limited residence time, a relatively high GHSV generally reduces the single-pass conversion of CO_2. However, it can kinetically enhance CO selectivity by shortening the subsequent residence and conversion time of the formed CO, thereby suppressing side reactions such as CO deep hydrogenation and methanation. Conversely, a low GHSV favors approaching equilibrium conversion but may simultaneously promote side reactions[26,33].

$$H_2(g)+CO_2(g)\rightarrow CO(g)+H_2O(g) \quad \Delta H^{\theta}_{298K}=+41.1\ kJ\cdot mol^{-1} \quad (1)$$

$$4H_2(g)+CO_2(g)\rightarrow CH_4(g)+2H_2O(g) \quad \Delta H^{\theta}_{298K}=-165.0\ kJ\cdot mol^{-1} \quad (2)$$

$$3H_2(g)+CO_2(g)\rightarrow CH_3OH(g)+H_2O(g) \quad \Delta H^{\theta}_{298K}=-49.5\ kJ\cdot mol^{-1} \quad (3)$$

$$r_{RWGS}=kp^{\alpha}_{CO_2}p^{\varepsilon}_{H_2}p^{\gamma}_{CO}\left[1-\frac{1}{K_{eq}}p^{-1}_{CO_2}p^{-1}_{H_2}p^{2}_{CO}\right] \quad (4)$$

The RWGS reaction typically proceeds through three distinct pathways: intermediate association mechanism with adsorbed intermediate species such as formate (*HCOO) or carboxylate (*COOH), and redox mechanism with direct redox on the surface of catalysts[27,34-38]. As illustrated in Figure 1b, in terms of the redox mechanism, CO_2 adsorbed on the catalyst surface is directly dissociated into CO, leaving adsorbed oxygen species (O_{ads}) on the catalyst surface. Subsequently, H_2 acts solely as a reducing agent to convert O_{ads} into H_2O. The rate-determining step is either the dissociation of CO_2 or the formation and desorption of water[39]. In the case of intermediate association mechanism, CO_2 is hydrogenated to form *COOH, which is generally considered the most direct precursor for CO production. The decomposition of *COOH involves breaking the C-O(H) bond, yielding *CO and hydroxyl species. While *CO species desorbs directly as CO, the hydroxyl species undergo further hydrogenation to form H_2O, which then desorbs from the surface of catalysts to complete the entire catalytic cycle. Conversely, the *HCOO species is relatively stable. Their conversion to CO typically requires dehydrogenation or structural rearrangement, regenerating *COOH or $*CO_2$ intermediates that subsequently decompose into *CO[40,41]. The reaction activity and CO selectivity along this pathway are governed by the adsorption capacities of CO_2 and H_2, the stability of the *COOH intermediate, and the desorption ability of CO[27,42]. Given the intricate thermodynamic properties and complex kinetic mechanisms of the RWGS reaction, catalyst design must carefully balance catalytic activity, CO selectivity, and structural stability during H_2 activation, CO_2 activation, and intermediate conversion[43,44]. Currently, catalytic systems employed for RWGS include non-precious metal catalysts (e.g. Ni, Cu, Fe, and Co)[45-54] and precious metal catalysts (e.g. Pt, Pd, Au, and Ru)[55-62]. Non-precious metals offer advantages of low cost and abundant availability but often suffer from insufficient low-temperature activity, low CO selectivity, and susceptibility to carbon deposition or sintering at high temperatures[37]. In comparison, Pt-based catalysts stand out in RWGS reactions due to their exceptional H_2 activation and electron transfer capabilities[63,64]. These catalysts also exhibit remarkable resistance to stable carbon deposition, alongside robust anti-sintering and anti-poisoning characteristics when exposed to high-temperature environments containing water vapor and CO_2 [65,66]. More importantly, the catalytic behavior of Pt is highly sensitive to its local structure, thereby possessing unique research value in the RWGS reaction[67,68].

Although Pt-based catalysts exhibit excellent catalytic properties in the RWGS reaction, Pt is a scarce and expensive metal resource, posing significant challenges for practical applications from the perspective of atomic economy[69]. Therefore, it is critical to improve the utilization efficiency of Pt atoms while maintaining or enhancing their activity and selectivity as well as robust stability. Meanwhile, it is also very important to maintain high catalytic performance and excellent stability under the ultra-high weight hourly space velocity condition so as to meet the requirements for large-scale industrial applications. In order to resolve the aforementioned problems and challenges, great efforts have been devoted to precisely regulate the geometric structures[70], electronic structures[71], particle sizes[72], coordination structures[73], interfacial structures[5], and metal-support interactions of Pt-based catalysts to simultaneously enhance the catalytic performance, selectivity, and stability[74]. Moreover, with the rapid development of in-situ/operando characterization techniques and theoretical calculations, the intrinsic active sites and the catalytic mechanisms of Pt-based catalysts have been deeply investigated during the RWGS reaction, which facilitate the rational design of the next-generation high-performance catalysts[75-77]. In recent years, many reviews about CO_2 hydrogenation to different products (e.g., CH_4, CO, CH_3OH, CH_3CH_2OH, High-carbon alkenes, alkanes, and alcohols, etc.) have been extensively reported[77-79]. Most of works primarily summarize the subject from the perspectives of generalized reaction networks, target product distributions, or common principles across various catalyst systems[80,81]. However, within the scope of such reviews, Pt-based catalysts are typically only briefly mentioned as one among many metal systems[82]. Their unique structural advantages, the characteristics of their true active sites, and the associated mechanistic implications in the RWGS reaction have not been thoroughly or systematically examined. Notably, existing reviews rarely

provide a unified discussion on the relationships among metal-support interfaces, particle size effects, single-atom coordination environments, bimetallic synergistic effects, and processes such as CO_2 activation, H_2 dissociation, conversion of key intermediates, as well as activity, selectivity, and stability, all from the perspective of local structure regulation in Pt-based catalysts. Therefore, a more targeted review focusing on the structural design and mechanistic research of Pt-based catalysts in the RWGS reaction is necessary.-

Based on this, the goal of this review is a relative comprehensive summary of recent research progress in structural regulation, identification of intrinsic active sites, and mechanistic insights of Pt-based catalysts. We significantly emphasize the innovative structural design of catalysts based on different synthetic strategies. Moreover, new research methodology is discussed in detail by the combination of the advanced in-situ/operando characterization techniques and theoretical studies. The intrinsic active sites and their potential structure-activity relationships are thoroughly elucidated at the atomic and molecular levels. Finally, based on these findings, the main challenges and future development trends are summarized, providing a new avenue for the rational design of Pt-based RWGS catalysts that are highly efficient, economically viable, and sustainable.

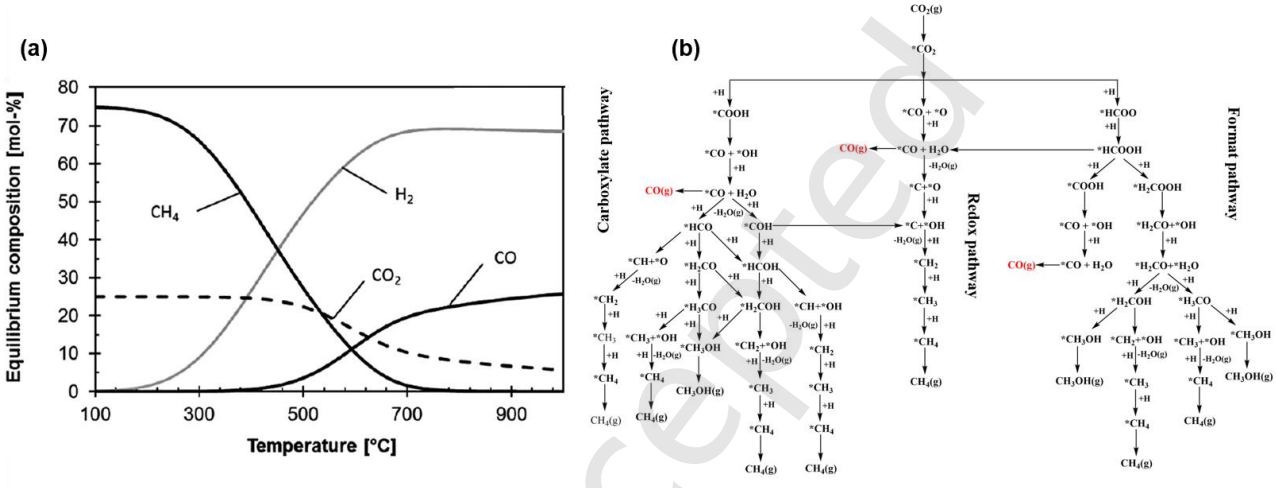

Figure 1. (a) Influence of temperature on the thermodynamic equilibrium of the RWGS reaction at 1 bar and H_2/CO_2 molar ratio of 3/1. Reprinted with permission from [26]. Copyright 2017, American Chemical Society. (b) Scheme for CO_2 hydrogenation mechanism. Reprinted with permission from [37]. Copyright 2013, WILEY-VCH Verlag.

2 Design strategy of Pt-based catalysts

Achieving high activity and structural stability is crucial for activating linear CO_2 molecules, which have high dissociation energy, and for timely desorption of adsorbed *CO species to prevent sintering-induced deactivation of active metals at elevated temperatures. Because the d-band center of Pt lies close to the Fermi level, Pt exhibits strong adsorption activity, leading to excessive CO adsorption on typical crystal planes such as Pt(111) and Pt(100). At low to medium temperatures (300-500 °C), the coverage of *CO increases rapidly, causing blockage of the metal surface by CO and competitive inhibition of *H and *CO_2 adsorption and subsequent activation. Moreover, the Pt surface lacks migratable surface oxygen species and variable valence centers, resulting in a high intrinsic energy barrier for CO_2 activation[83]. Consequently, the rate-determining steps often involve key transformations such as CO_2 → HOCO* or HOCO* → CO* + OH*. Given these mechanistic limitations, precise control of Pt sites has become an essential strategy to enhance the performance of Pt-based catalysts[84]. Numerous studies have demonstrated that constructing Pt-oxide interfaces or tuning the d-band center and geometric structure of Pt via a secondary metal can weaken Pt-CO bonding and optimize the adsorption strength of reaction intermediates[72]. Additionally, controlling particle size and morphology to selectively expose specific crystal planes and interface sites can better balance the inhibition of CO poisoning, enhancement of CO_2 activation, and optimization of intermediate desorption. To intuitively demonstrate the effects of various structural design strategies on the reaction performance of Pt-based RWGS catalysts, Table 1 summarizes the reaction conditions, CO_2 conversion, and product selectivity reported in representative studies conducted at 0.1 MPa. It should be noted that due to inconsistencies in the H_2/CO_2 ratio, reaction temperature, and space velocity across different studies, the purpose of Table 1 is not to provide a strict intrinsic activity ranking of the catalysts. Instead, it aims to summarize the overall optimization trends achieved by different structural designs in balancing CO_2 conversion and CO selectivity. In this section, we summarize the regulatory strategies for Pt-based catalysts based on previous research.

Table 1. Summary of Reaction Condition with CO_2 Conversion and Selectivity on Pt-based Catalysts under 0.1 MPa.

catalyst	H_2: CO_2 ratio	Temperature (℃)	GHSV (mL $gcat^{-1}$ h^{-1})	Conversion (%)	Selectivity (%)	
					CO	CH_4
Pt/CeO_2-AA-350[85]	3:1	200-450	72,000	46	>98	<2
Pt/CeO_2-IMP-350[85]	3:1	200-450	72,000	42	83	17
5Pt/CeO_2-IMP-350[85]	3:1	200-450	72,000	35	32	68
Pt_{ex}/Rutile[86]	4:1	800	600,000	75	100	
Pt_{en}/Rutile[86]	4:1	800	600,000	58	100	
Pt0.5W/SiO_2[87]	4:1	400	100,000	23.5	100	
MeCpPt/CeO_2[88]	1:1	320	114,000	8.3	99	1
Pt_{SA}/TiO_{2-x}[89]	3:1	330	80,000	20.4	99.6	0.6
0.02 wt% Pt/Fe_3O_4[90]	3:1	500	720,000	35	99.7	0.3
K80-Pt/KLTL zeolite[91]	1:1	500	30,000	27.4	>95	<5
$Pt_{cluster}$/PN-CeO_2[92]	3:1	350	12,000	30.1	98.5	1.5
Pt-K/mullite[93]	1:1	550	30,000	30.9	99.2	0.8
PtCr@SiO_2[94]	3:1	450	60,000	17	100	
PtCr-Cr_{int}@SiO_2[94]	3:1	450	60,000	36	100	
Pt-Cs/TiO_2[95]	4:1	400	30,000	21	100	
0.5Pt5Ce/Al_2O_3[96]	3:1	600	200,000	55	96.1	3.9
Pt-MoO_x/γ-Mo_2N[97]	3:1	300	300,000	18	100	
Pt-aCeO_2@SiO_2[98]	1:1	500	120,000	53.2	95	5
Pt-mixCeO_2@SiO_2[98]	1:1	500	120,000	50.8	88	12
Pt-cCeO_2[98]	1:1	500	120,000	51	44	56
Pt_{FEc}/CeO_2[99]	3:1	350	12,000	29.2	>99	0.5

Pt_{SAc}/CeO_2[99]	3:1	350	12,000	22.5	>99	
Pt_{NPs}/CeO_2[99]	3:1	350	12,000	16.1	>99	
PtNi/SBA-15[100]	2:1	400	49,000	24	99.49	0.51
Fe-Pt/CeO_2[101]	3:1	380	200,000	31.5	100	
PtFe/SiO_2[102]	3:1	450	60,000	44	>99.5	
Pt/TiO_2[84]	2:1	350	119.7	10.23	98.39	1.61
Pt/SiO_2[84]	2:1	350	24.7	8.99	99.99	
Pt-1VO_x@HPSNs[103]	1:1	500	144,000	28	100	

2.1 Modulation of metal-support interaction

In Pt-based catalysts, the intrinsic reaction rate of the RWGS reaction exhibits an almost linear correlation with the activity normalized by the perimeter length per unit of the Pt-support interface[104,105]. In contrast, it shows a weak correlation with the total Pt surface area or the number of metal active sites, indicating that the true active sites are concentrated at the Pt-oxide interface rather than on the bulk metal surface. Furthermore, due to differences in Fermi energy levels between the metal and the support in the supported catalyst, the interface facilitates electron rearrangement between the two materials to reduce the overall free energy. This drives electron redistribution across several atomic layers at the interface[106], accompanied by the formation of numerous oxygen vacancies (O_v) on the surface and interface. Key steps, including CO_2→*COOH and *COOH→CO + OH*, exhibit high sensitivity to interfacial charge distribution and O_v density[107], while *CO coverage and Pt-CO bonding strength govern the competition between CO desorption and methanation side reactions[74]. Accordingly, this section focuses on strong metal-support interaction (SMSI), electronic metal-support interaction (EMSI), and composite support interfaces, discussing how restructuring the structure and electronic state of Pt-reducible oxide interfaces regulates CO_2 activation pathways, suppresses over hydrogenation, and enhances high-temperature structural stability.

2.1.1 Strong Metal-Support Interaction

SMSI was first proposed by Tauster et al. in 1978 during their study of supported platinum group metal catalysts[108]. They observed that catalysts reduced at a low temperature of 473 K exhibited a high chemical adsorption capacity for probe molecules such as H_2 and CO. However, when the catalysts were reduced at a higher temperature of 773 K, their adsorption capacity for these probe molecules sharply decreased or even approached zero. Interestingly, the adsorption capacity was restored after the catalyst was oxidized at 673 K following reduction at 773 K. Based on these findings, Tauster et al. concluded that a strong chemical interaction occurs between metal particles and the support during reduction at 773 K, which they defined as SMSI. This phenomenon is fundamentally related to the work functions and surface energies of both the platinum and the support, which depend on the size of the platinum nanoparticles and the exposed crystal planes of the support. Numerous studies have shown that under certain conditions, surface species from the support migrate onto the metal particles, forming a non-stoichiometric oxide coating on the metal surface. This migration is a key factor contributing to SMSI[109-111]. The oxide overlayer effectively reduces the surface energy of the metal, partially covers the metal active sites, and precisely modulates the adsorption strength of reaction intermediates[57,112]. In 2000, Diebold et al. used Scanning Tunneling Microscopy (STM) and Low-Energy Helium Ion Scattering (LEIS) spectroscopy to observe the atomic structure of platinum encapsulated by TiO_2 on the TiO_2(110) surface[113]. Their experimental results confirmed that the TiO_{2-x} encapsulation layer consists of a double-layer $Ti_{1.1}O$ structure. Similarly, Zhang et al. reached the same conclusion in their study of Pt/TiO_2 catalysts using in-situ Transmission Electron Microscopy (TEM) and Electron Energy-Loss Spectroscopy (EELS)[114]. They found that after reduction at 773 K, a roughly double-layered titanium-oxygen overlayer encapsulated the 8 nm Pt nanoparticles (Figure 2a-b).

While the overlayer induced by SMSI enhances catalytic selectivity and stability, an excessively dense or thick support overlayer can physically block the metal active sites and hinder the diffusion of reactants to the interfacial active sites, thereby reducing the catalytic rate. In recent years, numerous studies have demonstrated that modifying the surface properties of oxide supports allows precise control over the thickness and compactness of the coating layer. This adjustment not only enhances the high-temperature stability of the interfacial structure but also selectively blocks certain over-hydrogenation sites. Zhang et al. proposed a novel strategy to regulate the interface sites of Pt-CeO_2 via ultrafast

laser induction, which constructs a permeable, encapsulated SMSI interface structure[115]. The core mechanism involves the utilization of a localized nanoconfined electric field generated by the laser at the metal-support interface, promoting the formation of surface defects on CeO_2 and inducing the generation of metastable CeO_x species. Driven by the interfacial electric field and surface energy, these CeO_x species migrate and spread over the surface of Pt nanoparticles, forming an ultrathin and porous CeO_x overlayer (Figure 2c-d). This enables the Pt/CeO_2 catalyst to maintain a stable SMSI structure while still participating effectively in the reaction. In addition to oxide layers, Chen et al. demonstrated that the Pt/Fe_3O_4 catalyst can regulate the metal-support interface through the dynamic phase transition of ferrite under reaction conditions[90]. The key point is that Fe_3O_4 undergoes co-evolution of reduction and carbonization in the reaction atmosphere, generating a highly active FeO_xC_y/FeC_x interface phase. During this process, Pt significantly lowers the energy barriers for the reduction and carburization of Fe_3O_4, accelerates the cleavage of Fe-O bonds, and facilitates the introduction of surface carbon species, thereby inducing the dynamic phase transition from Fe_3O_4 to FeO_x and then to FeC_x. As the reaction proceeds, the generated FeC_x species migrate toward the Pt surface and gradually spread under thermodynamic driving forces, forming a structure that partially to nearly completely encapsulates the Pt nanoparticles (Figure 2e-f). This partial coverage shields some adsorptive sites on the Pt surface, reducing CO adsorption capacity, while the structure remains dynamically stable throughout the reaction.

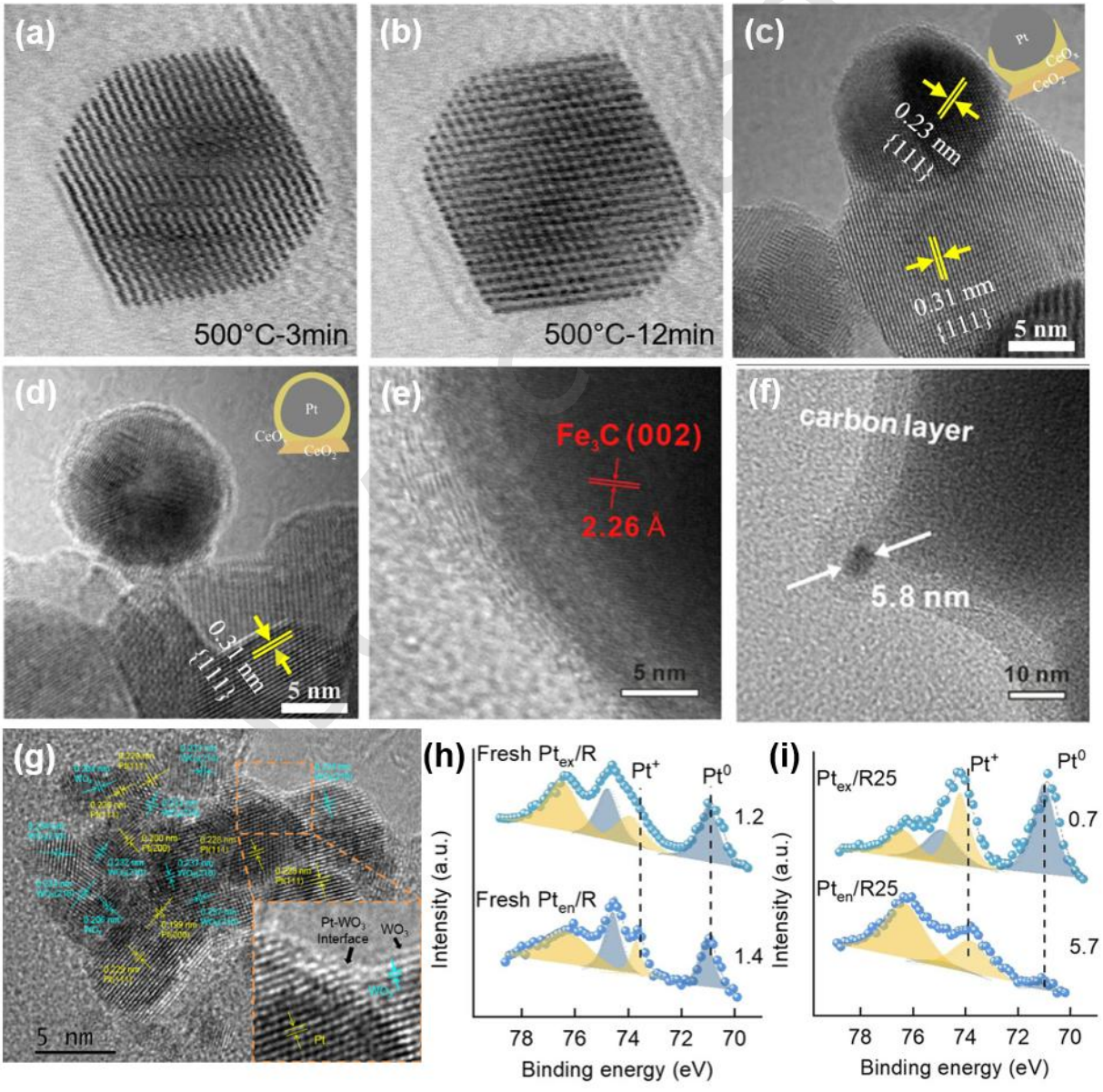

Figure 2. (a-b) Formation of a TiO_x overlayer on the surface of Pt NPs in the Pt/TiO_2 catalyst. Reprinted with permission from [114]. Copyright 2016, American Chemical Society. CeO_x overlayers induced by ultrafast laser irradiation: (c) 20 min, (d) 40 min. Reprinted with permission from [115]. Copyright 2021, Springer Nature. (e-f) TEM images and the corresponding SAED patterns of the Pt/Fe_3O_4 catalyst after reaction. Reprinted with permission from [90]. Copyright 2021, American Chemical Society. (g) HR-TEM image of Pt0.5W. The sample was prereduced at 400 °C. Reprinted with permission from [87]. Copyright 2024, American Chemical Society. In-situ Pt 4f XPS spectra: (h) fresh Pt/R catalysts, (i) Pt/R25 catalysts. Reprinted with permission from [86]. Copyright 2025, Wiley-VCH GmbH.

2.1.2 Electronic Metal-Support Interaction

Studies have shown that charge transfer occurs between the metal and the support concurrently with the generation of SMSI, specifically the EMSI. Beyond being perceived as a static transfer of electrons between the metal and the support, EMSI should be understood as a process of electronic state redistribution driven by the re-equilibration of the Fermi level at the interface, the involvement of defect states, and orbital hybridization[116-119]. From the perspective of band alignment, when Pt contacts reducible oxides, the conduction band edge, defect states, or localized f/d states of the support couple with the Pt 5d states to achieve Fermi level equilibrium at the interface. This interfacial coupling alters the occupation and density of states (DOS) distribution of the Pt 5d states, manifesting as an upward shift, downward shift, or broadening of the Pt d-band center relative to the Fermi level[120]. As the position of the Pt d-band center is closely related to adsorption strength, support-induced modulation of the electronic structure ultimately influences the adsorption and activation behaviors of CO_2, *CO, and H-related intermediates[121], thereby dictating the competition between CO formation and deep hydrogenation in the RWGS reaction[122]. Thus, the essence of EMSI is not electron transfer itself, but rather the regulation of Pt adsorption chemistry by the support through interfacial energy-level matching and DOS reshaping.

For the TiO_2 support, EMSI is primarily associated with the Ti 3d defect states induced by Ti^{3+}/O_v. The TiO_{2-x} surface formed after high-temperature reduction typically acts as an electron donor, transferring electrons to Pt during the interfacial Fermi level re-equilibration process. This electron transfer increases the electron density of Pt at the interface. However, when strong Pt-O-Ti bonding forms at the interface or when a TiO_{2-x} overlayer further develops, some Pt sites may exhibit $Pt^{\delta+}$ characteristics due to enhanced local oxygen coordination. Accordingly, EMSI in the TiO_2 system essentially represents a competition between the electron-donating effect of defects and the electron-withdrawing effect of interfacial oxygen coordination. The outcome depends on the degree of reduction, O_v concentration, and the mode of interfacial reconstruction. This competition enables reversible tuning of the Pt d-band center, which in turn influences the CO adsorption strength and the stability of the SMSI overlayer. Chen et al. loaded Pt nanoparticles onto the surface of TiO_2 and investigated the charge transfer behavior of the catalyst[123]. Characterization through conductivity measurements and X-ray photoelectron spectroscopy (XPS) revealed that the titania support was reduced during high-temperature treatment, allowing electrons to readily migrate through the thin surface TiO_2 layer to the Pt nanoparticle surfaces, where they became trapped, thus forming negatively charged Pt nanoparticles. Schierbaum et al. studied the $Pt/TiO_2(110)$ model catalyst using characterization techniques including XPS, ultraviolet photoelectron spectroscopy (UPS), and ion scattering spectroscopy (ISS)[124]. They found that the quantity of Ti^{3+} ions decreased significantly on the reduced $TiO_2(110)$ surface, indicating electron transfer from Ti^{3+} ions to Pt atoms. However, Hu et al.[86] discovered that high-temperature reduction treatment induces structural reconstruction on the Pt/rutile surface, generating a large number of O_v on the TiO_2 surface. Combined with XPS characterization, it was found that Pt NPs exhibited a positive valence state at the TiO_2 interface and showed strong adsorption toward the TiO_{2-x} overlayers. In contrast, O_v weakened the electron transfer from Pt nanoparticles to the rutile support, increasing the electron density of Pt. This facilitated the formation of Pt^0 species while simultaneously reducing the adsorption capacity of Pt toward the oxide overlayers (Figure 2h-i). This weakens the stabilization and spreading of the TiO_{2-x} overlayer on the Pt surface from the perspective of interfacial interaction energy, inhibits the formation of the TiO_{2-x} overlayer, and suppresses SMSI, thereby enhancing the stability of Pt/rutile under high-temperature RWGS reaction conditions.

For CeO_2 supports, the key to EMSI lies in the reversible transformation of Ce^{3+}/Ce^{4+} and the involvement of localized Ce 4f states. Since the Ce 4f energy level is close to the Fermi level of Pt, localized electrons tend to redistribute near the interface following the formation of O_v[125]. The relative energy levels between Ce 4f states and Pt 5d states can continuously fluctuate under specific temperature and local lattice distortion conditions, triggering electron transfer between Pt and CeO_2. Consequently, interfacial Pt typically exhibits electronic characteristics of coexisting $Pt^0/Pt^{\delta+}$ rather than a single valence state. Unlike simply strengthening the binding of Pt to adsorbates, CeO_2 tends to implement a relatively mild and dynamic modulation of the Pt d-band center through the synergy between Pt-O-Ce bonding and O_v. This modulation weakens the Pt-CO bonding strength while maintaining the capability for CO_2 activation. The research group of Núria López analyzed the fundamental principles and mechanisms regulating the EMSI at the Pt/CeO_2 interface[126]. First-principles Born-Oppenheimer molecular dynamics (BOMD) analysis revealed that at finite temperatures, surface atoms of CeO_2 undergo continuous thermal vibrations and local displacements, with these phonon excitations dynamically modulating the positions of Ce(4f) energy levels. When local lattice distortions transiently lower the Ce(4f) energy levels below the Fermi level of Pt, electrons can be injected from Pt into CeO_2. Conversely, when the structure recovers or new distortions occur, electrons may transfer back from CeO_2 to Pt. This indicates that EMSI is a process of electronic state redistribution jointly regulated by interfacial chemical bonds, local lattice distortions, and the reducibility of the oxide. Chen et al.[127] investigated the RWGS reaction over Pt/CeO_2 catalysts under atmospheric pressure at 200–500 °C. Due to the high electron density of the Pt d orbitals, charge transfer occurs between Pt and Ce^{3+}/Ce^{4+} pairs, forming electron-coupled interfacial sites of Pt-Ce^{3+}. Additionally, the generated O_v enhance the activation of CO_2. Consequently, the catalyst achieves a 25% CO_2 conversion and 100% CO selectivity at 500 °C.

For Fe_3O_4 supports, the EMSI characteristics are closely related to the mixed valence states of Fe^{2+}/Fe^{3+} and the carrier properties of Fe 3d orbitals. Compared to TiO_2 and

CeO_2, Fe_3O_4 functions more like a dynamic electron reservoir dominated by Fe 3d states. Under reducing or reactive atmospheres, Fe_3O_4 may undergo structural evolution involving FeO_x and even FeC_x phases, resulting in continuous changes to the local coordination environment and DOS distribution around Pt sites. Therefore, EMSI in Pt/Fe_3O_4 should not be viewed as a unidirectional electron injection or extraction with a fixed direction but rather as a dynamic modulation of the Pt d-band center driven by the adjustable ratio of Fe-O-Pt to Fe-C-Pt interfaces. This behavior is typically accompanied by interfacial reconstruction and partial surface overlayer formation, which helps mitigate excessively strong CO adsorption on Pt and enhances the stability of the interfacial structure under high-temperature RWGS conditions. In the dynamic phase transformation system of ferrite carbon compounds studied by Chen et al., the formation of FeC_x coating phases correlates with a downshift of the Pt d-band center. Pt acts as an electron donor, facilitating continuous and directional electron transfer to the Fe-based support via hydrogen spillover[90]. This process strengthens CO_2 adsorption and activation at the electronic structure level while weakening CO adsorption strength, ultimately achieving 100% CO selectivity (Table 1).

2.1.3 Composite Support Structure

Constructing a heterogeneous composite interface composed of an inert framework and a defect-enriched reducible phase is a core strategy for regulating the Pt-support interface[128]. This approach transforms the single-functional Pt-support surface into perimeter interfacial sites capable of both H_2 activation and CO_2 activation. It also employs defect sites as regulatory knobs to directionally modulate EMSI and SMSI, as well as reaction pathways, ultimately achieving synergistic optimization of activity, selectivity, and stability in the RWGS reaction. Bi et al.[87] introduced WO_x as a secondary oxide component into a Pt/SiO_2 system. Under reducing conditions, the WO_x species existed as low-polymerization polytungstate clusters that partially encapsulated Pt, preventing a significant decrease in activity caused by excessive overcoating. Consequently, abundant WO_x/Pt interfacial perimeter sites were formed. WO_x provided oxophilic sites and O_v for CO_2 activation, while Pt was responsible for H_2 dissociation (Figure 2g). Their synergistic interaction increased the intrinsic reaction rate by a factor of 8 times compared to Pt/SiO_2 and achieved 100% CO selectivity (Table 1). The electronic structure of the interfacial Pt sites deviates from that of bulk metals, significantly enhancing the adsorption and activation capacity of the interface toward CO_2[129]. Ma Ding et al. utilized the defects and interfacial chemistry of the MoO_3/γ-Mo_2N heterostructure to induce a significant EMSI[97]. MoO_3 on the surface of γ-Mo_2N was in-situ reduced to oxygen-vacancy-rich MoO_x ($2 < x < 3$), while simultaneously achieving atoms, thereby constructing a high-density Pt-MoO_x/γ-Mo_2N catalyst. This reduction occurs exclusively at the MoO_3/γ-Mo_2N heterointerfaces, whereas pure MoO_3 does not form MoO_x under the same RWGS reaction conditions. MoO_x exists as thin layers and defects, facilitating stable electron redistribution between MoO_x and Pt. Subsequently, isolated Pt atoms preferentially coordinate with oxygen atoms in MoO_x and aggregate to form stable Pt clusters during the reaction process (Figure 3a-c). This enabled a CO_2 conversion rate approaching thermodynamic equilibrium at 300 °C, with no significant deactivation observed over 300 hours (Table 1). Zhao et al. proposed a strategy for stabilizing Pt single atoms based on three-dimensional confinement[98]. This method utilizes the spatial confinement and interfacial effects of amorphous SiO_2 to restrict the crystallization and long-range ordered growth of CeO_2, preparing loose amorphous CeO_2 clusters rich in O_v. Furthermore, it employs surface O_v to trigger significant electron transfer from Pt to CeO_2, stabilizing atomically dispersed Pt. XPS characterization reveals that these defect-enriched CeO_2 clusters act as electron acceptors and anchoring sites, resulting in Pt existing predominantly in the Pt^{2+} and Pt^{4+} valence states at the Pt-CeO_x interface, rather than the Pt^0 state found in conventional Pt-CeO_x systems (Figure 3d-f). Benefiting from the interfacial regulation of this composite support, the catalyst simultaneously exhibits high CO_2 adsorption capacity, weak CO affinity, and excellent long-term stability. Chen et al. demonstrated another type of composite interface regulation via the physical mixing of Pt/Al_2O_3 with anatase TiO_2 diluents[130]. The communication effect between composite supports modifies the active intermediates and reaction pathways. Through close contact with Al_2O_3, TiO_2 facilitates the migration of adsorbed acetate species in air between the oxides, thereby eliminating the blockage of formate formation sites on Al_2O_3 (Figure 3g-h).

In this category of strategies, O_v, acting as defect states and local charge regulation centers, both drive and enhance charge redistribution between Pt and metal oxides by modifying the electron transfer capability of the oxide phase and the interfacial Pt-O-M bonding strength. This process consequently forms a favorable EMSI that optimizes the Pt charge state, CO adsorption strength, and CO_2 activation pathway. Additionally, the composite support interface influences the dispersion and coverage of oxide species on the Pt surface through interfacial bonding, thereby suppressing or regulating the SMSI. Due to the synergistic interaction between the inert framework and the reducible phase within the same system, Pt-based catalysts can simultaneously offer efficient H_2 dissociation sites and defect-enriched CO_2 activation sites on a single catalyst. This synergy establishes a more optimal intrinsic balance among catalytic activity, CO selectivity, and high-temperature structural stability in the RWGS reaction.

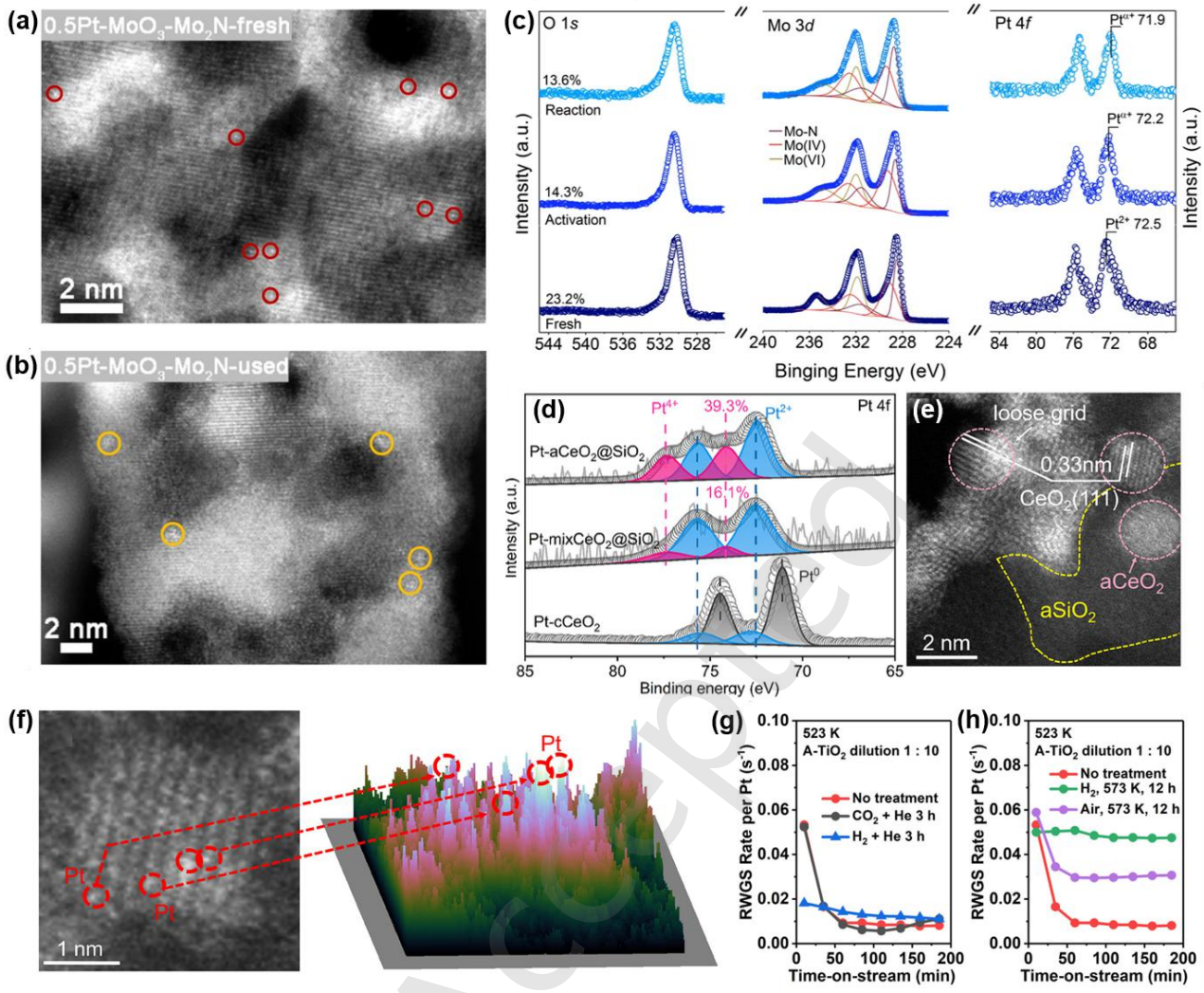

Figure 3. (a-b) Aberration-corrected HAADF-STEM images of fresh and used Pt-MoO_x/γ-Mo_2N catalysts. (c) XPS spectra of fresh 0.5 Pt-MoO_x/γ-Mo_2N and quasi in-situ XPS spectra of 0.5 Pt-MoO_x/γ-Mo_2N after the treatment of 5% H_2/Ar and 23% CO_2/69% H_2/Ar at 300 °C for 30 min. Reprinted with permission from [97]. Copyright 2022, Springer Nature. (d) XPS spectra of Pt 4f region for the Pt-aCeO_2@SiO_2, Pt-mixCeO_2@SiO_2 and Pt-cCeO_2 catalysts. (e) Atomic-scale HAADF-STEM images of Pt-aCeO_2@SiO_2 and (f) the corresponding plane intensity profile. Reprinted with permission from [98]. Copyright 2025, Wiley-VCH GmbH. Variations of the RWGS rate with TOS at 250 °C on Pt/Al_2O_3: A-TiO_2 = 1:10 after different pretreatments. Panel (g) shows results with the pretreatment of 5% CO_2 in He for 3 h (black), and 20% H_2 in He for 3 h (blue) at 250 °C, to compare with results with no pretreatment (red). Panel (h) shows results with a pretreatment of 20% H_2 in He for 12 h (purple) and air for 12 h (green) at 300 °C, to compare with results with no pretreatment (red). Reprinted with permission from [130]. Copyright 2021, American Chemical Society.

2.2 Regulation of Pt particle size

In addition to regulating interfacial chemistry, the Pt particle size also determines the number of available interfacial perimeter sites per unit mass of Pt, as well as their local geometric configurations[131]. Studies have shown that when nanoparticle size falls below 4 nm, the proportion of coordinatively unsaturated sites increases markedly[132]. This variation in coordinatively unsaturated sites affects the bonding interactions between reactant molecules and the catalyst, thereby influencing catalytic activity. Consequently, it is generally accepted that the proportion of active reaction sites increases as metal particle size decreases[133]. On the other hand, the electronic structure of Pt nanoparticles also changes with decreasing particle size. When the size of metal nanoparticles is reduced beyond a certain threshold, their energy bands split, modifying the electronic structure such that the metal clusters exhibit a discrete-like band structure, as illustrated in Figure 4a. Building on the interfacial electronic structure, this section focuses on how the Pt particle size and coordination environment of Pt particles reshape the dominant active sites and regulate the selectivity between CO and CH_4.

The overall reaction rate and apparent activity exhibit a clear dependence on particle size. Larger Pt nanoparticles have a coordination environment closer to the intrinsic metallic state, with significantly weaker interfacial electronic effects. In contrast, smaller Pt nanoparticles exhibit a higher contact ratio with the support, placing Pt in a stronger Pt-O-M interaction environment and inducing more pronounced support-mediated electronic effects [134] and driving more readily it undergoes interfacial reconstruction by the reaction atmosphere and temperature, thereby triggering MSI to varying degrees[135-137]. Maurer et al. used atomically dispersed Pt_{SAc} as a reference and compared it with approximately 1 nm Pt nanoparticles (NPs) formed by

reducing Pt_{SAc} in 2% H_2 at 400 °C for 30 minutes[138]. Operando high-energy-resolution fluorescence-detected X-ray absorption near-edge structure (HERFD-XANES) analysis revealed that, with increasing reaction temperature, Pt NPs only the Pt^0 valence state without any change in electronic structure. In contrast, during the heating process, the Pt_{SAc} catalyst underwent Pt cluster formation, and its valence state evolved continuously in the sequence of $Pt^{4+} \rightarrow Pt^{2+} \rightarrow Pt^{\delta+}$-CO $\rightarrow Pt^{n\delta+}$-CO (Figure 4b). This demonstrates stronger support-induced charge modulation and a more significant EMSI.

As the Pt particle size decreases, the dominant active sites shift from those favoring metal surface reactions to those that activate the lattice oxygen of the oxide support and participate in the interfacial reaction pathway. Xie et al. prepared Pt/CeO_2 catalysts with three different particle sizes (5 nm, 2 nm, and atomically dispersed Pt) via surface pre-reduction and conventional impregnation methods[99]. Catalytic tests indicate that CO selectivity decreases significantly as Pt particle size increases. In-situ FTIR of CO desorption shows that larger Pt species exhibit stronger CO adsorption, facilitating the further reaction of surface *CO with H to form CH_4. Conversely, atomically dispersed Pt creates a distinct local chemical environment due to its interaction with the support, resulting in weaker CO adsorption and thereby attenuating the sequential hydrogenation pathway of CO to CH_4 (Figure 4c-e). Leo et al. clearly distinguished and compared the structures and reaction behaviors of Pt single atoms, oxidized Pt clusters, and metallic Pt clusters within the same system[139]. Based on CO probe infrared spectroscopy (CO-IR) analysis, Pt single atoms exhibit only a single, clearly assignable CO adsorption configuration. In contrast, oxidized and metallic Pt clusters display superimposed responses from multiple adsorption sites, indicating stronger CO adsorption properties (Figure 5a-c).The size effect does not exhibit a direct linear correlation with catalytic activity, but rather depends on the degree of coordinative unsaturation and the chemical environment induced by particle size[140-143]. By comparing fully exposed Pt clusters (Pt_{FEc}/CeO_2), single-atom Pt (Pt_{SAc}/CeO_2), and Pt nanoparticles (Pt_{NPs}/CeO_2), Xie et al. [85] found that variations in Pt particle size significantly reconstruct the local coordination structure at the Pt-CeO_2 interface. In Pt_{FEc}/CeO_2, Pt exists in a low-coordination $Pt^{\delta+}$ state and is tightly coupled with O_v enriched on the CeO_2 surface (Figure 4f). This structure reduces the electron density of Pt clusters, thereby weakening the Pt-CO bonding strength. In contrast, single-atom Pt is confined by excessively strong Pt-O coordination and exists in the Pt^{4+} state, making it difficult to balance activity and selectivity simultaneously. Meanwhile, Pt nanoparticles promote methanation due to their strong H_2 dissociation ability and high CO adsorption capacity.

2.3 Single-atom platinum catalysts

From the perspective of the size effect, Pt single atoms are fully interfacialized geometrically[144-146]. The site-specific electronic structure, reactant adsorption configuration, and conversion capabilities of key intermediates are no longer governed by Pt-Pt coordination but are instead highly dependent on chemical bonding and electronic coupling with the support[147-152]. Generally, the local configurations of single-atom Pt can be summarized into types such as Pt-N_x, Pt-O_x, and Pt-S_x. However, in current research on Pt-based catalysts for the RWGS reaction, Pt-O_x sites on oxide supports remain the most prevalent and have been the subject of the most comprehensive mechanistic investigations. Therefore, this section focuses on discussing how the Pt-O_x coordination environment influences the CO_2 adsorption mode, the energy barriers of key elementary steps, and product selectivity.

Distinct from simply considering single-atom Pt as highly dispersed Pt species, the catalytic behavior of Pt-O_x sites is fundamentally governed by their coordination saturation, site accessibility, and the synergistic effects with O_v or interfacial defects. For Pt-O_x sites with highly saturated and geometrically confined coordination environments, although this configuration favors the stabilization of single-atom Pt, the accessibility of Pt sites is compromised, limiting their ability to dissociate H_2. Additionally, due to insufficient vacancy accessibility at the Pt centers, CO_2 tends to adsorb only weakly, thereby inhibiting the initial activation of CO_2 and the formation of key intermediates.

In contrast, moderately decoordinated Pt-O_x sites coupled with defect sites generally exhibit a more open local geometric configuration and a more balanced electronic state distribution. This enables Pt to maintain a certain degree of metallicity or $Pt^{\delta+}$ character and form synergistic units with adjacent O_v or interfacial oxygen species. Under these conditions, Pt sites are more favorable for H_2 activation, while neighboring defect sites or interfacial oxygen facilitate the adsorption and polarization of linear CO_2 molecules, promoting their transformation into a bent configuration and thereby lowering the formation energy barrier of oxygen-containing intermediates. Furthermore, the local electronic states of Pt are modulated by oxygen coordination and defect coupling, weakening the Pt-CO interaction compared to metallic Pt nanoparticles. This effect shortens the residence time of *CO on Pt sites and suppresses further hydrogenation to CH_4. Using Pt_1/TiO_2 as a model, Chen et al. proposed a strategy to achieve high catalytic activity and structural stability through the reversible regulation of Pt particle size and chemical environment[153]. X-ray absorption spectroscopy (XAS) reveals that in the fresh Pt_1/TiO_2 catalyst, Pt is highly dispersed as single atoms and forms a highly saturated Pt-O coordination environment with the surface oxygen of TiO_2, which significantly restricts catalytic activity. After reduction treatment, some Pt_1 species migrate to form small, amorphous Pt_n aggregates. This process reduces the Pt-O coordination number, transforms the local electronic environment of Pt into a more open metallic state, and enhances the RWGS reaction activity by nearly fivefold. Subsequently, these Pt_n aggregates are redispersed into Pt_1 after mild oxidation treatment. Unlike the fresh samples, the Pt_1 after redispersion exhibits a significantly reduced degree of coordination with surface oxygen, presenting a more open coordination environment and thus markedly enhancing RWGS reaction activity (Figure 4g-h). The Phillip Christopher group proposed a Pt single-atom regulation strategy integrating site homogenization

and environmental responsiveness[154]. Pt single atoms (0.5 wt%) were uniformly anchored at specific sites on 5 nm anatase TiO_2 nanocrystals. In-situ atomic-resolution microscopy and spectroscopic characterization combined with first- principles calculations demonstrated that Pt single atoms dynamically regulate their local coordination number and valence state under different environmental conditions. Under oxidizing conditions, Pt forms a high-coordination, oxygen-enriched Pt-O configuration. Under mild reducing conditions, it transforms into a Pt-O-Ti interfacial structure bonded to the surface sites of TiO_2. In a stronger reducing environment, it further evolves into nearly neutral $Pt^{\delta+}$ species (Figure 5d), thereby decreasing the activation energy from approximately 75 to 48 kJ/mol and resulting in a 2-5-fold increase in catalytic activity.

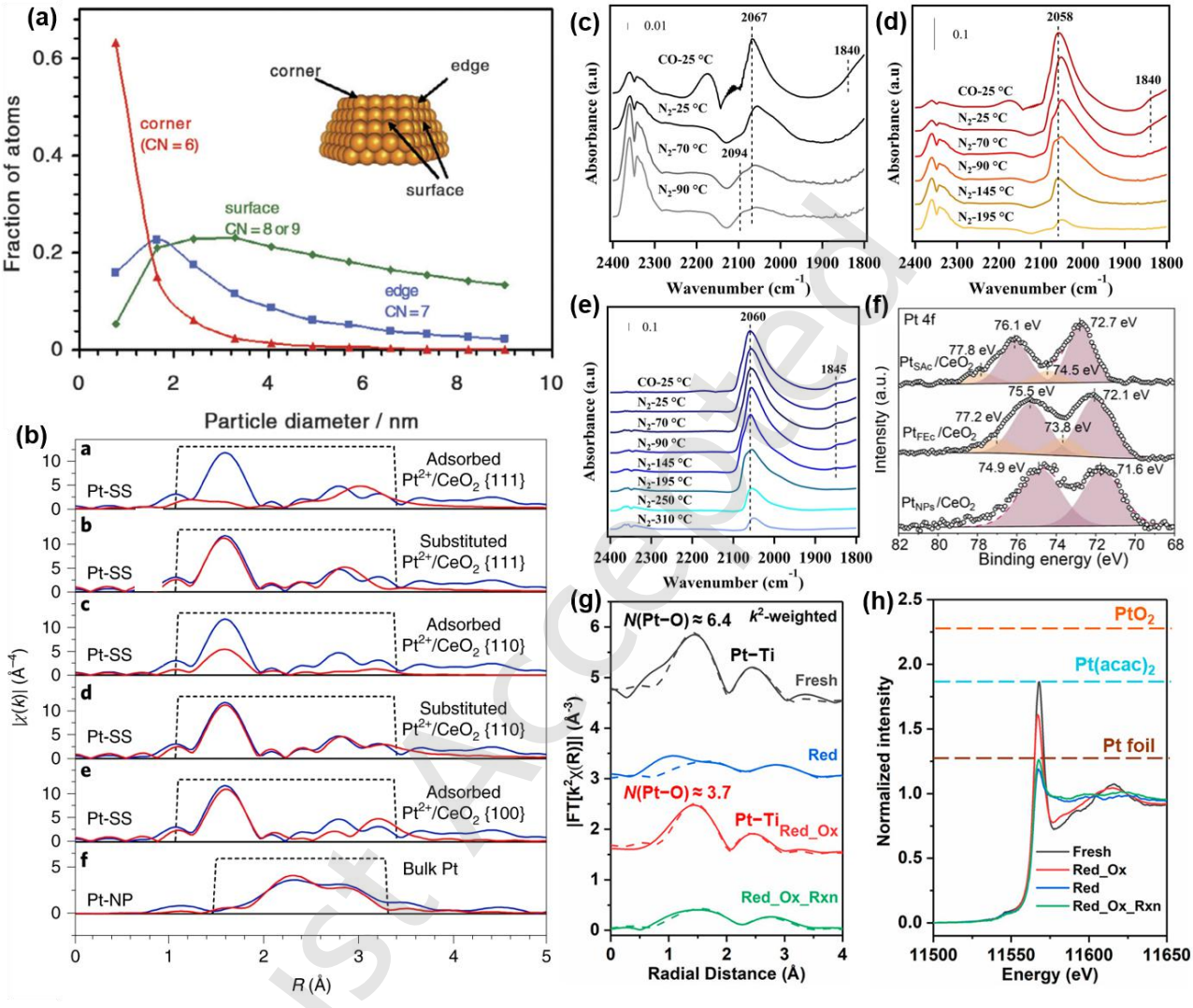

Figure 4. (a) Geometric and electronic structures of single atoms, clusters, and nanoparticles. Reprinted with permission from [155]. Copyright 2017, Elsevier Ltd. (b) FT k^3-weighted EXAFS data of different Pt/CeO_2 catalysts. Reprinted with permission from [138]. Copyright 2020, Springer Nature. In-situ FTIR of CO desorption on (c) Pt/CeO_2-AA-350, (d) Pt/CeO_2-IMP-350 and (e) $5Pt/CeO_2$-IMP-350 catalysts after pre-reduction at 350 °C in 20 % H_2/N_2 for 1 h. Reprinted with permission from [85]. Copyright 2021, Elsevier B.V. (f) Quasi in-situ XPS spectra of Pt/CeO_2 catalysts for Pt 4f regions. Reprinted with permission from [99]. Copyright 2025, Elsevier B.V. Pt L_3-edge XAS results on Pt_1/TiO_2: (g) the EXAFS, (h) the XANES. Reprinted with permission from [153]. Copyright 2021, The Authors.

Owing to the unique configuration of single atoms, while Pt_1 maintains high catalytic activity, structural stability remains a major challenge. The anchoring interaction between single-atom Pt and the support is difficult to sustain under high-temperature reducing atmospheres, and Pt_1 tends to migrate when induced by CO[156]. Meanwhile, the weak dependence of the RWGS reaction on interfacial O renders the Pt_1 structure metastable, resulting in its thermodynamic and kinetic tendency to transform into Pt-Pt aggregated states. Numerous studies have demonstrated that Pt single-atom catalysts can significantly suppress migration and sintering at high temperatures by strengthening MSI, thereby intrinsically enhancing catalyst structural stability[157,158]. John Jones proposed the atom trapping strategy for single-atom regulation[159]. Under high-temperature air calcination conditions, the Pt nanoparticles originally present on the CeO_2 surface undergo volatile migration to form mobile PtO_2 species, which then form strong Pt-O-Ce bonds with the surface oxygen of CeO_2 and are firmly anchored, thus converting into highly dispersed isolated Pt single atoms (Figure 5e-f). These Pt atoms are forcibly confined as interfacial sites, and their stability

derives from strong EMSI rather than Pt-Pt coordination. Lang et al. also achieved highly loaded and thermally stable dispersion of Pt single atoms on the defect-free surface of Fe_2O_3 by utilizing the strong covalent metal-support interaction (CMSI) between Pt-O and the support[160] (Figure 5g). These fully interfacialized and atomically dispersed Pt species shift the stability-determining factor of the catalyst from defect density control to chemical bond strength control, thereby challenging the traditional perception that highly loaded single-atom catalysts must rely on high-density defects. Kang et al. proposed an amine-molecule-assisted in-situ anchoring strategy[89]. By synergistically regulating the interaction between Pt species and interfacial O_v of TiO_{2-x}, Pt single atoms are embedded into the O_v to form a well-defined $Pt^{\delta+}$-O_v-Ti^{3+} anchored structure, thereby establishing SMSI to suppress Pt sintering (Figure 5h-i).

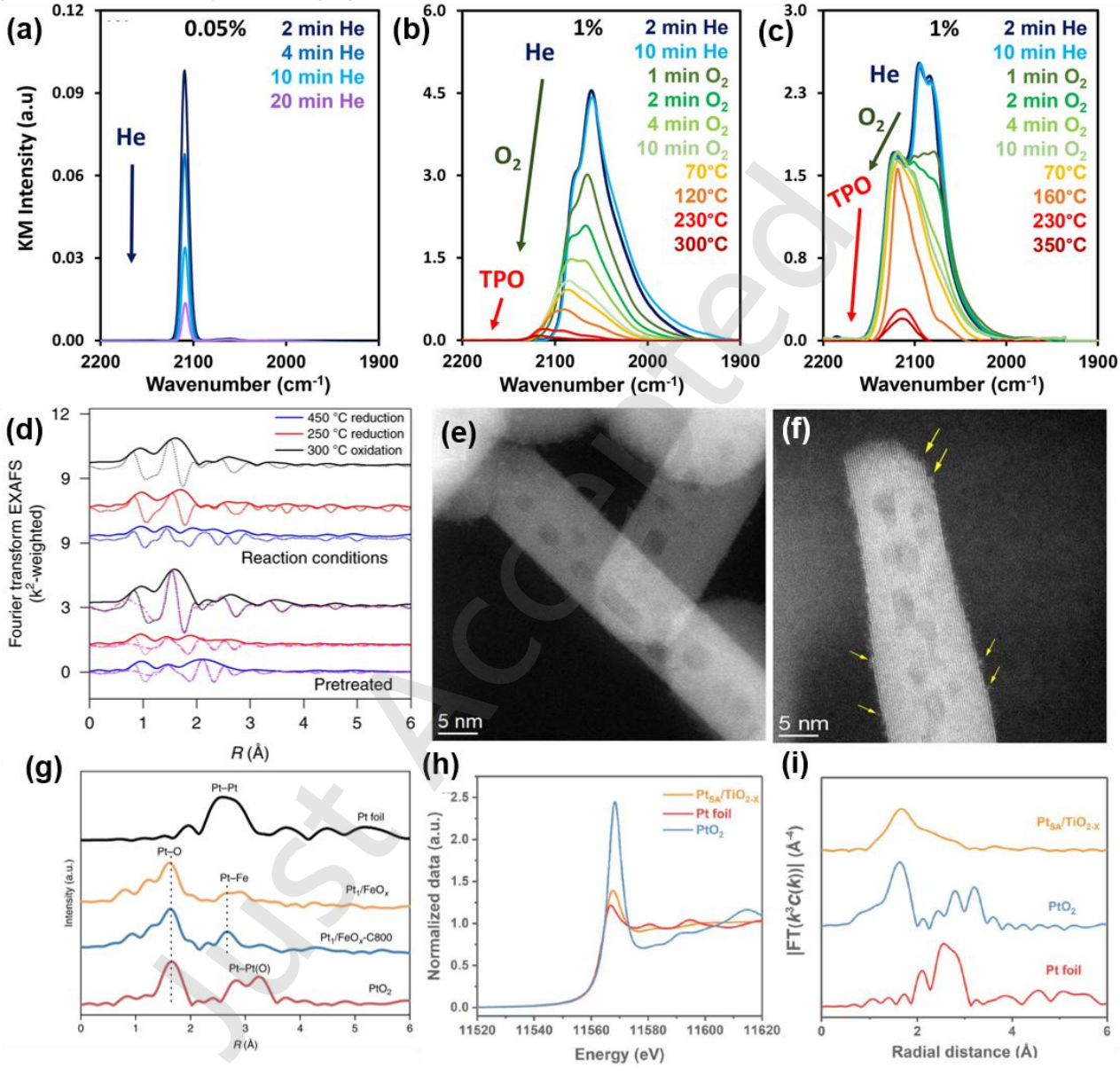

Figure 5. Site-specific signatures of CO adsorbed to Pt_{iso}, Pt_{metal}, and Pt_{ox}. (a) IR spectra of CO adsorbed at room temperature and saturation coverage on a pre-reduced 0.05 wt % SEA catalyst during He flushing. (b) CO adsorbed to a reduced 1 wt % DI catalyst during a He and O_2 flush at room temperature and a TPO ramp. (c) CO adsorbed to an oxidized 1 wt % DI catalyst during the identical protocol as (b). Reprinted with permission from [139]. Copyright 2017, American Chemical Society. (d) EXAFS of catalysts after each pretreatment and under CO oxidation reaction conditions. Reprinted with permission from [154]. Copyright 2019, Springer Nature. HAADF AC-STEM images of Pt/CeO_2 treated at 800 °C in an air flow for 10 h: (e) before treatment, (f) after three cycles of CO oxidation at 300 °C. Reprinted with permission from [159]. Copyright 2016, American Association for the Advancement of Science. (g) Fourier transform radial distribution function of the Pt L_{III}-edge k^3-weighted EXAFS spectra of Pt_1/FeO_x before and after calcination in comparison with PtO_2 and Pt foil. Reprinted with permission from [160]. Copyright 2019, Springer Nature. (h) XANES spectra of the Pt L_3-edge over the Pt_{SAc}/TiO_{2-x}, Pt foil and PtO_2. (h) Fourier-transformed EXAFS spectra of Pt_{SAc}/TiO_{2-x}, Pt foil and PtO_2. Reprinted with permission from [89]. Copyright 2024, Science China Press.

2.4 Bimetallic catalysts

Single Pt sites often face challenges such as the difficulty in balancing activity and selectivity, limited reaction pathways, and uncontrollable structural evolution under high

temperatures or reaction atmospheres. In recent years, the introduction of a second metal to construct Pt-M bimetallic catalysts has been proven to be an effective regulation strategy, whose core lies in the precise modulation of Pt local structure, electronic state, and interfacial chemistry by the second metal, thereby systematically reshaping the catalytic reaction process itself[161-165]. Existing studies have demonstrated that the catalytic behavior of Pt can be regulated through multiple structural modes, including forming Pt-M alloys or intermetallic compounds, constructing adjacent heteronuclear diatomic sites, and introducing alkali metal promoters with well-defined chemical functions at the metal-support interface, thereby reshaping the local electronic structure and proximal coordination environment of Pt[166].

The second metal can directionally modulate the d-band center of Pt and the adsorption strength of key intermediates, weakening the excessive Pt–CO bonding under reaction conditions by altering the proximal atomic environment of Pt. This process alleviates CO poisoning and increases the CO desorption rate. Additionally, the metal's reversible redox behavior can participate in the cleavage of C-O and O-H bonds, further modifying the reaction pathway and significantly enhancing the CO_2 conversion rate. Kattel et al. introduced Co into Pt to fabricate nanoalloy catalysts supported on various oxide supports, aiming to create a Pt-Co subsurface structure while maintaining Pt-dominated surface chemistry and amplifying the reaction characteristics at the metal-oxide interface[167]. Combined with thermodynamic stability predictions of Pt-terminated structures using density functional theory (DFT), the results demonstrate that Co primarily modulates Pt in the form of a subsurface layer rather than replacing Pt as the primary surface adsorption site. The PtCo-oxide interface formed in this manner further governs the reaction process. Hansen et al. prepared a series of SiO_2-supported Pt_xFe_y alloy nanoparticles via the SOMC method[102]. As the Fe content increased, the degree of Pt-Fe alloying was enhanced, resulting in a CO formation rate nine times higher than that of monometallic Pt@SiO_2, while Fe@SiO_2 exhibited almost no catalytic activity. XAS results revealed that the stability of the Pt-Fe alloy and the rapid redox dynamics of surface Fe transformed the formate reaction pathway of Pt@SiO_2 into a more efficient redox catalytic pathway (Figure 6a-b). Liu et al. constructed Pt_3Ni intermetallic compounds supported on mesoporous SBA-15 support[100]. In-situ XAS results indicated that Ni tends to form a significant MSI with the SiO_2 support, leading to the dispersion of partial Ni into stable Ni-silicate phases. Under conditions of mass conservation, the remaining Ni metal components form Pt-rich Pt_3Ni alloys, which eliminate Ni-Ni interactions (Figure 6c-d). CO adsorption diffuse reflectance infrared Fourier transform spectroscopy (CO-DRIFTS) results showed that these specific Pt-Ni sites and Ni-silicate phases effectively suppress the strong interaction between CO and Pt NPs as well as Ni atoms, endowing the catalyst with high activity and selectivity for CO generation in the RWGS reaction (Figure 6e). Wang et al. employed atomically spatially confined adjacent Pt-Fe hetero-dual sites as the core and achieved directional reconstruction of Pt catalysts by controllably anchoring Fe atoms at positions adjacent to Pt atoms on the surface of commercial CeO_2[101]. HAADF-STEM characterization showed that Pt and Fe were atomically dispersed on the CeO_2 surface while maintaining adjacency, with no independent metal clusters observed. Compared with Pt/CeO_2, the introduction of Fe significantly modulated the local electronic structure and proximal coordination environment of Pt. As the Fe content decreased, the average distance between Pt and Fe increased accordingly, and the catalytic activity decreased simultaneously (Figure 6f). This indicates that the promotional effect of this configuration depends on the adjacent, rather than random, site configuration.

2.5 Regulation of functional catalytic additives

In addition to the direct involvement of secondary metals in reactions through alloy formation or adjacent heteronuclear sites, promoter regulation primarily focuses on reconstructing the interfacial chemical environment and reaction field surrounding Pt[168]. Alkali metal promoters generally do not serve as new active metal centers in the RWGS reaction. Instead, they systematically regulate the adsorption and activation behaviors, as well as the reaction pathways of CO_2 and *CO, by modifying the acid-base properties, charge distribution, and local electric field at the Pt-support interface[64,169-172].

Yang et al. proposed a strategy for the synergistic regulation of the structure, electronic properties, and reaction pathways of Pt-based zeolite catalysts by introducing the alkali metal promoter potassium (K)[91]. With the addition of K, the dispersion degree of Pt increased from 80.9% to 87.1%. The introduction of K gradually disrupted the microporous structure of the zeolite and covered the Pt^0 sites on the Pt surface, thereby constructing a stable Pt-K interface (Figure 6g-h). The presence of the promoter K induced the formation of Pt-O(OH)-K interfacial sites, which enhanced CO_2 adsorption and activation capacity while simultaneously weakening the bonding strength of Pt-CO species. Liang et al. also utilized the alkali metal promoter K to construct Pt-KO_x interfacial interactions rather than relying on a particle size effect between Pt and the mullite support[93]. The introduction of K resulted in an elevated reduction temperature of Pt species and the appearance of a $Pt^{\delta+}$ signal, clearly indicating the formation of a strong interaction between K_2O and Pt (Figure 6i). In addition to K, Torres-Sempere employed the alkali metal promoter cesium (Cs) to extensively regulate the surface acid-base properties of the TiO_2 support[95]. Compared with the undoped system, Cs did not compromise the high dispersion characteristics of Pt or the specific surface area of the support. The core mechanism involves the reconstruction of surface hydroxyl groups and the electronic structure of TiO_2 by Cs. Analysis using the Tauc plot method indicated that the band gap of the catalyst after Cs doping changed by approximately 0.1 eV compared with that of the undoped sample, reflecting that Cs can neutralize hydroxyl sites on the TiO_2 surface and form surface titanate species, thereby modulating the electronic structure and insulating properties of the support. This directly leads to a change in the reaction mechanism upon Cs introduction: the O_v-dominated redox mechanism over

Pt/TiO_2 is transformed into a formyl/acyl-associated pathway synergized by Cs-modified surface Lewis acid-base sites and the frustrated Lewis pair (FLP)-assisted CO_2 reduction pathway over Pt-Cs/TiO_2.

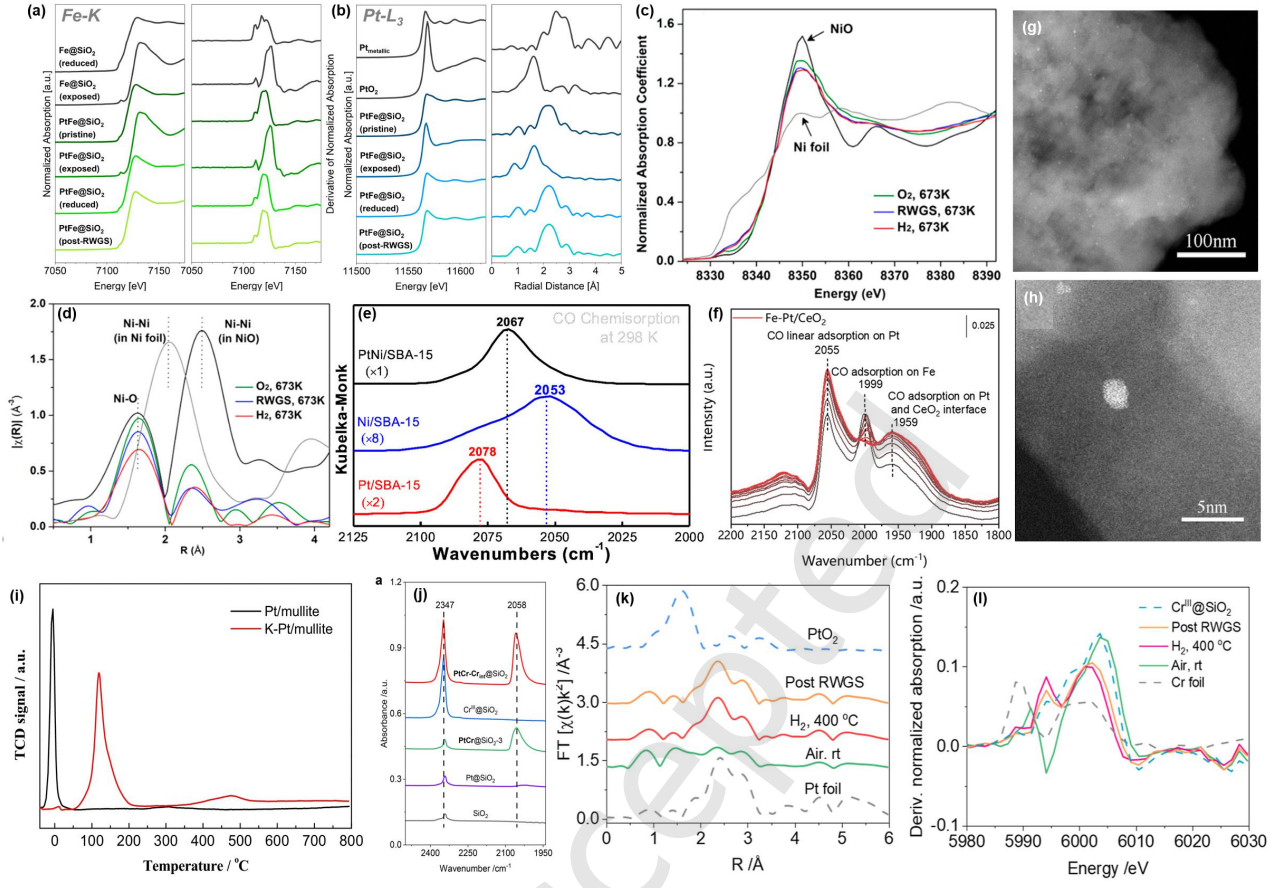

Figure 6. XANES under various conditions for (a) PtFe@SiO_2 (Fe-K edge), (b) PtFe@SiO_2 (Pt-L_3 edge). Reprinted with permission from [102]. Copyright 2024, American Chemical Society. XAS data measured at the (c, d) Ni K-edge. (e) DRIFTS band of CO atop adsorption on metallic sites of Ni, Pt, and PtNi catalysts (after activation in H_2/673 K) recorded at 298 K with helium flow. Reprinted with permission from [100]. Copyright 2018, American Chemical Society. In-situ DRIFT spectra of the RWGS reaction over (f) Fe-Pt/CeO_2. Reprinted with permission from [101]. Copyright 2023, American Chemical Society. Aberration-corrected transmission electron microscope images of K_{80}-Pt/L catalyst under the scale bar of (g) 100 nm and (h) 5 nm. Reprinted with permission from [91]. Copyright 2017, Elsevier B.V. (i) H_2-TPR profiles of Pt/mullite and K-Pt/mullite catalysts. Reprinted with permission from [93]. Copyright 2016, Elsevier B.V. (j) FT-IR of CO_2 adsorbed on different catalysts under 10-15 mbar CO_2 pressure at room temperature. XAS spectra of PtCr-Cr_{int}@SiO_2 at Pt L_3-edge and Cr K-edge under different conditions: (k) corresponding k^2-weighted Fourier transforms of EXAFS spectra of Pt L_3-edge, (l) corresponding first derivative spectra of Cr K-edge. Reprinted with permission from [94]. Copyright 2025, American Chemical Society.

From the perspective of catalytic design, the regulatory roles of alkali metal promoters and transition metals in Pt-based catalysts are inherently different yet highly complementary[173]. Alkali metal promoters generally do not form new metal reaction centers; instead, they function by modulating the interfacial chemical environment surrounding Pt, thereby weakening the Pt-CO interaction and altering the reaction mechanism. In contrast, transition metals directly participate in the formation of active sites through alloying with Pt or by forming heteronuclear diatomic sites, modulating the local electronic structure of Pt and facilitating the catalytic reaction process. Zhou et al. leveraged the regulatory advantages of both strategies and established a dual-promotion mechanism that synergizes Pt-Cr alloying with promoter-like interfacial Cr(III) species[94]. The introduction of Cr not only modulates the local electronic structure and chemical environment of Pt but also enables Cr(III) to act as Lewis acidic interfacial sites, significantly enhancing CO_2 adsorption capacity (Figure 6j-l). Furthermore, a formate-mediated associated reaction pathway is initiated between the PtCr alloy and Cr(III) species, proceeding in parallel with the redox pathway on the alloy sites. A clear comparison between the two pathways demonstrates that the rational design of Pt-based catalysts has evolved from optimizing single active sites to a multidimensional strategy focused on the synergistic regulation of active centers and their reaction microenvironments.

To regulate the local geometric configuration and interfacial electronic structure of Pt-based catalysts, multiple strategies have been employed, including metal-support interface reconstruction, control of Pt particle size and coordination environment, engineering of bimetallic active sites, and incorporation of functional promoters. By modifying the reaction energy barriers of key steps, such as CO_2 → HOCO* conversion, H_2 dissociation capacity, *CO adsorption strength, and the relative conversion between reaction pathways, these structural adjustments effectively establish the intrinsic correlation between catalyst structure

and RWGS reaction activity, CO/CH_4 selectivity, and high-temperature structural stability. This approach advances traditional empirical optimization toward a reaction mechanism–oriented synergistic design framework.

3 Identification of active sites and mechanistic studies

In heterogeneous catalysis, catalytic performance depends on the structural characteristics of genuine active sites and their dynamic reaction pathways. Relying solely on static characterization of products before and after the reaction makes it difficult to accurately identify active centers and their underlying mechanisms[174]. In-situ spectroscopy can track the evolution of intermediates and changes in electronic structure in real time[175]. When combined with first-principles calculations, it enables quantitative analysis of adsorption configurations, reaction energy barriers, and electron transfer, thereby revealing the nature of active sites and catalytic mechanisms[176-178].

For Pt-based catalysts, different working-state structures not only alter the dispersion and valence state of Pt but also determine the adsorption and activation modes of CO_2, the dissociation sites of H_2, and the stability of key intermediates. These effects arise from the regulation of the local coordination environment of Pt sites, metal–support interfacial electronic coupling, and the proximity of defect sites. Therefore, this section focuses not only on identifying the true active sites but also on establishing the relationship between the active site structure and the reaction pathways illustrated in Figure 1b. Furthermore, it aims to elucidate how this relationship influences the activity, CO selectivity, and stability of RWGS.

3.1 In-situ characterization techniques

The advancement of in-situ and operando characterization techniques has enabled the direct monitoring of changes in Pt coordination environments, surface species, and electronic states under realistic reaction conditions[179]. Techniques such as in-situ XANES/EXAFS, environmental TEM (ETEM)and in-situ Raman can identify the Pt coordination structure, surface chemical species, and the mechanisms of synergistic effects between different active sites at the molecular level[49,180]. Under RWGS reaction conditions, Pt exists in a state where Pt^0 and $Pt^{\delta+}$ coexist or undergo dynamic interconversion, and its average coordination number and local structure exhibit reversible changes with atmospheric switching[181].

In-situ XANES/EXAFS is a key technique for identifying the active structure of Pt catalysts. XANES sensitively reflects changes in the average valence state and electron density of Pt, while EXAFS quantitatively provides coordination information on Pt-O, Pt-Pt, and Pt-M bonds. This enables differentiation among single atoms, sub-nanometer clusters, nanoparticles, and interfacial sites under reaction conditions. For instance, in a single-atom system, Liang et al.[88] developed a MeCpPt/CeO_2 single-atom catalyst coordinated with methylcyclopentadienyl ligands (MeCp) through the half-reaction of atomic layer deposition (ALD). In-situ XANES and differential XANES spectra revealed a significant decrease in the intensity of the Pt-O coordination peak and the emergence of characteristic Pt-H signals under H_2 pretreatment and CO_2/H_2 reaction conditions. This indicates that the original structure, anchored as Pt^{2+}-O-Ce, was partially dissociated during the reduction process, forming MeCpPt(H) working-state species characterized by low Pt-O coordination and concomitant weak Pt-H interactions (Figure 7a-c). In interfacial systems, Xu et al.[103] employed in-situ XAFS spectroscopy to investigate the Pt-VO_x catalyst and found that electron transfer occurs from Pt to VO_x during the RWGS reaction, accompanied by the formation of low-coordination Pt structures. Additionally, VO_x generates reversible redox couples, demonstrating that the Pt-VO_x interface is directly involved in the reaction cycle.

In turn, ETEM provides unique real space evidence for the direct observation of catalyst structural reconstruction under reactive atmospheres. ETEM/operando TEM enables real-time monitoring of active species migration, particle sintering, interface encapsulation, shell collapse, and the interconversion among single atoms, clusters, and nanoparticles under controlled atmospheres and elevated temperatures. This approach reveals the structural mechanisms underlying genuine active sites or activity degradation. Yang et al.[182] employed in-situ HR-TEM/ETEM to track the crystal face-dependent structural reconstruction of TiO_2 in real time under realistic RWGS reaction conditions. At 500 °C in a pure H_2 atmosphere, the TiO_2 surface experienced oxygen loss, forming Ti_3O_5 (312) facets that hindered oxygen diffusion. Upon switching the atmosphere to CO_2, the surface was re-oxidized through oxygen incorporation, driving the structural transformation from the Ti_3O_5 lattice back to TiO_2. During this transformation, atomic displacement initially occurred on the stepped (110) facets, while atomic row merging was observed on the high-index (112) facets and the (101) facets remained relatively stable. When exposed to the RWGS reaction atmosphere, the TiO_2 surface exhibited distinct crystal face-dependent dynamic structural changes. Specifically, the (112) and (110) facets displayed pronounced merging and splitting of atomic columns, accompanied by intense surface reconstruction and oxygen exchange. Conversely, the thermodynamically stable (101) facets maintained structural integrity (Figure 7d-f). These findings directly confirm that the active sites for the RWGS reaction are concentrated on high-index and stepped crystal facets, whereas the (101) facets are intrinsically inert toward the reaction. In recent research, Bamonte et al.[183] conducted continuous monitoring of the structural evolution of a Pt-OMS-2 (α-MnO_2) catalyst under realistic reaction atmospheres via ETEM. The results demonstrated that Pt existed as isolated single atoms prior to the reaction through isomorphous substitution of Mn sites. Under reaction conditions, a 1×2 MnO_2 tunnel structure emerged at 250 °C, indicating an in-situ phase transformation of the catalyst. Upon heating to 300 °C, ETEM enabled real-time visualization of the gradual formation of Mn_3O_4 at the tips of the rod-like particles, revealing continuous structural reconstruction of the support during the catalytic process. Notably, no Pt aggregation was detected throughout the reaction upon further heating to 350 °C, suggesting that single-atom Pt maintains high structural stability within this

dynamic reaction temperature window (Figure 7g-i).

In contrast to ETEM and in-situ XANES/EXAFS, in-situ Raman spectroscopy overcomes their limitations in monitoring support framework vibrations, O_v, and surface oxygen-containing species. It is particularly effective for tracking phase transitions, the reconstruction of surface M-O species, and structural variations related to O_v and lattice oxygen within reducible oxide-supported catalytic systems under reaction conditions. Keturakis et al.[184] employed in-situ Raman spectroscopy to elucidate the bulk phase transformation and surface species reconstruction of the CrO_3/Fe_2O_3 catalyst during the RWGS reaction. The results revealed that the catalyst transformed from Fe_2O_3 to catalytically active Fe_3O_4 under varying H_2: CO_2 molar ratios. Meanwhile, surface Cr^{6+} species were irreversibly reduced to Cr^{3+} during the catalytic process. Further in-situ Raman redox cycling experiments demonstrated that the catalyst retained Fe_3O_4 as the dominant phase after reaching the RWGS steady state, with surface Cr^{3+} remaining in the reduced state (Figure 7g-k). These findings indicate that chromium acts solely as a structural promoter and does not participate in the redox cycle. Meanwhile, this technique enables the tracking of active interfacial structure evolution by monitoring M-O bond vibrations. In the $PtFe/CeO_2$ system, Xie et al.[99] employed in-situ Raman spectroscopy and observed that H_2 reduction significantly enhanced the intensity of the defect D band, indicating that high-temperature reduction effectively generates abundant surface O_v. Additionally, a peak corresponding to the Pt-O-Ce bridge bond appeared and intensified with increasing reduction temperature, confirming that the reducing atmosphere drives interfacial structural reconstruction. The in-situ formation of $Pt^{\delta+}$-O-Ce^{3+} active sites and O_v synergistic centers was identified as the key to the high low-temperature RWGS activity (Figure 8f).

To further clarify the real-time changes of reactants at the active sites, in-situ diffuse reflectance infrared Fourier transform spectroscopy (in-situ DRIFTS) enables the identification of reaction intermediates and pathways[185,186]. In various Pt-based systems, in-situ DRIFTS has clearly observed surface species such as CO*, carboxylate (COOH*), and formate (HCOO*), and their evolution with temperature, reactant partial pressure, and time provides critical information for identifying active sites and determining reaction mechanisms[187-189]. Xie et al.[99] employed in-situ DRIFTS to achieve real-time tracking of the evolution of surface-active species and the response of local structures under realistic reaction conditions at 350 °C. Characteristic vibrational peaks assigned to Ce^{4+}-OH, Ce^{3+}-OH, and Ce^{4+}-OH-like oxyhydroxide species were observed in an H_2 atmosphere. These signals intensified continuously over time, indicating that H_2 dissociated at $Pt^{\delta+}$-O-Ce^{3+} sites, and the generated *H species continuously spilled over onto the CeO_2 surface to form -OH groups. Subsequently, upon the introduction of CO_2, the formation of bicarbonate intermediates was monitored in real time, confirming that dual active sites promote the conversion of CO_2 to HCOO* species via the bicarbonate pathway (Figure 8g). In the $MeCpPt/CeO_2$ single-atom system, in-situ DRIFTS results indicated that CO_2 is primarily adsorbed on the CeO_2 surface, while CO formation depends on the MeCpPt(H) sites[88]. Further monitoring of intermediate adsorption confirmed that single-atom Pt sites serve as the main active sites in this system. Lei et al.[98] observed both a weak and narrow band corresponding to linear CO adsorption and a band assigned to bidentate CO adsorption on the Pt-aCeO_2@SiO_2 catalyst through in-situ CO-DRIFTS studies. This observation indicates that the active sites are closely associated with the high-valent Pt-O-Ce interfacial sites, which are modulated by the SMSI (Figure 7l-n).

The aforementioned diverse in-situ techniques can not only resolve the dynamic reconstruction of the Pt structure and valence state during the reaction process but also provide direct evidence for the identification of distinct active centers and interfacial structures[47]. By integrating these observations with catalytic performance data and mechanistic analysis, we can more precisely identify which sites dominate CO_2 activation and enhance RWGS activity, which sites improve CO selectivity by regulating CO adsorption and inhibiting deep hydrogenation, and which structural features contribute to stabilizing the active sites during operation and maintaining long-term performance.

Among the various working-state structures revealed by in-situ characterization, the key active sites in highly efficient RWGS catalytic systems are often not isolated metal atoms but rather composite sites located at the interfaces between metals and supports or metal-oxide promoters[190]. On reducible supports, a defining feature of Pt interfacial sites is their strong coupling with O_v and variable-valence cations. Pt atoms are frequently anchored to surface O_v, forming stable $Pt^{\delta+}$-O_v-M^{n+} structures. On one hand, O_v donates electrons to Pt, inducing a partial positive charge or charge redistribution on Pt, thereby modulating its adsorption strength toward reaction intermediates such as CO, H, and OH. On the other hand, the M^{n+}-O_v network itself acts as a crucial redox site for CO_2 adsorption and activation. Additionally, O_v exerts a strong anchoring effect on interfacial sites. Consequently, these structures synergistically enhance both RWGS activity and CO selectivity by regulating the balance between CO_2 activation capacity and CO adsorption strength, while providing a favorable foundation for maintaining the active state of interfacial sites. Combining steady-state kinetics with in-situ infrared spectroscopy, Bi et al.[87] demonstrated that CO_2 is more readily activated at the WO_x/Pt interface. The intensity ratio of linearly bonded to bridge-bonded CO adsorbed on the catalyst, formed from CO_2 hydrogenation, was significantly reduced, while the intensity of the gas-phase CO peak was approximately 1.3 times higher than that observed for Pt/SiO_2. These findings indicate that the interfacial peripheral sites formed by WO_x overlayers not only enhance the adsorption and activation of CO_2 but also weaken CO adsorption on Pt (Figure 8a-b). This clearly demonstrates that the truly efficient active centers in RWGS are often located at interfacial peripheral regions rather than isolated metal sites. Similarly, using in-situ infrared spectroscopy, Lei et al.[98] further showed that CO_2 preferentially adsorbs on defective CeO_2 surfaces as CO_3^{2-} species, H_2 dissociates at single-atom Pt sites, and subsequent conversion to CO and H_2O occurs at the Pt-O-Ce interfacial sites, with products rapidly desorbing from the Pt

sites (Figure 8c). This phenomenon is attributed to the predominance of $Pt^{\delta+}$ species in the high-valence Pt-O-Ce single-atom interfacial structure, which weakens CO adsorption at the Pt sites. Simultaneously, the strong anchoring effect of O_v on the single-atom Pt maintains the stability of the interfacial structure, enabling the catalyst to operate stably for up to 16 hours. It is worth noting that

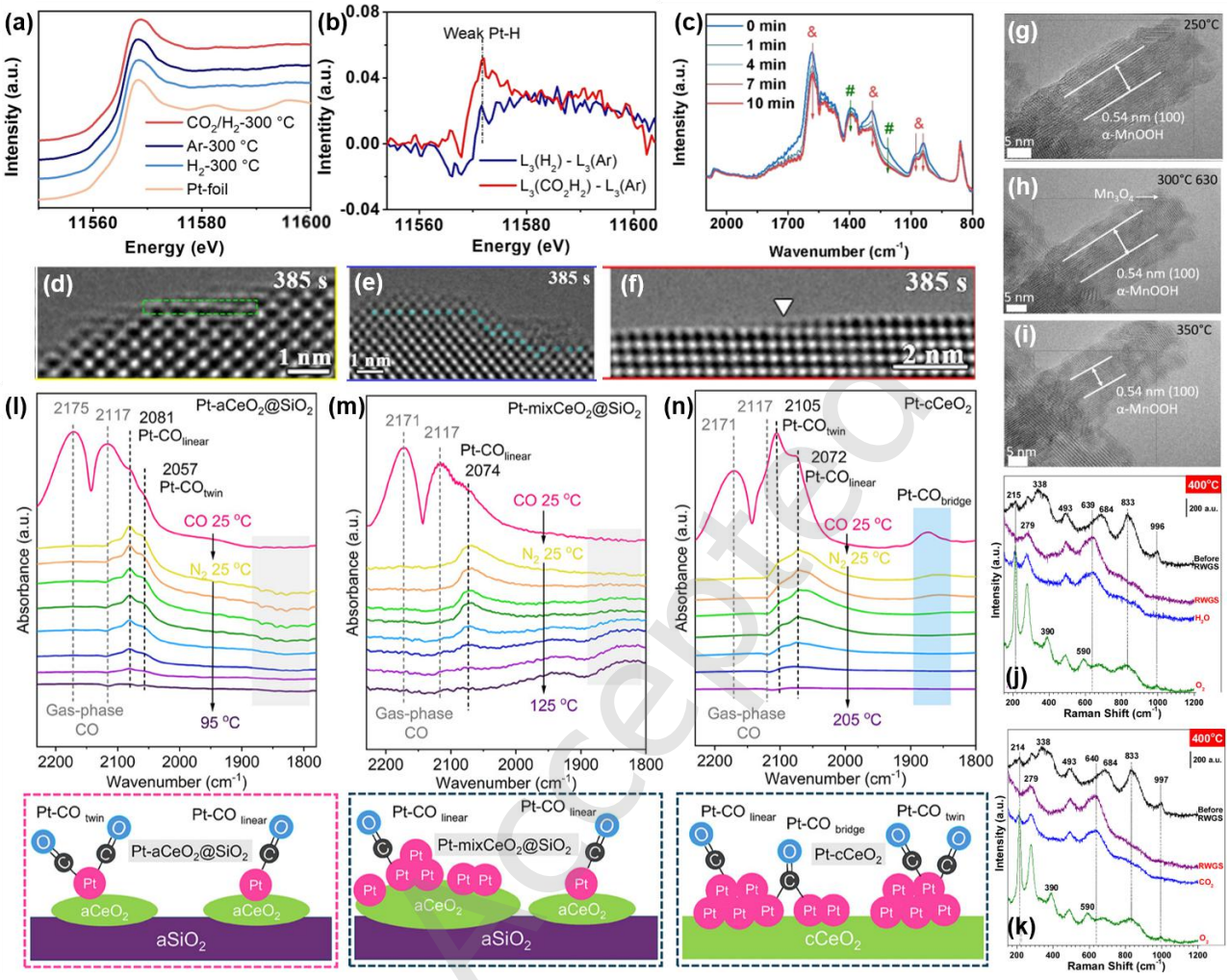

Figure 7. (a) In-situ XANES spectra of MeCpPt/CeO_2 after sequentially introducing H_2/Ar ($L_3(H_2)$), Ar (L_3(Ar)) and CO_2/H_2/Ar ($L_3(CO_2H_2)$) at 300 °C. (b) Difference spectra of $L_3(H_2)-L_3$(Ar) and $L_3(CO_2H_2)$-L_3(Ar) to reveal the Pt-H contribution. (c) In-situ DRIFTS spectra of MeCpPt/CeO_2 at 300 °C after CO_2/H_2 absorption Reprinted with permission from [88]. Copyright 2024, Wiley-VCH GmbH. In-situ HRTEM visualization of RWGS reaction dynamics on TiO2 surfaces under CO_2/H_2 gas flow, capturing RWGS reaction dynamics on (d) the (112) facet, (e) the stepped (110) facet, (f) and the (101) facet. Reprinted with permission from [182]. Copyright 2025, American Chemical Society. E-TEM image of Pt-OMS-2 under reaction conditions at (g) 250 °C, (h) 300 °C, (i) 350 °C. Reprinted with permission from [183]. Copyright 2026, Elsevier B.V. In-situ Raman spectroscopy before, during, and after the RWGS reaction with a supported 9% CrO_3/Fe_2O_3 catalyst: (A) 2.5% H_2O/Ar oxidizing treatment after the RWGS reaction; (B) 33% CO_2/Ar oxidizing treatment after the RWGS reaction. Reprinted with permission from [184]. Copyright 2016, American Chemical Society. In-situ FTIR of CO desorption and corresponding coordination structure models on (l) Pt-aCeO_2@SiO_2, (m) Pt-mixCeO_2@SiO_2, and (n) Pt-cCeO_2. Reprinted with permission from [98]. Copyright 2025, Wiley-VCH GmbH.

although interfacial sites can simultaneously provide electronic coupling and defect participation, optimizing both CO_2 activation and H_2 dissociation simultaneously at a single site remains challenging in some systems.

Compared to single active sites, dual active sites facilitate a synergistic division of labor for CO_2 adsorption and activation, as well as H_2 dissociation, both in terms of spatial distribution and functional properties. This synergy enhances the reaction rate and CO selectivity[191-195]. Meanwhile, such site-partitioning behavior helps prevent the excessive accumulation of reactants and intermediates on individual metal sites, mitigates the tendency toward deep hydrogenation, and to some extent reduces the risk of deactivation caused by locally high coverage, thereby promoting long-term stable operation. Li et al.[92] developed a Pt cluster/PN-CeO_2 catalyst by introducing frustrated Lewis pairs (FLPs) onto a CeO_2 support. In-situ DRIFTS analysis of the dynamic evolution of surface species during the reaction revealed that, under the RWGS reaction atmosphere, the characteristic peak of Ce^{3+}-OH gradually diminished, while the Ce^{4+}-OH peak emerged. This observation confirmed that CO_2 is preferentially activated at FLP sites induced by defects on the CeO_2 surface. Conversely, under an H_2 atmosphere, combined results from in-situ DRIFTS, H_2-TPR, and XPS analyses demonstrated that Pt clusters exhibit excellent hydrogen molecule dissociation

ability and serve as the primary sites for H_2 activation. Therefore, the dual active sites of Pt clusters and FLPs (Ce^{3+}-O-Ce^{3+}) achieve a synergistic division of labor in the adsorption and activation of CO_2 and H_2. This synergy not only eliminates competitive adsorption but also prevents Pt deactivation caused by excessive CO coverage on Pt sites, which is crucial for attaining high activity at low temperatures (Figure 8d-e). By combining in-situ isotope-labeled FTIR (H_2/D_2) and -OD evolution experiments, Xie et al.[99] was found that CO_2 is adsorbed and activated at O_v sites on the support in the Pt_{FEc}/CeO_2 system,, and the resulting CO_2 intermediates are further converted by the -OH species on the support surface (Figure 8h-i). The dual active sites of $Pt^{\delta+}$-O-Ce^{3+} and O_v collectively enable near-equilibrium CO_2 conversion at 350 °C and stable operation for 550 hours.

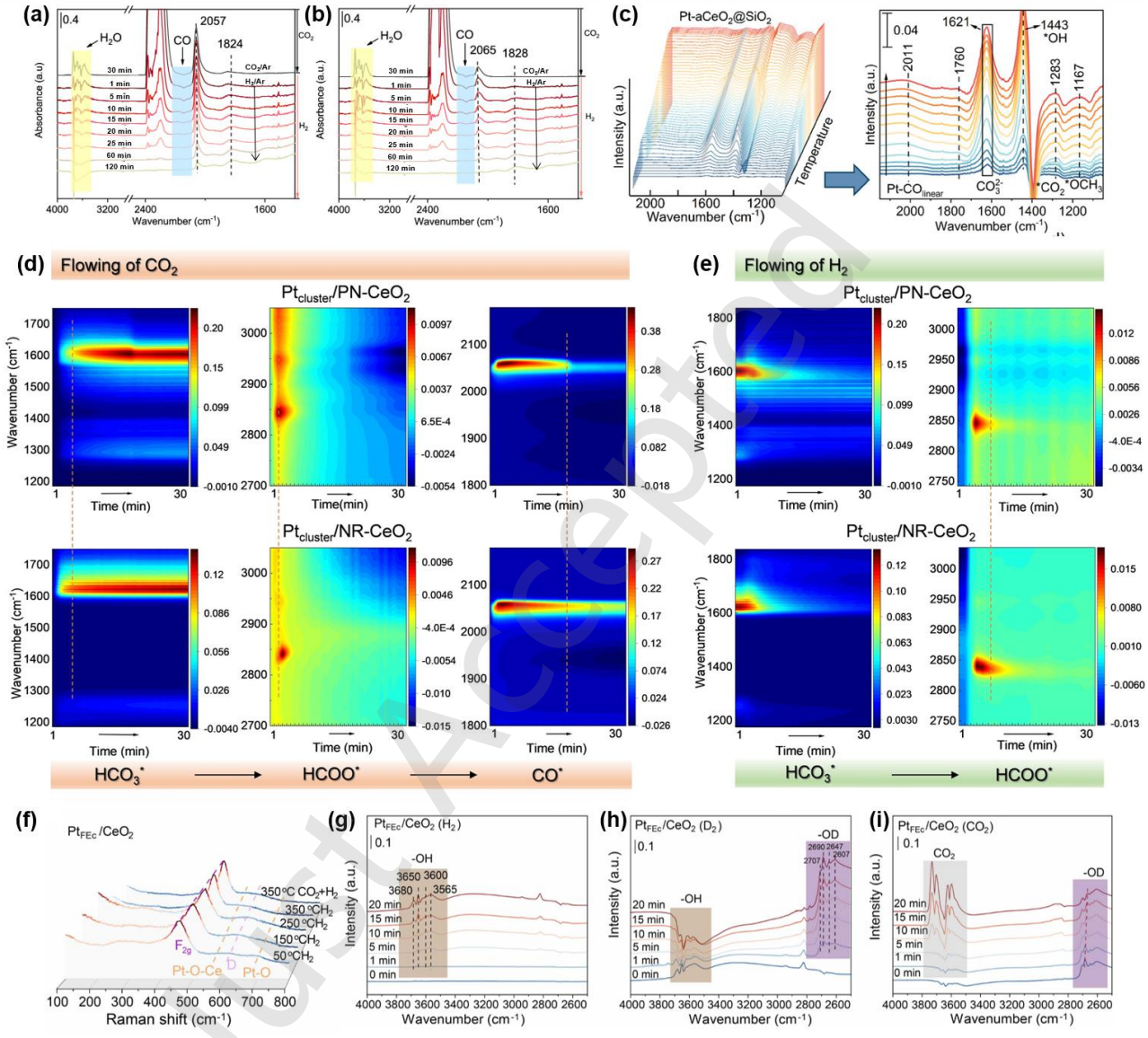

Figure 8. In-situ FTIR spectra of CO_2 hydrogenation on (a) Pt/SiO_2 and (b) Pt0.5W at 400 °C. Reprinted with permission from [87]. Copyright 2024, American Chemical Society. (c) In-situ FTIR of Pt-aCeO_2@SiO_2 collected at different temperatures under reaction gas flow. In-situ DRIFTS spectra of $Pt_{cluster}/PN\text{-}CeO_2$ and $Pt_{cluster}/NRCeO_2$ under flowing (d) CO_2 and (e) H_2. Reprinted with permission from [92]. Copyright 2023, Wiley-VCH GmbH. (f) In-situ Raman spectra of Pt_{FEc}/CeO_2. In-situ DRIFT spectra of (g) the -OH groups evolution during H_2 adsorption, (h) H_2 and D_2 isotope labeling experiments, and (i) the -OD groups evolution during CO_2 adsorption on the Pt_{FEc}/CeO_2 catalyst. Reprinted with permission from [99]. Copyright 2025, Elsevier B.V.

Another significant contribution of in-situ characterization is its ability to distinguish multiple parallel reaction pathways and clarify their corresponding structural origins. By tailoring the interfacial composition or introducing bimetallic components, and combining in-situ DRIFTS with kinetic measurements, researchers have found that the RWGS reaction often proceeds simultaneously via different pathways. As illustrated in Figure 1b, the distinct reaction pathways of Pt-based catalysts in the RWGS reaction depend on the synergistic regulation of oxygen, hydrogen, and oxygen-containing intermediates at the interface. When the Pt-oxide interface or alloy sites contain reversible redox components, CO_2 activation is more likely to proceed via the generation, migration, and elimination of surface oxygen species, favoring the redox pathway. In contrast, the *COOH associative pathway is more readily favored at Pt-support interfaces, O_v-adjacent sites, or bifunctional sites with efficient H_2 dissociation and hydrogen spillover capabilities.

This is because Pt efficiently dissociates and activates H_2, while defect sites or interfacial O sites can adsorb and polarize CO_2, converting it from a stable linear molecule to a more reactive bent adsorbed state. When H spills over to the interface, it combines with the activated CO_2 molecules, facilitating the formation of $*CO_2 + H \rightarrow *HOCO$ (Figure 1b). Additionally, when the interface structure promotes the formation and accumulation of bidentate formate species, sites on the interface or support surface that can stably anchor the O-C-O skeleton in a bidentate configuration enable hydrogen to preferentially add to the oxygen-related configuration of CO_2, resulting in the formation of relatively more stable formate species.

These different pathways correspond to varying stabilities of key intermediates and rate-determining steps, which in turn influence the activity and CO selectivity of the RWGS reaction[196]. Liang et al.[93] confirmed through in-situ CO-DRIFTS that only *CO adsorption peaks were detected on the Pt/mullite catalyst, indicating that the reaction follows a redox pathway. Upon K doping, formate intermediates form at the Pt-KO_x interface, which opens a new formate pathway and simultaneously weakens CO adsorption (Figure 9a-c). Chen et al.[130] tracked the dynamic evolution of surface intermediates during the RWGS process by means of in-situ DRIFTS to elucidate the pathway differences of distinct interfacial sites. For the Pt/Al_2O_3 system, various surface carbon-containing species were clearly observed via in-situ DRIFTS. Upon cutting off the CO_2 supply, the signals of weakly adsorbed bicarbonates and carbonates disappeared rapidly. Under an H_2 atmosphere, monodentate formate decayed much faster than bridged ones, indicating that the Pt-Al_2O_3 interfacial sites mainly follow the formate pathway. In contrast, when in-situ DRIFTS measurements were performed under the same conditions on a physically mixed system of Pt/Al_2O_3 and anatase TiO_2, *CO accumulated over time, while all formate-related peaks disappeared completely, and a broad peak attributable to TiO_2-bound acetate species emerged (Figure 9d-f). This demonstrated that acetate migration covered the formate formation sites at the Pt-Al_2O_3 interface, switching the reaction pathway to the more favorable carboxyl route. This confirms that the carboxyl pathway primarily occurs at the metal-support interface, whereas the formate pathway is highly dependent on the proximal synergy between these interfacial sites and Pt.

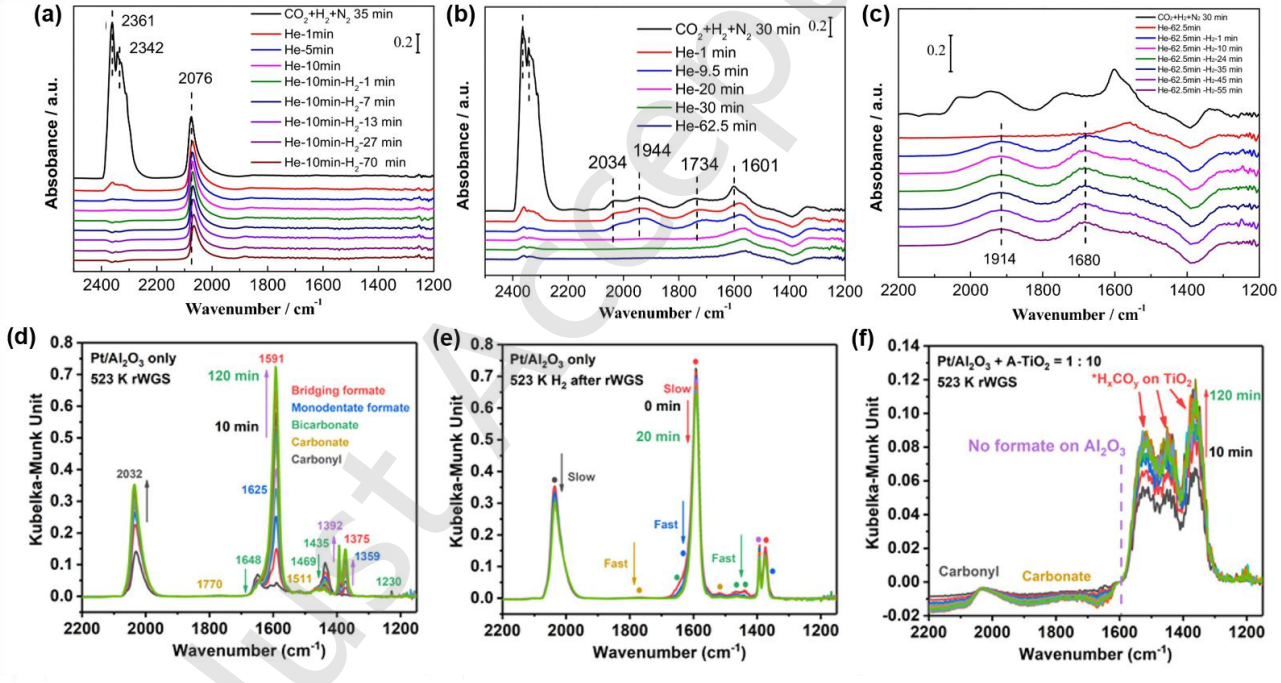

Figure 9. DRIFT spectra collected at 300 °C when the gas was switched from feed gas to He, followed by switching the gas flow to H_2 over (a) reduced Pt/mullite and (b-c) reduced K-Pt/mullite. Reprinted with permission from [93]. Copyright 2016, Elsevier B.V. In-situ DRIFT spectra of the Pt/Al_2O_3 single sample: (d) during 2 h of the RWGS reaction, (e) under a H_2 atmosphere at 250 °C. (f) The Pt/Al_2O_3: A-TiO_2 = 1:10 mixed sample exhibits the same spectra as those in (d). Reprinted with permission from [130]. Copyright 2021, American Chemical Society.

Building on this foundation, the reconstruction of active site functionality through the introduction of a second metal has added a new dimension to the tunability of reaction pathways. Its role is not only to construct additional synergistic sites but also to reshape CO_2 activation and the conversion modes of surface intermediates by altering the local electronic structure, interfacial composition, and redox properties around Pt, thereby triggering the switching of reaction pathways or the parallel coupling of different pathways. Using in-situ DRIFTS, Hansen et al.[102] observed only weak formate signals at single Pt metal sites under an H_2 atmosphere, indicating that CO_2 activation primarily depends on the hydrogen-mediated formate pathway. In contrast, for the bimetallic PtFe@SiO_2 catalyst, in-situ DRIFTS and in-situ XAS spectra revealed that Fe sites undergo a reversible redox dynamic between Fe^0 and Fe^{n+} under reaction conditions, enabling the direct formation of CO from CO_2 even in the absence of H_2. On the other hand, Pt is mainly responsible for the efficient dissociation of H_2. This series of in-situ observations directly demonstrates that Fe, acting as a promoter, triggers a switch in the reaction pathway from the hydrogen-mediated mechanism to the

redox mechanism by altering the functional division of labor among active sites surrounding Pt (Figure 10a-b). Additionally, the dynamic alloying cycle of FeO_x-PtFe inhibits particle agglomeration and maintains the structure of active sites, thereby enabling both high activity and excellent stability under low-temperature conditions. In the PtCr-Cr_{int}@SiO_2 catalyst system, Zhou et al.[94] confirmed the stable existence of PtCr alloys using in-situ XAS. Combined with in-situ DRIFTS to probe the response of Pt sites to CO_2, it was found that Pt@SiO_2 and SiO_2 exhibited almost no CO_2 adsorption, whereas CO adsorption peaks appeared on PtCr@SiO_2. This indicates that the Pt-Cr alloy sites possess the ability to directly activate and dissociate CO_2, following an alloy-site-dominated redox pathway. In contrast, significantly enhanced CO_2 adsorption signals and characteristic peaks of formate intermediates were observed at the Pt-Cr(III) interfacial sites, demonstrating that these interfacial sites initiate an additional formate-mediated pathway with synergistic hydrogen supply from Pt (Figure 10c-f). These two types of sites operate in parallel, enhancing CO_2 activation efficiency while maintaining structural stability after 50 hours of continuous operation.

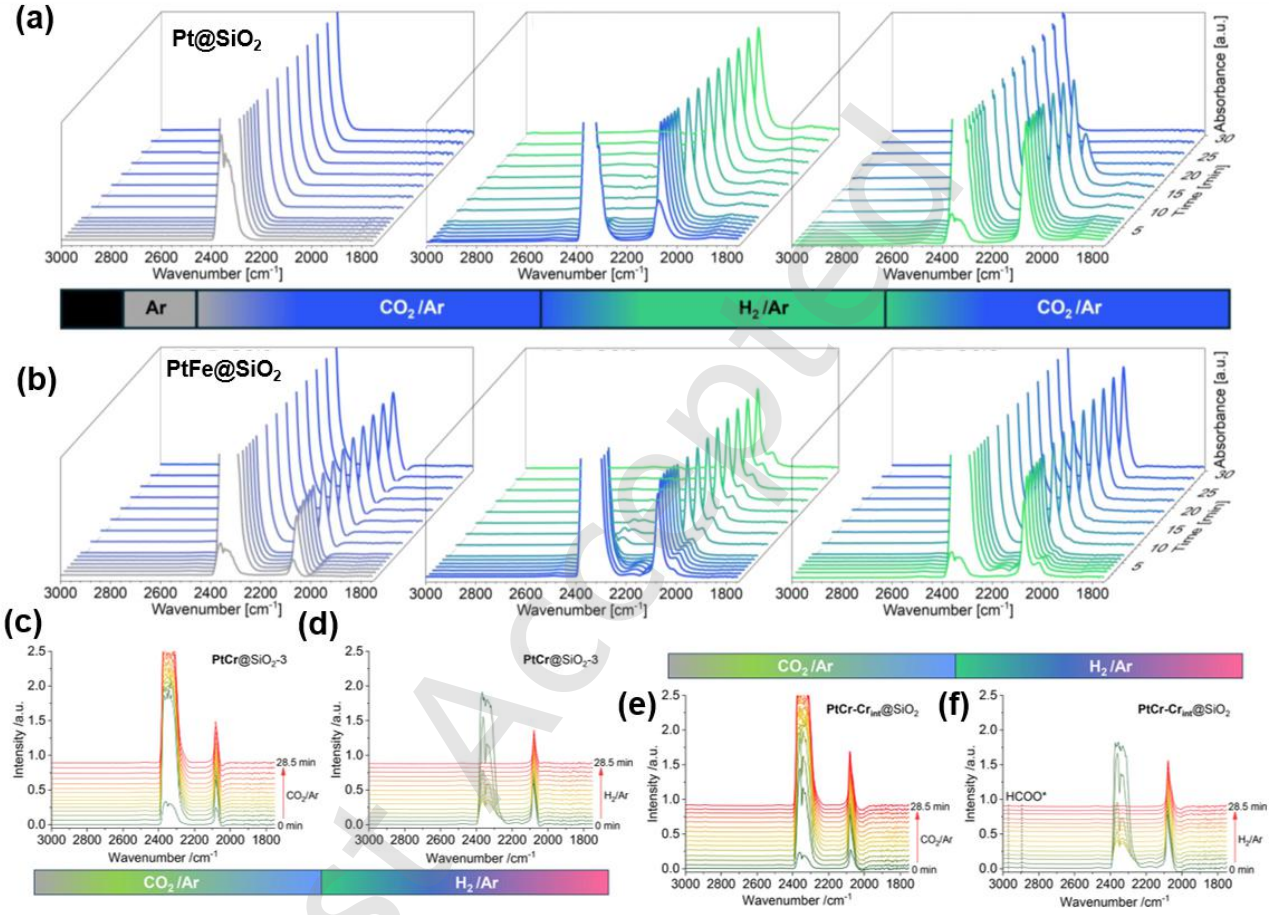

Figure 10. In-situ DRIFTS for (a) Pt@SiO_2 and (b) PtFe@SiO_2 under CO_2/Ar, H_2/Ar, and CO_2/Ar. Reprinted with permission from [102]. Copyright 2024, American Chemical Society. In-situ gas-switching DRIFTS for PtCr@SiO_2-3 under (c) CO_2/Ar and (d) H_2/Ar, and in-situ gas-switching DRIFTS for PtCr-Cr_{int}@SiO_2 under (e) CO_2/Ar and (f) H_2/Ar. Reprinted with permission from [94]. Copyright 2025, American Chemical Society.

In recent years, in-situ and operando characterization techniques have made significant progress in elucidating MSI, single-atom catalysts, interfacial catalysis, and energy conversion processes. However, their capabilities remain limited in resolving the origins of electronic structures, variations in energy barriers, and detailed analyses of synergistic effects. Therefore, it is essential to combine these techniques with DFT calculations to perform quantitative analyses of the structures of distinct active sites and reaction pathways, with the goal of deepening the understanding of Pt-based RWGS reaction mechanisms at the atomic scale.

3.2 Theoretical studies

Compared to experimental approaches, theoretical calculations can elucidate the energy changes and structural evolution of each elementary reaction step at the atomic and electronic scales. This capability provides a quantitative basis for understanding why different active sites exhibit varying activity and CO selectivity[197]. Therefore, theoretical studies are used not only to determine the reaction pathways and rate-determining steps (RDS)[198] but, more importantly, to explain how the structure of the Pt active site directly correlates with macroscopic performance by regulating the initial CO_2 activation capacity, the stability of key intermediates, and the ease of CO desorption.

A central focus of theoretical calculations is the intrinsic differences in reaction pathways across distinct active sites[199]. Pt active sites primarily manifest as ideal crystal facets, step or defect sites, and Pt-support interfacial structures[200,201]. Theoretical studies typically involve constructing structural models with varying configurations to systematically compare CO_2 adsorption, the stability of

key intermediates, and the associated reaction energy barriers. For isolated Pt(111) sites, low-coordination active sites, such as edge-bridge sites on Pt NPs favor intermediate adsorption but exhibit excessively weak bonding to CO_2. This weak interaction causes CO_2 to desorb before hydrogenation to form *COOH or *HCOO intermediates, making it difficult for Pt NPs alone to catalyze the conversion of CO_2 to CO[84]. Therefore, stable CO_2 adsorption has become a prerequisite for enhancing overall conversion efficiency. Extensive theoretical studies have demonstrated that the CO_2 activation ability is primarily determined by the coordination environment of metal active centers, with metal-support interfacial sites serving as the core factor regulating the coordination environment and electronic structure. In the atomically dispersed state of Pt, the low coordination number and partial positive charge of Pt can enhance the linear adsorption and polarization of CO_2, facilitate the formation of intermediates, and reduce the initial activation energy. In the Pt_1/TiO_2 system, Chen et al.[153] observed that Pt_1/TiO_2 with highly oxygen-coordinated Pt exhibited almost no Pt-CO adsorption peaks, whereas its catalytic performance increased several-fold after reduction. Combined with theoretical calculations, it was found that under a reducing atmosphere, the local coordination of Pt atoms transformed from a fully oxidized state to a partially reduced state, forming accessible $Pt^{\delta+}$ and Pt^0 species located near the surface region. At this point, the coupling between the d-orbitals of Pt and the antibonding orbitals of CO_2 was enhanced, significantly reducing the initial activation energy barrier of the $*CO_2 \rightarrow *COOH$ step.

Modulated by the metal-support interfacial structure, the unique geometric and electronic characteristics of interfacial sites significantly influence the adsorption and activation behaviors of reactant molecules[202]. Xie et al.[99] constructed geometric models of Pt clusters on the CeO_2 surface and near O_v defects. Energy analysis revealed that the O_v sites provided by CeO_2 can substantially modulate the electron density of the metal, rendering Pt partially positively charged and forming a stable Pt-O-Ce bridge structure at the interface. Energy profile calculations demonstrated that the heterolytic cleavage of H_2 at the $Pt^{\delta+}$-O-Ce^{3+} sites exhibits the lowest energy barrier, whereas a higher potential energy is required on the surface of pure Pt clusters. In contrast, CO_2 molecules adsorb in a bent configuration at the O_v sites, forming formate intermediates (Figure 11a-b). The Ma Ding group constructed a Pt_4-MoO_x model via DFT calculations[97]. At the interface between Pt clusters and O_v, CO_2 forms a stable adsorption configuration in which the carbon atom coordinates with Pt and the oxygen atom coordinates with O_v-rich Mo^{n+} sites. This configuration significantly enhances the polarization and bending of the CO_2 molecule, thereby reducing the energy barrier of subsequent reaction steps. In contrast, CO_2 adsorption is weak on MoO_x without Pt or on the Pt_4-MoO_3 surface without O_v (Figure 11c-e). These results indicate that simply increasing Pt exposure is insufficient to ensure high RWGS activity. The crucial factor is enhancing the initial CO_2 activation capacity via low-coordination structures or interface-induced electronic regulation.

In addition, the binding strength of *CO determines CO selectivity[203-205]. In Pt-based RWGS catalytic systems, the type and distribution of active sites directly govern the intermediate configurations formed during the CO_2 hydrogenation process, thereby influencing CO selectivity. The COOH pathway exhibits a lower energy barrier for C-O bond scission and is both thermodynamically and kinetically more favorable than the pathway leading to HCOO formation. At the Pt/oxide interface, oxide sites provide additional acid-base functionality and electronic modulation effects, which significantly stabilize the COOH intermediate and reduce the energy barrier for C-O bond scission. These interfacial sites interact with oxygen defects on the support, enabling the stabilization of bent CO_2 adsorption configurations and facilitating their combination with active hydrogen to form *COOH. This configuration features a low energy barrier for C-O bond cleavage, favoring the rapid formation and desorption of CO. For instance, at the Ti_3O_6/PtCo interface, the calculated energy barriers for COOH formation and dissociation are both lower than those on pure Pt, allowing the RWGS pathway to proceed at lower temperatures while maintaining high CO selectivity[167].

Having established the decisive role of CO binding energy and intermediate configurations in CO selectivity, it is essential to further investigate the electronic and structural modulation effects exerted by support properties in this process. Using Pt/TiO_2 and Pt/SiO_2 as examples, Kinetic Monte Carlo (KMC) simulations, by integrating surface reaction energy barriers and adsorption kinetic parameters, revealed that at the Pt/TiO_2 interface, the significant synergy between Pt edge and corner sites and O_v markedly reduces the activation energy of the $*CO_2 \rightarrow *COOH$ step in the carboxyl pathway, facilitates H_2 dissociation and hydrogen atom migration, and promotes *CO desorption (Figure 11f-g). In contrast, on Pt/SiO_2, the absence of metal-support electronic coupling results in difficult CO_2 activation and a higher propensity for C-O bond scission, leading to the preferential formation of CH_4[84]. A similar phenomenon has also been observed in Pt-Co model systems. DFT potential energy surface calculations indicate that on Ti_3O_6/PtCo(111), $*CO_2$ adsorbs stably in a bent configuration at the Pt-Ti interface and is hydrogenated to the COOH intermediate. The free energy required for CO desorption at 300 °C is significantly lower than that for the CO hydrogenation step. In contrast, on Zr_3O_6/PtCo(111), although the *COOH pathway is retained, the enhanced interfacial O-Zr^{4+} interaction leads to a marked increase in the binding energies of C, O-bidentate and O-monodentate intermediates (Figure 11h-i). Consequently, the CO binding energy rises to -2.00 eV, resulting in hindered CO desorption[167]. These two studies collectively demonstrate that CO formation and desorption depend not only on the nature of metal active sites but are also significantly modulated by the electronic structure of the support and interfacial synergistic effects. Supports with strong electron-donating capacity or the ability to form O_v facilitate the stabilization of COOH intermediates and promote CO desorption, thereby enhancing the selectivity of the RWGS reaction.

The identification of reaction pathways and key RDS constitutes a crucial theme in theoretical studies. In heterogeneous catalytic reactions, the overall reaction rate

and final selectivity are governed by the slowest elementary step. The redox pathway regulates the reaction rate through two primary steps: the re-oxidation step, in which surface O/OH species are hydrogenated to form H_2O, and the C-O bond cleavage step in CO_2. These steps are closely associated with different types of Pt active sites. At Pt–support interfacial sites, O and OH species bind strongly at the interface, resulting in high-coverage blocking adsorbates. Further hydrogenation of strongly adsorbed OH to weakly adsorbed H_2O requires breaking the Pt-O/M-O bonds and forming an H-O-H molecule (Figure 1b), which leads to a higher activation energy. Feng et al. employed first-principles potential energy surface calculations and found that the direct CO_2 dissociation pathway on a Pt-O_v-Ti interfacial model has the lowest energy barrier[206]. Microkinetic simulations revealed that CO_2 activation and CO formation are relatively accelerated at the Pt-O_v-Ti interface, whereas the elementary step involving the recombination of highly covered H and OH to form H_2O exhibits the greatest kinetic resistance and thus controls the overall reaction rate.

Association mechanism typically involves either the adsorption and activation of CO_2 at the Pt/support interface to form COOH intermediates or the cleavage of COOH to generate CO and OH species. Consequently, the rate of this step is directly determined by the ability of reaction intermediates or transition states to adsorb onto and transform at active sites[207].

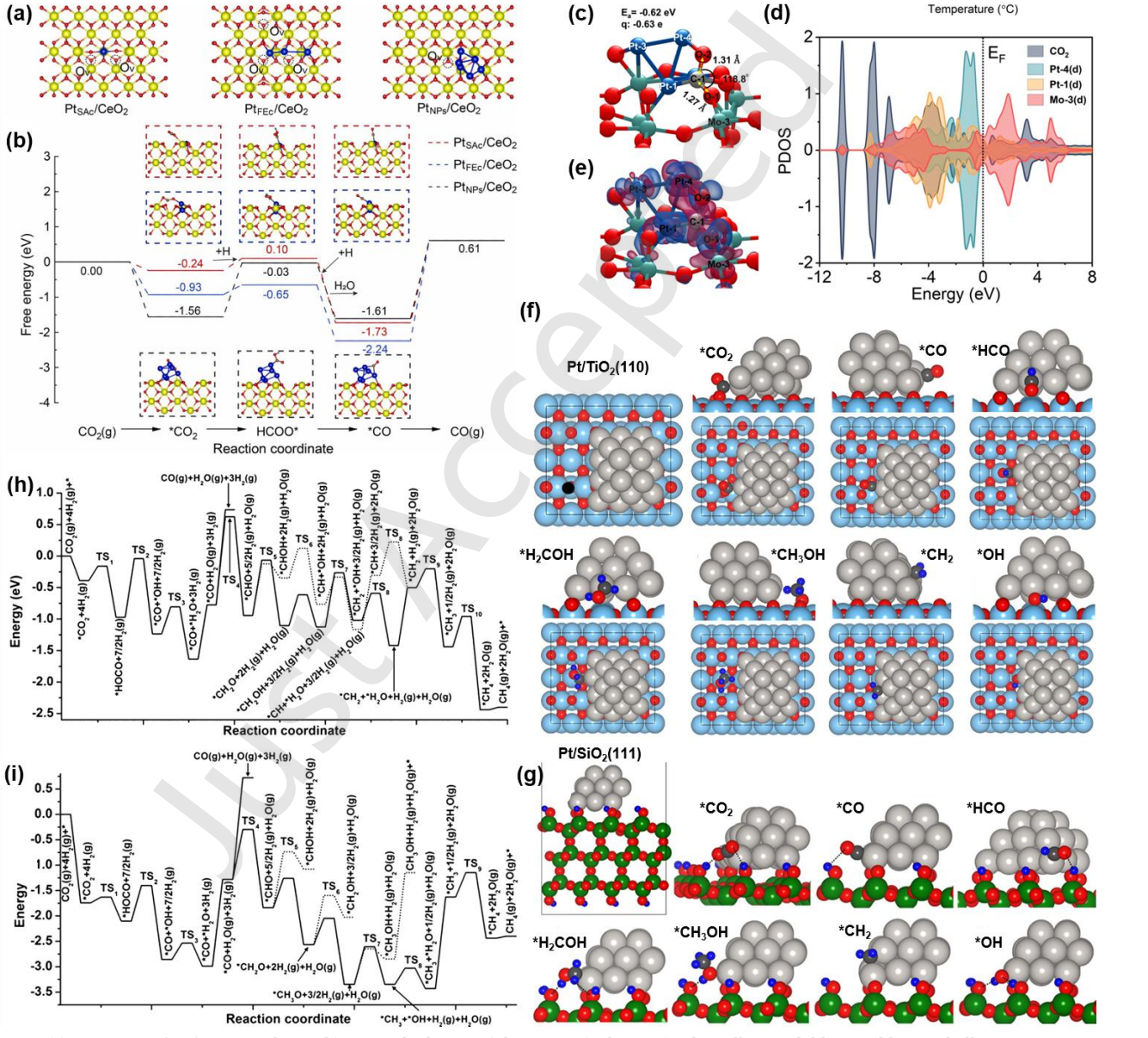

Figure 11. (a) Top view of Pt/CeO_2 catalysts. (b) DFT calculation of the RWGS (Side view). The yellow, red, blue, and brown balls represent Ce, O, Pt, and C atoms, respectively. Reprinted with permission from [99]. Copyright 2025, Elsevier B.V. (c) Adsorption structure of CO_2 on the Pt_4-MoO_x surface model (denoted as CO_2/Pt_4-MoO_x-I). (d) Projected electronic density of states (PDOS) of the CO_2 adsorbate. (e) Electron transfer between adsorbed CO_2 and Pt_4-MoO_x surface according to the differential charge density analysis. The blue and red colors represent the electron accumulation and depletion, respectively. Reprinted with permission from [97]. Copyright 2022, Springer Nature. DFT optimized geometries of (f) Pt/TiO_2(110) and (g) Pt/SiO_2(111) catalyst models with O_v, and side (top) and top (bottom) views. Ti: Light blue, Si: green, Pt: light gray, C: dark gray, O: red, and H: blue. Reprinted with permission from [84]. Copyright 2016, Elsevier Inc. Potential energy diagrams for the synthesis of CO and CH_4 through the RWGS and CO hydrogenation pathway on model hydroxylated (h) Ti_3O_6/PtCo(111) and (i) Zr_3O_6/PtCo(111) surfaces. Reprinted with permission from [167]. Copyright 2016, WILEY-VCH Verlag GmbH & Co.

In contrast, metallic Pt step and terrace sites lack lattice oxygen that can participate in the redox cycle. All O species exist as adsorbed O* or OH*. Cleavage of the CO-O bond in CO_2 on metallic Pt requires simultaneous rearrangement of the bonding between C, O and the metal surface, which significantly increases the transition-state energy and renders this step rate-determining in the microkinetic analysis. Qi et al. combined DFT with microkinetic modeling[208]. On Pt(111), they indicate that metallic Pt sites exhibit strong C-binding ability and moderate O-binding ability. A subsequent degree-of-rate-control analysis quantified the sensitivity of all intermediates and transition states, showing that the transition state for CO-O bond cleavage in the $CO_2 \rightarrow CO + O^*$ step has the highest degree of rate control, whereas the contributions of other species are negligible. Thus, the metallic Pt(111) sites responsible for CO-O bond cleavage are identified as the key active sites for the high-temperature RWGS reaction.

At contiguous metallic sites with high H_2 activation capability but weak CO_2 adsorption, the CO_2 transition state intermediate cannot be effectively stabilized, making the energy barrier for the $*CO_2 \rightarrow *COOH$ step the kinetic bottleneck of the RWGS reaction[209,210]. Li et al. constructed a bifunctional interface model incorporating Pt clusters and FLP sites, and systematically analyzed the reaction pathways and variations in key energy barriers using DFT calculations[92]. The results revealed that the RWGS process follows a typical *COOH intermediate pathway in this dual-active-site system. Pt clusters primarily facilitate the heterolytic cleavage of H_2 molecules to form adsorbed hydrogen (H*). One of the H* atoms migrates to the FLP sites via spillover and reacts with CO_2 adsorbed on the FLP sites to generate the *COOH intermediate. Subsequent hydrogenation promotes the decomposition of *COOH into *CO and surface hydroxyl groups (OH*), followed by the smooth desorption of CO. The free energy profile demonstrated that the pathway $*CO_2 \rightarrow *COOH \rightarrow *CO + *OH$ is the most favorable on the Pt cluster/PN-CeO_2 surface. Further analysis of key energy barriers confirmed that the initial activation of CO_2 exhibits the largest free energy change and thus serves as the RDS of the overall reaction (Figure 12a). In the sub-nanometric Pt_{FEc}/CeO_2 cluster model, the RWGS process was similarly found to follow a typical *COOH intermediate pathway. Pt cluster sites enable efficient H-H bond cleavage and hydrogen supply, while O_v and Ce^{3+} sites facilitate CO_2 polarization and the formation of carboxyl intermediates. The energy barriers for CO_2 adsorption and activation steps are significantly higher than those for subsequent hydrogenation or CO desorption steps, thus serving as the RDS of the reaction[99].

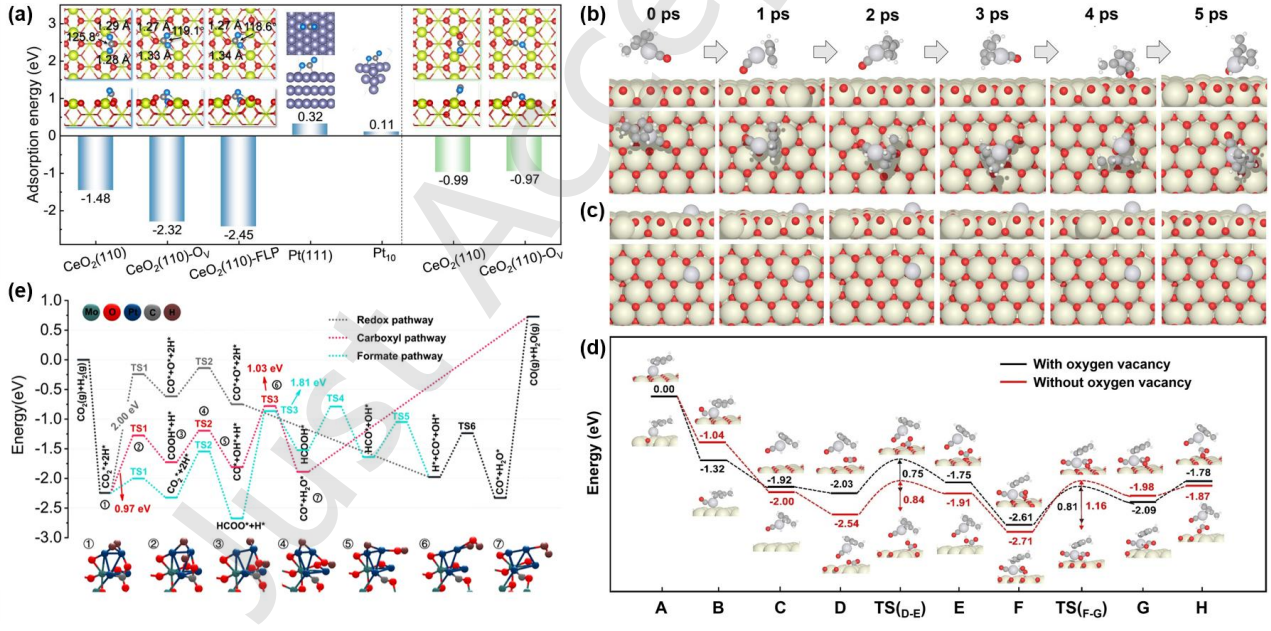

Figure 12. (a) The adsorption behaviors of CO_2 and CO on the CeO_2(110) surface with various active sites. The red and yellow balls represent the O and Ce atoms of CeO_2, respectively. Reprinted with permission from [92]. Copyright 2023, Wiley-VCH GmbH. (b) The dynamic mobilization of the MeCpPt(H)CO complex on the CeO_2 surface at 300 °C from AIMD simulation. (c) The dynamic state of a single Pt atom fixed on the CeO_2 surface at 300 °C from the AIMD simulation. (d) DFT-calculated energy profile (eV) for the RWGS reaction through operando mobile catalysis (Ce: ivory, O: red, H: white, C: gray, Pt: light gray). Reprinted with permission from [88]. Copyright 2024, Wiley-VCH GmbH. (e) Energy profiles of the three reaction routes (redox, carboxyl, and formate) on Pt_4-MoO_x, depicted in gray, red, and cyan, respectively. Reprinted with permission from [97]. Copyright 2022, Springer Nature.

At Pt sites exhibiting strong interfacial interactions with support defects or metal oxides, the electronic structure of single-atom Pt sites is modulated by support O_v or support metal ions[211]. This modulation significantly enhances the capacity for bent CO_2 adsorption and polarization, lowers the energy barrier for the initial hydrogenation step forming *COOH[212], and consequently shifts the RDS to the cleavage of *COOH into CO and *OH[213,214]. In the MeCpPt/CeO_2 system, ab initio molecular dynamics (AIMD) simulations revealed that compared to stationary Pt atoms, the MeCpPt(H)CO complex can migrate rapidly on the CeO_2 surface. This high mobility substantially increases the spatial

contact probability between Pt active centers and carbonate intermediates on the CeO_2 surface, facilitating the rapid hydrogenation and conversion of surface carbonates into *COOH. Subsequently, *COOH cleaves into *CO and *OH at the Pt-O_v synergistic sites (Figure 12b-d). At the Pt-O_v interface, the energy barrier for the *COOH → CO + *OH step is higher than those for the *CO_2 → *COOH step and the subsequent *OH hydrogenation step, thus identifying it as the key RDS[88]. In the Pt-MoO_x/γ-Mo_2N system, a comparison of the free energy profiles revealed that the highest energy barrier of the carboxyl pathway is significantly lower than those of the redox and formate pathways, confirming that the reaction proceeds via a carboxyl-mediated associative mechanism (Figure 12e). Combined with experimental results, it is inferred that the *COOH → *CO + *OH step in this pathway serves as the key RDS[97].

Integrating in-situ characterization with theoretical calculations, the efficient catalysis of the RWGS reaction stems from the synergistic effects of specific Pt-support interfaces or bifunctional active sites. In-situ techniques have revealed the spatial and functional division of labor of these sites in CO_2 activation and H_2 dissociation, while theoretical calculations have quantified the reaction energy barriers and identified the location of the key RDS.

Thus, the structural design of Pt-based catalysts not only alters the dispersion and valence state of Pt but also governs the CO_2 activation capacity, the ease of *COOH/*HCOO intermediate conversion, and CO desorption behavior by modulating the local coordination environment, interfacial electronic coupling, and defect neighborhoods[215]. These factors collectively influence the activity and CO selectivity of the RWGS reaction. In systems exhibiting strong anchoring effects or stable interfacial configurations, these characteristics further contribute to maintaining the working-state structure and ensuring long-term operational stability.

4 Conclusion and outlook

In recent years, due to the high cost and scarcity of Pt, enhancing the atomic utilization efficiency of Pt and precisely regulating the intrinsic structures of active sites have proven to be effective strategies for enhancing the activity, selectivity, and stability of the RWGS reaction. This review summarizes recent advances in the structural design and mechanistic understanding of Pt-based catalysts for the RWGS reaction. The studies discussed collectively demonstrate that high RWGS activity and CO selectivity do not arise from isolated metallic Pt sites alone, but from a range of structurally well-defined active centers, including Pt-reducible oxide interfaces, defect-anchored single atoms, sub-nanometric Pt clusters, and functionally divided bimetallic ensembles. Across these systems, a consistent picture emerges in which the local coordination environment, oxidation state, and dynamic reconstruction of Pt under reaction conditions jointly govern CO_2 activation, intermediate stabilization, and CO desorption.

In terms of Pt-based RWGS catalysts with high activity, high CO selectivity, and excellent stability, metal-support and metal–promoter interfaces serve as intrinsic active sites. Combined in-situ spectroscopic and kinetic studies reveal that the most active centers are the metal-support interfacial sites. These sites couple metallic or partially oxidized Pt with oxygen vacancies and variable-valence cations. Such interfacial ensembles enhance CO_2 bending adsorption and polarization, stabilize carboxyl (COOH) intermediates, and weaken CO binding compared to metallic Pt surfaces. Promoters and secondary metals improve RWGS performance through well-defined electronic and structural effects rather than simple additive behavior. Alkali and alkaline-earth cations modulate the basicity and O_v concentration of oxide supports, resulting in stronger CO_2 adsorption but weaker CO binding at Pt adjacent sites. Transition metals reconstruct Pt active sites at the atomic level by redistributing redox and hydrogen-activation functions across different local environments.

The combination of in-situ methods with theoretical tools such as DFT and microkinetic simulations reveals the dynamic nature of Pt active centers and clarifies the dominant reaction pathways at different site types. At O_v-rich Pt–O_v–M^{n+} interfaces, redox pathways can become dominant, with the OH + H → H_2O step typically controlling the overall reaction rate. In contrast, on metallic Pt terraces and steps that lack lattice O, CO–O bond cleavage generally exhibits the highest degree of rate control. For the associative mechanism, both theoretical and kinetic analyses consistently indicate that the CO_2 → *COOH and *COOH → CO + OH steps are usually rate-determining. These findings demonstrate that both the identity and population of active sites are dynamic, and that reaction pathways and RDS with the distribution of interfacial and metallic sites.

Despite these advances, Pt-based RWGS catalytic systems still face several critical challenges: The atomic structure of the true active sites under realistic RWGS conditions remains a subject of debate. Existing in-situ techniques can monitor trends in Pt valence states and average coordination, but they still face challenges in providing direct, time-resolved images of specific $Pt^{\delta+}$–O_v–M^{n+} motifs and their rapid reconstruction under conditions of high temperature, high space velocity, and elevated CO partial pressure. The synergistic effects among defects, variable-valence cations, and $Pt^{\delta+}$ species at composite sites near the interface have been shown to be crucial for strong CO_2 activation and weak CO adsorption. However, the specific roles of different active site types in regulating reaction pathways and rate-limiting steps remain not fully understood. Additionally, Pt single atoms tend to migrate and agglomerate under high-temperature RWGS conditions due to CO-induced mobility, posing challenges to achieving long-term structural stability while maintaining high CO selectivity. Although Pt-based systems exhibit excellent activity at high temperatures, maintaining high CO_2 conversion and CO selectivity at low temperatures and high space velocities remains difficult due to thermodynamic limitations, competing methanation reactions, and mass-transfer constraints.

Future research should focus on several unresolved issues specific to Pt-based catalysts for the RWGS reaction. First, it is necessary to further clarify the dynamic structure-performance relationship of Pt active sites under real reaction conditions. It is essential to further develop and integrate complementary operando techniques capable of

simultaneously probing the oxidation state of Pt, its coordination geometry, local environment, and surface intermediates under realistic RWGS conditions. These approaches should enable direct observation of active-site reconstruction during reaction initiation, steady-state operation, and deactivation. Furthermore, it is essential to establish a quantitative correlation between interfacial species such as $Pt^{\delta+}$-O_v-M^{n+} and CO_2 activation, CO selectivity, and the rate-determining step. Such a combined strategy is anticipated to provide clearer evidence regarding the nature and dynamic evolution of interfacial active sites and to elucidate how they respond to variations in temperature, gas composition, and GHSV.

Secondly, achieving the long-term stability of single-atom and sub-nanometer Pt species under high-temperature RWGS conditions remains a critical prerequisite for enhancing Pt atom utilization efficiency. To achieve a balance between high Pt atomic utilization and structural stability, future synthesis strategies should focus on anchoring Pt atoms and clusters at well-defined defect sites, O_v, and heteroatom dopants within reducible oxides or composite supports. Techniques such as vacancy engineering, strong CMSI, structural confinement by the support, and controlled encapsulation can effectively suppress Pt migration while preserving accessible interfacial sites. Moreover, combining single Pt atoms with adjacent oxide redox centers and metallic nanodomains may produce hybrid single-atom plus interface structures that sustain high CO selectivity under elevated temperatures and high GHSV.

Finally, to overcome the bottleneck of simultaneously enhancing activity, CO selectivity, and stability under low-temperature and high GHSV conditions, the design of Pt-based RWGS catalysts should place greater emphasis on interfacial synergy and reaction network regulation. Building on the understanding of functional site division in bimetallic catalysts and composite interfaces, future catalyst development should intentionally construct bimetallic or multi-component interfaces where H_2 activation and CO_2 activation occur at distinct yet electronically coupled sites. Pt-rich sites can be engineered for rapid H_2 dissociation and moderate CO binding, while promoter-rich sites are optimized for strong CO_2 adsorption, *COOH stabilization, and efficient C-O bond cleavage. Concurrently, defect-rich composite supports featuring hierarchical porosity and an optimal hydrophobic/hydrophilic balance can reduce water accumulation, enhance mass and heat transfer, and sustain high catalytic activity and CO selectivity under low-temperature, high-GHSV conditions.

Data availability

All data needed to support the conclusions in the paper are presented in the manuscript and/or the Electronic Supplementary Material. Additional data related to this paper may be requested from the corresponding author upon request.

Acknowledgements

This work was supported by the National Natural Science Foundation of China (No. 22572021, No. 22379023, No. 52301011), the China Postdoctoral Science Foundation (No. 2023M740555, 2025M771070, and 2025T180292), Heilongjiang Provincial Postdoctoral Science Foundation (LBH-Z23001, LBH-Z24003), Heilongjiang Provincial Key Research and Development Program Guidance Category Project (GZ20220073, GZ2024012), Heilongjiang Provincial Natural Science Foundation Outstanding Youth Fund Project (YQ2024B002, YQ2025B002), and the Foundation of State Key Laboratory of Catalysis (Grant No. N-22-07).

Declaration of competing interest

All the contributing authors report no conflict of interests in this work.

Author contribution statement

Xiaoyu Hu: Writing-review & editing, Writing-original draft. Yingnan Tan: Writing-review & editing, Writing-original draft. Yuanyuan Ma: Project administration, writing manuscript. Xiaohan Zhao: Writing-review & editing, Writing-original draft, Investigation, Conceptualization. Deming Rao: Writing-review & editing, Writing-original draft. Pan Yin: Writing-review & editing, Writing-original draft. Bin Wang: Writing-review & editing, Writing-original draft. Tingting Cui: Writing-review & editing, Supervision, Resources, Funding acquisition, Formal analysis. Ming Xu: Supervision, Funding acquisition, Project administration, Resources, Formal analysis, Conceptualization.

Informed consent

Not applicable

Ethics statement

Not applicable

Use of AI statement

None

References

[1] Koytsoumpa, E.I.; Bergins, C.; Kakaras, E. The CO_2 economy: Review of CO_2 capture and reuse technologies. *J. Supercrit. Fluid.* **2018**, 132, 3-16.

[2] Sullivan, I.; Goryachev, A.; Digdaya, I.A.; Li, X.Q.; Atwater, H.A.; Vermaas, D.A.; Xiang, C.X. Coupling electrochemical CO_2 conversion with CO_2 capture. *Nat. Catal.* **2021**, 4, 952-958.

[3] Saleh, T.A. Nanomaterials and hybrid nanocomposites for CO_2 capture and utilization: environmental and energy sustainability. *RSC Adv.* **2022**, 12, 23869-23888.

[4] González-Castaño, M.; Dorneanu, B.; Arellano-García, H. The reverse water gas shift reaction: a process systems engineering perspective. *REACT. CHEM. ENG.* **2021**, 6, 954-976.

[5] Beck, A.; Frey, H.; Huang, X.; Clark, A.H.; Goodman, E.D.; Cargnello, M.; Willinger, M.; van Bokhoven, J.A. Controlling the Strong Metal-Support Interaction Overlayer Structure in Pt/TiO_2 Catalysts Prevents Particle Evaporation. *Angew. Chem. Int. Ed.* **2023**, 62, e202301468.

[6] Zhu, Z.T.; Tsai, H.H.; Parker, S.T.; Lee, J.H.; Yabuuchi, Y.; Jiang, H.Z.H.; Wang, Y.; Xiong, S.Y.; Forse, A.C.; Dinakar, B.; Huang, A.D.; Dun, C.; Milner, P.J.; Smith, A.; Martins, P.G.; Meihaus, K.R.; Urban, J.J.; Reimer, J.A.; Neaton, J.B.; Long, J.R. High-Capacity, Cooperative CO_2 Capture in a Diamine-Appended Metal-Organic Framework through a Combined Chemisorptive and Physisorptive Mechanism. *J. Am. Chem. Soc.* **2024**, 146, 6072-6083.

[7] Peng, M.; Ge, Y.Z.; Gao, R.; Yang, J.; Li, A.W.; Xie, Z.H.; Yu, Q.L.; Zhang, J.; Asakura, H.; Zhang, H.; Liu, Z.; Zhang, Q.; Deng, J.; Zhou, J.H.; Zhou, W.; Hutchings, G.J.; Ma, D. Thermal catalytic reforming for hydrogen production with zero CO_2 emission. *Science* **2025**, 387, 769-775.

[8] Ghoshray, A.; Lorusso, M. Energy consumption, CO_2 emissions and economic growth in selected ASEAN countries. *Lett. Spat. Resour. Sci.* **2025**, 18, 2.

[9] Wang, P.; Pei, A.; Chen, Z.X.; Sun, P.L.; Hu, C.Y.; Wang, X.; Zheng, N.F.; Chen, G.X. Integrated system for electrolyte recovery, product separation, and CO_2 capture in CO_2 reduction. *Nat. Commun.* **2025**, 16, 731.

[10] Jiang, M.; Wang, Z.-Q.; Li, Z.; Liu, Z.; Yin, Y.; Tian, F.; Li, A.; Xu, H.; Gong, X.-Q.; He, Y. Ambient-Pressure C-C Coupling of CO_2 Hydrogenation by NiFe/TiO_2 Bimetallic Catalyst. *J. Am. Chem. Soc.* **2025**, 147, 33495-33506.

[11] Qin, X.T.; Xu, M.; Guan, J.X.; Feng, L.; Xu, Y.; Zheng, L.R.; Wang, M.; Zhao, J.W.; Chen, J.L.; Zhang, J.; Xie, J.L.; Yu, Z.H.; Zhang, R.Q.; Li, X.M.; Liu, X.; Liu, J.X.; Zheng, J.R.; Ma, D. Direct conversion of CO and H_2O to hydrocarbons at atmospheric pressure using a TiO_{2-x}/Ni photothermal catalyst. *Nat. Energy* **2024**, 9, 154-162.

[12] Triviño, M.L.T.; Arriola, N.C., Jr.; Kang, Y.S.; Seo, J.G. Transforming CO_2 to valuable feedstocks: Emerging catalytic and technological advances for the reverse water gas shift reaction. *Chem. Eng. J.* **2024**, 487, 150369.

[13] Ye, J.Y.; Dimitratos, N.; Rossi, L.M.; Thonemann, N.; Beale, A.M.; Wojcieszak, R. Hydrogenation of CO_2 for sustainable fuel and chemical production. *Science* **2025**, 387.

[14] Ye, R.; Ma, L.; Mao, J.; Wang, X.; Hong, X.; Gallo, A.; Ma, Y.; Luo, W.; Wang, B.; Zhang, R.; Duyar, M.S.; Jiang, Z.; Liu, J. A Ce-CuZn catalyst with abundant Cu/Zn-O_V-Ce active sites for CO_2 hydrogenation to methanol. *Nat. Commun.* **2024**, 15, 2159.

[15] Ye, R.-P.; Ding, J.; Gong, W.; Argyle, M.D.; Zhong, Q.; Wang, Y.; Russell, C.K.; Xu, Z.; Russell, A.G.; Li, Q.; Fan, M.; Yao, Y.-G. CO_2 hydrogenation to high-value products via heterogeneous catalysis. *Nat. Commun.* **2019**, 10, 5698.

[16] Bown, R.M.; Joyce, M.; Zhang, Q.; Reina, T.R.; Duyar, M.S. Identifying Commercial Opportunities for the Reverse Water Gas Shift Reaction. *Energy Technol-Ger* **2021**, 9, 2100554.

[17] Zhang, M.; Zhu, Y.; Yan, J.; Xie, J.; Yu, T.; Peng, M.; Zhao, J.; Xu, Y.; Li, A.; Jia, C.; He, L.; Wang, M.; Zhou, W.; Wang, R.; Jiang, H.; Shi, C.; Rodriguez, J.; Ma, D. A Highly Active Molybdenum Carbide Catalyst with Dynamic Carbon Flux for Reverse Water-Gas Shift Reaction. *Angew. Chem. Int. Edit.* **2025**, 64, e202418645.

[18] Saravanan, A.; Kumar, P.S.; Vo, D.V.N.; Jeevanantham, S.; Bhuvaneswari; Narayanan, V.A.; Yaashikaa, P.R.; Swetha, S.; Reshma, B. A comprehensive review on different approaches for CO_2 utilization and conversion pathways. *Chem. Eng. Sci.* **2021**, 236, 116515.

[19] Zhang, B.Z.; Huang, S.Y.; Li, Y.; Shen, J.; Tian, X.; Ding, M.Y. Highly dispersed Cu on hollow spherical CeO_2: An efficient and stable catalyst for the RWGS reaction. *Appl. Catal. B-Environ.* **2025**, 366, 125003.

[20] Sun, J.Q.; Tao, L.; Ye, C.L.; Wang, Y.; Meng, G.; Lei, H.Y.; Zheng, S.K.; Xing, C.; Tao, X.; Wu, P.F.; Chen, J.A.; Du, S.X.; Wang, D.S.; Li, Y.D. MOF-Derived Ru_1Zr_1/Co Dual-Atomic-Site Catalyst with Promoted Performance for Fischer-Tropsch Synthesis. *J. Am. Chem. Soc.* **2023**, 145, 7113-7122.

[21] Cai, Y.; Wang, M.L.; Zhao, S.; Liu, X.; Xie, J.Z.; Liu, X.W.; Xu, Y.; Zhang, J.; Zeng, L.Z.; Qian, F.; Gao, Z.R.; Cen, Z.Y.; Liu, X.C.; Wang, H.; Xu, B.J.; Hutchings, G.J.; Yang, Y.; Li, Y.W.; Wen, X.D.; Ma, D. Trace-level halogen blocks CO_2 emission in Fischer-Tropsch synthesis for olefins production. *Science* **2025**, 390, 516-520.

[22] Xiao, Z.R.; Zhang, H.; Tan, X.Y.; Ye, F.; Zhang, Y.R.; Gu, J.M.; Li, J.J.; Sun, K.H.; Zhang, S.L.; Zou, J.J.; Wang, D.S. Comprehensive Insight into External Field-Driven CO_2 Reduction to CO: Recent Progress and Future Prospects. *Adv. Mater.* **2025**, 15, 2500988.

[23] Daza, Y.A.; Kuhn, J.N. CO_2 conversion by reverse water gas shift catalysis: comparison of catalysts, mechanisms and their consequences for CO_2 conversion to liquid fuels. *RSC Adv.* **2016**, 6, 49675-49691.

[24] Choi, S.; Sang, B.-I.; Hong, J.; Yoon, K.J.; Son, J.-W.; Lee, J.-H.; Kim, B.-K.; Kim, H. Catalytic behavior of metal catalysts in high-temperature RWGS reaction: In-situ FT-IR experiments and first-principles calculations. *Sci. Rep.* **2017**, 7, 41207.

[25] Markowitsch, C.; Andritz, M.; Lindenthal, L.; Cotter, T.; Drexler, H.; Rameshan, C.; Lehner, M. Process intensification of the rWGS reaction by a perovskite-based catalyst. *Chem. Eng. J.* **2024**, 500.

[26] Kaiser, P.; Unde, R.B.; Kern, C.; Jess, A. Production of Liquid Hydrocarbons with CO_2 as Carbon Source based on Reverse Water-Gas Shift and Fischer-Tropsch Synthesis. *Chem-Ing-Tech* **2013**, 85, 489-499.

[27] Wang, X.; Shi, H.; Szanyi, J. Controlling selectivities in CO_2 reduction through mechanistic understanding. *Nat. Commun.* **2017**, 8, 513.

[28] Gong, Y.T.; Jing, Y.X.; Liu, X.H.; Wang, Y.Q.; Guo, Y. In Situ Surface Restructuring of γ-Mo_2N for Enhanced Reverse Water-GasShift Reaction. *ACS Catal.* **2025**, 15, 8337-8344.

[29] Bahmanpour, A.M.; Signorile, M.; Kröcher, O. Recent progress in syngas production via catalytic CO_2 hydrogenation reaction. *Appl. Catal. B-Environ.* **2021**, 295, 120319.

[30] Cui, X.J.; Liu, Y.Q.; Mei, Y.A.; Li, J.M.; Zhang, H.; Zhu, S.H.; Niu, Y.L.; Deng, T.S. Enhancing methanol selectivity of commercial Cu/ZnO/Al_2O_3 catalyst in CO_2 hydrogenation by surface silylation. *Appl. Catal. B Environ.* **2023**, 339, 123099.

[31] Zhou, C.; Zhang, J.; Fu, Y.; Dai, H. Recent Advances in the Reverse Water-Gas Conversion Reaction. *Molecules* **2023**, 28, 7657.

[32] Su, X.; Yang, X.; Zhao, B.; Huang, Y. Designing of highly selective and high-temperature endurable RWGS heterogeneous catalysts: recent advances and the future directions. *J. Energy. Chem.* **2017**, 26, 854-867.

[33] Deka, D.R.; Peter, S.C. Engineering CO_2-to-CO Conversion: Integrating Catalyst Design, Mechanistic Investigation, Reactor Fundamentals, TEA–LCA Evaluations, and AI-Driven Optimization. *ACS Catal.* **2026**, 16, 4290-4314.

[34] Yao, X.S.; Wei, Z.H.; Mei, J.Y.; Guo, X.H.; Tian, X.X. The reverse water gas shift reaction (RWGS) mechanism study on the γ-MoC(100) surface. *RSC Adv.* **2025**, 15, 460-466.

[35] Wang, X.R.; Xia, W.; Zhang, Y.L.; Wang, D.; Dong, M.Y.; Chen, K.; Liu, D.; Lu, B.W. Tailoring CeO_2 catalysts via oxygen vacancies and Ni loading: Boosting RWGS reaction performance and uncovering underlying mechanisms. *Mol. Catal.* **2026**, 589, 115615.

[36] Rabee, A.I.M.; Cisneros, S.; Zhao, D.; Kreyenschulte, C.R.; Bartling, S.; Kondratenko, V.; Kubis, C.; Kondratenko, E.V.; Brückner, A.; Rabeah, J. Uncovering the synergy between gold and sodium on ZrO_2 for boosting the reverse water gas shift reaction: In-situ spectroscopic investigations. *Appl. Catal. B-Environ.* **2024**, 345, 123685.

[37] Kattel, S.; Liu, P.; Chen, J.G. Tuning Selectivity of CO_2 Hydrogenation Reactions at the Metal/Oxide Interface. *J. Am. Chem. Soc.* **2017**, 139, 9739-9754.

[38] Zhang, C.; Xiao, Z.; Guo, X.; Tan, X.; Gu, J.; Li, J.; Li, G.; Zou, J.-J.; Wang, D. Investigating the role of advanced catalysts and technologies in enhancing CO_2 conversion via reverse water-gas shift reaction. *Chem. Eng. J.* **2025**, 519, 165414.

[39] Sun, Z.T.; Huang, J.L.; Zhou, L.; Zhang, Y. Synergistic effects of promoters on adjusting the reaction pathway over iron catalysts for CO_2 hydrogenation to CO. *Catal. Sci. Technol.* **2025**, 15, 2964-2976.

[40] Chen, J.; Su, S.Y.; Wang, C.Q.; Li, Q.; Wang, H.L.; Xu, W.J.; Li, X.L.; Jia, H.P. Understanding CO_2 reduction via reverse water-gas shift triggered by electromagnetic induction at moderate condition. *Chem. Eng. J.* **2023**, 476, 146712.

[41] Bobadilla, L.F.; Santos, J.L.; Ivanova, S.; Odriozola, J.A.; Urakawa, A. Unravelling the Role of Oxygen Vacancies in the Mechanism of the Reverse Water-Gas Shift Reaction by Operando DRIFTS and Ultraviolet-Visible Spectroscopy. *ACS Catal.* **2018**, 8, 7455-7467.

[42] Du, X.; Li, R.; Xin, H.; Fan, Y.; Liu, C.; Feng, X.; Wang, J.; Dong, C.; Wang, C.; Li, D.; Fu, Q.; Bao, X. In-Situ Dynamic Carburization of Mo Oxide with Unprecedented High CO Formation Rate in Reverse Water-Gas Shift Reaction. *Angew. Chem. Int. Edit.* **2024**, 63, e202411761.

[43] Shen, J.; Tian, X.; Ding, M.Y. Structurally stabilized spinel-type Fe-Al catalyst for the reverse water-gas shift reaction. *Chem. Eng. J.* **2025**, 525, 170357.

[44] Chang, X.; Yu, C.; Yang, C.; Xie, H.; Xia, S.; Fang, Z.; Li, J.; Zhang, S.; Liu, F.; Wang, T.; Tan, Y.; Chen, X.; Shi, S.; Guo, Q.; Xu, Q.; Hu, J.; Ding, H.; Huang, C.; Zhou, C.; Zhu, J.; Yang, X.; Yang, W. Groove-Confined Cobalt Catalyst for Low-Temperature CO_2 Activation. *J. Am. Chem. Soc.* **2025**, 147, 16164-16170.

[45] Gao, Z.Y.; Meng, Y.; Shen, H.; Xie, B.; Ni, Z.M.; Xia, S.J. Theoretical study on low temperature reverse water gas shift (RWGS) mechanism on monatomic transition metal M doped

C_2N catalyst (M=Cu, Co, Fe). *Mol. Catal.* **2021**, 516, 111992.

[46] Wang, L.; Liu, H.; Chen, Y.; Yang, S. Reverse water-gas shift reaction over co-precipitated Co-CeO_2 catalysts: Effect of Co content on selectivity and carbon formation. *Int. J. Hydrogen Energ.* **2017**, 42, 3682-3689.

[47] Li, W.; Liu, B.; Guo, Q.; Guo, W.; Zhang, S.; Qu, Y. Reaction-induced regioselective reconstruction of Ni-doped $Ce(OH)_3/CeO_2$ enables exceptional activity and selectivity for reverse water-shift reaction. *Nat. Commun.* **2025**, 16, 7335.

[48] Lin, S.; Wang, Q.; Li, M.; Hao, Z.; Pan, Y.; Han, X.; Chang, X.; Huang, S.; Li, Z.; Ma, X. Ni-Zn Dual Sites Switch the CO_2 Hydrogenation Selectivity via Tuning of the d-Band Center. *ACS Catal.* **2022**, 12, 3346-3356.

[49] Lin, L.; Liu, J.; Liu, X.; Gao, Z.; Rui, N.; Yao, S.; Zhang, F.; Wang, M.; Liu, C.; Han, L.; Yang, F.; Zhang, S.; Wen, X.-d.; Senanayake, S.D.; Wu, Y.; Li, X.; Rodriguez, J.A.; Ma, D. Reversing sintering effect of Ni particles on γ-Mo_2N via strong metal support interaction. *Nat. Commun.* **2021**, 12, 6978.

[50] Choi, Y.; An, B.-S.; Sim, G.D.; Jung, U.; Park, Y.; Koo, K.Y. Synthesis of CuO catalysts supported on Fe-modified mixed oxides with high CO formation rates in low-temperature CO_2 hydrogenation. *Appl. Catal. B-Environ.* **2025**, 377, 125475.

[51] Jiao, J.Q.; Lin, R.; Liu, S.J.; Cheong, W.C.; Zhang, C.; Chen, Z.; Pan, Y.; Tang, J.G.; Wu, K.L.; Hung, S.F.; Chen, H.M.; Zheng, L.R.; Lu, Q.; Yang, X.; Xu, B.J.; Xiao, H.; Li, J.; Wang, D.S.; Peng, Q.; Chen, C.; Li, Y.D. Copper atom-pair catalyst anchored on alloy nanowires for selective and efficient electrochemical reduction of CO_2. *Nat. Chem.* **2019**, 11, 222-228.

[52] Li, Z.-Y.; Liu, H.-X.; Wu, J.-H.; Yang, F.; Ma, C.; Wang, W.-W.; Wang, F.R.; Jia, C.-J. Efficient Surface to Bulk Catalysis in the Reverse Water-Gas Shift Reaction by the FeO_x/Fe_3C Catalyst. *J. Am. Chem. Soc.* **2026**, 148, 1129-1140.

[53] Qu, Q.Y.; Mao, Y.; Ji, S.F.; Liao, J.W.; Dong, J.C.; Wang, L.G.; Wang, Q.C.; Liang, X.; Zhang, Z.D.; Yang, J.R.; Li, H.J.; Zhou, Y.F.; Wang, Z.Y.; Waterhouse, G.I.N.; Wang, D.S.; Li, Y.D. Engineering the Lewis Acidity of Fe Single-Atom Sites via Atomic-Level Tuning of Spatial Coordination Configuration for Enhanced Oxygen Reduction. *J. Am. Chem. Soc.* **2025**, 147, 6914-6924.

[54] Choi, Y.; Sim, G.D.; Jung, U.; Park, Y.; Youn, M.H.; Chun, D.H.; Rhim, G.B.; Kim, K.Y.; Koo, K.Y. Copper catalysts for CO_2 hydrogenation to CO through reverse water-gas shift reaction for e-fuel production: Fundamentals, recent advances, and prospects. *Chem. Eng. J.* **2024**, 492, 152283.

[55] Chen, L.; Allec, S.I.; Nguyen, M.-T.; Kovarik, L.; Hoffman, A.S.; Hong, J.; Meira, D.; Shi, H.; Bare, S.R.; Glezakou, V.-A.; Rousseau, R.; Szanyi, J. Dynamic Evolution of Palladium Single Atoms on Anatase Titania Support Determines the Reverse Water–Gas Shift Activity. *J. Am. Chem. Soc.* **2023**, 145, 10847-10860.

[56] Zhu, Y.; Guo, S.; Zhuang, N.; Ping, Q.; Zhang, J.; An, Z.; Song, H.; Shu, X.; Xi, W.; Zheng, L.; Zhang, R.; He, J. High-Density Dispersion of Atomic Pt (Ru, Rh, Pd, Ir) Induced by Meso-Stable Penta-Coordinated FeIII in the Topological Transformation of Layered Double Hydroxides. *ACS Catal.* **2023**, 14, 56-66.

[57] Xin, H.; Lin, L.; Li, R.; Li, D.; Song, T.; Mu, R.; Fu, Q.; Bao, X. Overturning CO_2 Hydrogenation Selectivity with High Activity via Reaction-Induced Strong Metal-Support Interactions. *J. Am. Chem. Soc.* **2022**, 144, 4874-4882.

[58] Wang, H.; Wang, L.; Lin, D.; Feng, X.; Niu, Y.; Zhang, B.; Xiao, F.-S. Strong metal-support interactions on gold nanoparticle catalysts achieved through Le Chatelier's principle. *Nat. Catal.* **2021**, 4, 418-424.

[59] Tang, Y.; Asokan, C.; Xu, M.; Graham, G.W.; Pan, X.; Christopher, P.; Li, J.; Sautet, P. Rh single atoms on TiO_2 dynamically respond to reaction conditions by adapting their site. *Nat. Commun.* **2019**, 10, 4488.

[60] Feng, Q.C.; Zhao, S.; Wang, Y.; Dong, J.C.; Chen, W.X.; He, D.S.; Wang, D.S.; Yang, J.; Zhu, Y.M.; Zhu, H.L.; Gu, L.; Li, Z.; Liu, Y.X.; Yu, R.; Li, J.; Li, Y.D. Isolated Single-Atom Pd Sites in Intermetallic Nanostructures: High Catalytic Selectivity for Semihydrogenation of Alkynes. *J. Am. Chem. Soc.* **2017**, 139, 7294-7301.

[61] Ji, S.F.; Chen, Y.J.; Fu, Q.; Chen, Y.F.; Dong, J.C.; Chen, W.X.; Li, Z.; Wang, Y.; Gu, L.; He, W.; Chen, C.; Peng, Q.; Huang, Y.; Duan, X.F.; Wang, D.S.; Draxl, C.; Li, Y.D. Confined Pyrolysis within Metal-Organic Frameworks To Form Uniform Ru3 Clusters for Efficient Oxidation of Alcohols. *J. Am. Chem. Soc.* **2017**, 139, 9795-9798.

[62] Meng, Q.L.; Liu, H.X.; Xu, K.; Wang, W.W.; Jia, C.J. CeO_{2-x} modified Ru/γ-Al_2O_3 catalysts for ammonia decomposition reaction. *J. Rare Earth.* **2023**, 41, 801-809.

[63] Peng, M.; Ge, Y.; Gao, R.; Yang, J.; Li, A.; Xie, Z.; Yu, Q.; Zhang, J.; Asakura, H.; Zhang, H.; Liu, Z.; Zhang, Q.; Deng, J.; Zhou, J.; Zhou, W.; Hutchings, G.J.; Ma, D. Thermal catalytic reforming for hydrogen production with zero CO_2 emission. *Science* **2025**, 387, 769-775.

[64] Gao, Z.; Li, A.; Liu, X.; Peng, M.; Yu, S.; Wang, M.; Ge, Y.; Li, C.; Wang, T.; Wang, Z.; Zhou, W.; Ma, D. Shielding Pt/γ-Mo_2N by inert nano-overlays enables stable H_2 production. *Nature* **2025**, 638, 690-696.

[65] Goguet, A.; Meunier, F.; Breen, J.; Burch, R.; Petch, M.; Faurghenciu, A. Study of the origin of the deactivation of a Pt/CeO_2 catalyst during reverse water gas shift (RWGS) reaction. *J. Catal.* **2004**, 226, 382-392.

[66] Becka, R.; Bajohr, S.; Kolb, T. Review on CO_2 Activation via Catalytic Reverse Water-Gas Shift Reaction. *Chem. Ing. Tech.* **2025**, 97, 860-881.

[67] Huang, Z.; Yuan, Y.; Song, M.; Hao, Z.; Xiao, J.; Cai, D.; Ibrahim, A.-R.; Zhan, G. CO2 hydrogenation over mesoporous Ni-Pt/SiO_2 nanorod catalysts: Determining CH_4/CO selectivity by surface ratio of Ni/Pt. *Chem. Eng. Sci.* **2022**, 247, 117106.

[68] Song, M.; Huang, Z.; Chen, B.; Liu, S.; Ullah, S.; Cai, D.; Zhan, G. Reduction treatment of nickel phyllosilicate supported Pt nanocatalysts determining product selectivity in CO_2 hydrogenation. *J. CO_2 Util.* **2021**, 52, 101674.

[69] Yu, J.; Peng, G.; Peng, L.; Chen, Q.; Su, C.; Shang, L.; Zhang, T. Recent advancements in two-dimensional transition metal dichalcogenide materials towards hydrogen-evolution electrocatalysis. *Green Energy & Environ.* **2025**, 10, 1130-1152.

[70] Zhu, Z.; Feng, K.; Li, C.; Tang, R.; Xiao, M.; Song, R.; Yang, D.; Yan, B.; He, L. Stabilization of Exposed Metal Nanocrystals in High - Temperature Heterogeneous Catalysis. *Adv. Mater.* **2021**, 34, 2108727.

[71] Zhang, Y.; Chen, F.; Yang, X.; Guo, Y.; Zhang, X.; Dong, H.; Wang, W.; Lu, F.; Lu, Z.; Liu, H.; Liu, H.; Xiao, Y.; Cheng, Y. Electronic metal-support interaction modulates Cu electronic structures for CO_2 electroreduction to desired products. *Nat. Commun.* **2025**, 16, 1956.

[72] Aunkon, R.H.; Choi, H.; Shimogawa, R.; Wang, H.; Zhang, L.; Reece, C.; Li, Y.; Kim, H.Y.; Frenkel, A.I. Low-Temperature Catalyst Redispersion: A Route to Enhanced Stability of Supported Metal Catalysts? *ACS Catal.* **2025**, 15, 19709-19720.

[73] Zhu, Y.; Yuk, S.F.; Zheng, J.; Nguyen, M.-T.; Lee, M.-S.; Szanyi, J.; Kovarik, L.; Zhu, Z.; Balasubramanian, M.; Glezakou, V.-A.; Fulton, J.L.; Lercher, J.A.; Rousseau, R.; Gutiérrez, O.Y. Environment of Metal-O-Fe Bonds Enabling High Activity in CO_2 Reduction on Single Metal Atoms and on Supported Nanoparticles. *J. Am. Chem. Soc.* **2021**, 143, 5540-5549.

[74] Rabee, A.I.M.; Zhao, D.; Cisneros, S.; Kreyenschulte, C.R.; Kondratenko, V.; Bartling, S.; Kubis, C.; Kondratenko, E.V.; Brückner, A.; Rabeah, J. Role of interfacial oxygen vacancies in low-loaded Au-based catalysts for the low-temperature reverse water gas shift reaction. *Appl. Catal. B-Environ.* **2023**, 321, 122083.

[75] Feng, L.; Zhao, J.-W.; Wei, W.-Y.; Wang, H.-Y.; Jiang, Y.-Q.; Liu, J.-X.; Li, W.-X. Nature of Reverse Water-Gas Shift Reactions at Metal–Oxide Interfaces Uncovered via Interpretable Machine Learning. *J. Am. Chem. Soc.* **2026**, 3602–3613.

[76] Zhao, Y.; Adiyeri Saseendran, D.P.; Huang, C.; Triana, C.A.; Marks, W.R.; Chen, H.; Zhao, H.; Patzke, G.R. Oxygen Evolution/Reduction Reaction Catalysts: From In Situ Monitoring and Reaction Mechanisms to Rational Design. *Chem. Rev.* **2023**, 123, 6257-6358.

[77] Lu, X.; Tan, K.B.; Zhao, J.; Zhan, G. Advances in integrated catalysts for CO_2 thermal hydrogenation to multicarbon products. *Chem Catal.* **2025**, 5, 101264.

[78] Jiang, X.; Nie, X.; Guo, X.; Song, C.; Chen, J.G. Recent Advances in Carbon Dioxide Hydrogenation to Methanol via Heterogeneous Catalysis. *Chem. Rev.* **2020**, 120, 7984-8034.

[79] Wang, D.; Xie, Z.; Porosoff, M.D.; Chen, J.G. Recent advances in carbon dioxide hydrogenation to produce olefins and aromatics. *Chem* **2021**, 7, 2277-2311.

[80] Liu, S.; Song, M.; Cha, X.; Hu, S.; Cai, D.; Li, W.; Zhan, G.

Nickel phyllosilicates functionalized with graphene oxide to boost CO selectivity in CO_2 hydrogenation. *Sep. Purif. Technol.* **2022**, 287, 120555.

[81] Zhang, S.; Cai, D.; Du, G.; Zhu, W.; Yang, J.; Wen, X.; Yan, X.; Zhou, Y.; Ali, S.; Tan, K.B.; Sun, K.; Zhan, G. Atomic-layer-deposited ZnO tailors $Ni^{\delta-}$–$ZnO^{\delta+}$ interfaces to switch CO_2 hydrogenation selectivity from CH_4 to CO. *Appl. Catal. B Environ.* **2026**, 383, 126092.

[82] Bahmanpour, A.M.; Signorile, M.; Kröcher, O. Recent progress in syngas production via catalytic CO_2 hydrogenation reaction. *Appl. Catal. B Environ.* **2021**, 295, 120319.

[83] Foppa, L.; Silaghi, M.-C.; Larmier, K.; Comas-Vives, A. Intrinsic reactivity of Ni, Pd and Pt surfaces in dry reforming and competitive reactions: Insights from first principles calculations and microkinetic modeling simulations. *J. Catal.* **2016**, 343, 196-207.

[84] Kattel, S.; Yan, B.; Chen, J.G.; Liu, P. CO_2 hydrogenation on Pt, Pt/SiO_2 and Pt/TiO_2: Importance of synergy between Pt and oxide support. *J. Catal.* **2016**, 343, 115-126.

[85] Zhao, Z.; Wang, M.; Ma, P.; Zheng, Y.; Chen, J.; Li, H.; Zhang, X.; Zheng, K.; Kuang, Q.; Xie, Z.-X. Atomically dispersed Pt/CeO_2 catalyst with superior CO selectivity in reverse water gas shift reaction. *Appl. Catal. B-Environ.* **2021**, 291, 120101.

[86] Hu, X.; Xu, D.; Jiang, J. Strong Metal-Support Interaction between Pt and TiO_2 over High-Temperature CO_2 Hydrogenation. *Angew. Chem. Int. Edit.* **2024**, 64, e202419103.

[87] Bi, W.; Wang, J.; Zhang, R.; Ge, Q.; Zhu, X. Tuning Interfacial Sites of WO_x/Pt for Enhancing Reverse Water Gas Shift Reaction. *ACS Catal.* **2024**, 14, 11205-11217.

[88] Liang, H.; Zhang, B.; Hong, M.; Yang, X.; Zhu, L.; Liu, X.; Qi, Y.; Zhao, S.; Wang, G.; van Bavel, A.P.; Wen, X.; Qin, Y. Operando Mobile Catalysis for Reverse Water Gas Shift Reaction. *Angew. Chem. Int. Edit.* **2024**, 63, e202318747.

[89] Kang, X.; Liu, J.; Xie, Y.; Wang, D.; Liu, Q.; Yu, P.; Tian, C.; Fu, H. Pt single atoms in oxygen vacancies boost reverse water-gas shift reaction by enhancing hydrogen spillover. *Sci. China Mater.* **2024**, 67, 3579-3588.

[90] Chen, H.; Zhao, Z.; Wang, G.; Zheng, Z.; Chen, J.; Kuang, Q.; Xie, Z. Dynamic Phase Transition of Iron Oxycarbide Facilitated by Pt Nanoparticles for Promoting the Reverse Water Gas Shift Reaction. *ACS Catal.* **2021**, 11, 14586-14595.

[91] Yang, X.; Su, X.; Chen, X.; Duan, H.; Liang, B.; Liu, Q.; Liu, X.; Ren, Y.; Huang, Y.; Zhang, T. Promotion effects of potassium on the activity and selectivity of Pt/zeolite catalysts for reverse water gas shift reaction. *Appl. Catal. B-Environ.* **2017**, 216, 95-105.

[92] Li, W.; Gan, J.; Liu, Y.; Zou, Y.; Zhang, S.; Qu, Y. Platinum and Frustrated Lewis Pairs on Ceria as Dual-Active Sites for Efficient Reverse Water-Gas Shift Reaction at Low Temperatures. *Angew. Chem. Int. Edit.* **2023**, 62, e202305661.

[93] Liang, B.; Duan, H.; Su, X.; Chen, X.; Huang, Y.; Chen, X.; Delgado, J.J.; Zhang, T. Promoting role of potassium in the reverse water gas shift reaction on Pt/mullite catalyst. *Catal. Today* **2017**, 281, 319-326.

[94] Zhou, W.; Yao, C.; Dery, S.; Grings, J.; Wang, W.; Brack, E.; Paterson, J.; Southouse, J.; Copéret, C. Disentangling the Promotional Roles of Interfacial and Alloyed Sites in PtCr Catalysts for CO_2 Hydrogenation. *J. Am. Chem. Soc.* **2025**, 147, 41425-41432.

[95] Torres-Sempere, G.; Blay-Roger, R.; Luque-Álvarez, L.A.; Santos, J.L.; Bobadilla, L.F.; Pastor-Pérez, L.; Centeno, M.A.; Hernández, W.Y.; Yousef, I.; Odriozola, J.A.; R. Reina, T. Subnanometric Pt clusters dispersed over Cs-doped TiO_2 for CO_2 upgrading via low-temperature RWGS: operando mechanistic insights to guide an optimal catalyst design. *J. Mater. Chem. A* **2024**, 12, 1779-1792.

[96] Jiang, N.; Wang, W.; Liu, H.; Wu, M.; Jia, C. Alumina supported platinum-ceria catalyst for reverse water gas shift reaction. *J. Rare Earths* **2025**, 43, 284-294.

[97] Liu, H.-X.; Li, J.-Y.; Qin, X.; Ma, C.; Wang, W.-W.; Xu, K.; Yan, H.; Xiao, D.; Jia, C.-J.; Fu, Q.; Ma, D. Pt_n-O_v synergistic sites on MoO_x/γ-Mo_2N heterostructure for low-temperature reverse water-gas shift reaction. *Nat. Commun.* **2022**, 13, 5800.

[98] Lei, J.; Wu, Z.; Ye, D.; Feng, Y.; Tian, Y.; Niu, J.; Cheng, C.; Wang, Y.; Li, S.; Zhao, C. Amorphous Silica Induced Loose CeO_2 Clusters with Isolated Pt Atoms for Efficient Reverse - Water Gas Shift Reaction. *Angew. Chem. Int. Edit.* **2025**, 64, e202511913.

[99] Xie, J.; Feng, Y.; Wang, X.; Li, X.; Yu, J.; Gao, A.; Jiang, J.; Chang, Q.; Dai, Y.; Liu, W.; Guo, S. Fully exposed platinum clusters for the efficient reverse water-gas shift reaction at low temperatures. *Appl. Catal. B-Environ.* **2025**, 373, 125341.

[100] Liu, D.; Li, Y.; Kottwitz, M.; Yan, B.; Yao, S.; Gamalski, A.; Grolimund, D.; Safonova, O.V.; Nachtegaal, M.; Chen, J.G.; Stach, E.A.; Nuzzo, R.G.; Frenkel, A.I. Identifying Dynamic Structural Changes of Active Sites in Pt-Ni Bimetallic Catalysts Using Multimodal Approaches. *ACS Catal.* **2018**, 8, 4120-4131.

[101] Wang, H.; Bootharaju, M.S.; Kim, J.H.; Wang, Y.; Wang, K.; Zhao, M.; Zhang, R.; Xu, J.; Hyeon, T.; Wang, X.; Song, S.; Zhang, H. Synergistic Interactions of Neighboring Platinum and Iron Atoms Enhance Reverse Water-Gas Shift Reaction Performance. *J. Am. Chem. Soc.* **2023**, 145, 2264-2270.

[102] Hansen, C.; Zhou, W.; Brack, E.; Wang, Y.; Wang, C.; Paterson, J.; Southouse, J.; Copéret, C. Decoding the Promotional Effect of Iron in Bimetallic Pt–Fe-nanoparticles on the Low Temperature Reverse Water–Gas Shift Reaction. *J. Am. Chem. Soc.* **2024**, 146, 27555-27562.

[103] Xu, C.; Kuwahara, Y.; Yamada, T.; Zhou, S.; Yamashita, H. Hollow porous silica nanoreactors encapsulating VO_x-decorated Pt nanoparticles for the reverse water-gas shift reaction. *Chem. Eng. J.* **2024**, 497, 154484.

[104] Heyl, D.; Rodemerck, U.; Bentrup, U. Mechanistic Study of Low-Temperature CO_2 Hydrogenation over Modified Rh/Al_2O_3 Catalysts. *ACS Catal.* **2016**, 6, 6275-6284.

[105] Lang, R.; Du, X.R.; Huang, Y.K.; Jiang, X.Z.; Zhang, Q.; Guo, Y.L.; Liu, K.P.; Qiao, B.T.; Wang, A.Q.; Zhang, T. Single-Atom Catalysts Based on the Metal-Oxide Interaction. *Chem. Rev.* **2020**, 120, 11986-12043.

[106] Liu, J.; Chen, L.; Liu, X. Deep Insight into Characterizing the Metal-Support Interface in Heterogeneous Catalysis. *ACS Catal.* **2024**, 14, 1987-2002.

[107] Xu, M.; Peng, M.; Tang, H.; Zhou, W.; Qiao, B.; Ma, D. Renaissance of Strong Metal-Support Interactions. *J. Am. Chem. Soc.* **2024**, 146, 2290-2307.

[108] S. J. Tauster, S.C.F., and R. L. Garten. Strong Metal-Support Interactions. Group 8 Noble Metals Supported on TiO_2. *J. Am. Chem. Soc.* **1978**, 100, 170-175.

[109] Wang, H.; Gao, Z.; Sun, B.; Mu, S.; Dang, F.; Guo, X.; Ma, D.; Shi, C. Engineering metal-support interaction to construct catalytic interfaces and redisperse metal nanoparticles. *Chem Catal.* **2023**, 3, 100768.

[110] Ding, Y.; Chen, J.; Lian, X.; Tian, Z.; Geng, X.; Wang, Y.; Liu, Y.; Wang, W.; Wang, M.; Xiao, Y.; Jin, T.; Sun, M.; Yang, Z.; Zhang, K.H.L.; Zhong, J.-Q.; Chen, W. Revealing the effect of metal-support interactions at the $Ni/In_2O_3(111)$ interface on the selective CO_2 hydrogenation. *Appl. Catal. B-Environ.* **2024**, 343, 123508.

[111] Belgamwar, R.; Verma, R.; Das, T.; Chakraborty, S.; Sarawade, P.; Polshettiwar, V. Defects Tune the Strong Metal-Support Interactions in Copper Supported on Defected Titanium Dioxide Catalysts for CO_2 Reduction. *J. Am. Chem. Soc.* **2023**, 145, 8634-8646.

[112] Du, P.; Qi, R.; Zhang, Y.; Gu, Q.; Xu, X.; Tan, Y.; Liu, X.; Wang, A.; Zhu, B.; Yang, B.; Zhang, T. Single-atom-driven dynamic carburization over Pd_1–FeO_x catalyst boosting CO_2 conversion. *Chem* **2022**, 8, 3252-3262.

[113] Dulub, O.; Hebenstreit, W.; Diebold, U. Imaging Cluster Surfaces with Atomic Resolution: The Strong Metal-Support Interaction State of Pt Supported on $TiO_2(110)$. *Phys. Rev. Lett.* **2000**, 84, 3646-3649.

[114] Zhang, S.; Plessow, P.N.; Willis, J.J.; Dai, S.; Xu, M.; Graham, G.W.; Cargnello, M.; Abild-Pedersen, F.; Pan, X. Dynamical Observation and Detailed Description of Catalysts under Strong Metal–Support Interaction. *Nano Lett.* **2016**, 16, 4528-4534.

[115] Zhang, J.; Zhu, D.; Yan, J.; Wang, C.-A. Strong metal-support interactions induced by an ultrafast laser. *Nat. Commun.* **2021**, 12, 6665.

[116] Sang, K.; Zuo, J.; Zhang, X.; Wang, Q.; Chen, W.; Qian, G.; Duan, X. Towards a molecular understanding of the electronic metal-support interaction (EMSI) in heterogeneous catalysis. *Green Energy & Environ.* **2023**, 8, 619-625.

[117] Yang, J.R.; Li, W.H.; Tan, S.D.; Xu, K.N.; Wang, Y.; Wang, D.S.; Li, Y.D. The Electronic Metal-Support Interaction Directing the Design of Single Atomic Site Catalysts: Achieving High Efficiency Towards Hydrogen Evolution. *Angew. Chem. Int.*

Edit. **2021**, 60, 19085-19091.

[118] Ye, D.; Wu, Z.; Wang, T.; Zhu, R.; Feng, Y.; Lei, J.; Tian, Y.; Zou, Z.; Wu, H.; Cheng, C.; Tang, S.; Li, S. Anti-Sintering Ni-W Catalytic Layer on Reductive Tungsten Carbides for Superior High-Temperature CO_2 Reduction. *Adv. Mater.* **2025**, 37, 2504431.

[119] Sun, C.; Zhou, Y.; Zhang, J.; Yu, J.; Wang, L.; Zhang, L. Potassium-Modulated Ni/Carbon Catalyst for Efficient Photothermal CO_2 Reduction: Unveiling the Role of Electronic Metal–Support Interactions. *Adv. Funct. Mater.* **2025**, n/a, e16103.

[120] Besenbacher, F.; Chorkendorff, I.; Clausen, B.S.; Hammer, B.; Molenbroek, A.M.; Nørskov, J.K.; Stensgaard, I. Design of a Surface Alloy Catalyst for Steam Reforming. *Science* **1998**, 279, 1913-1915.

[121] Tang, X.; Yu, A.W.; Yang, Q.Q.; Yuan, H.Y.; Wang, Z.H.; Xie, J.Z.; Zhou, L.H.; Guo, Y.; Ma, D.; Dai, S. Significance of Epitaxial Growth of PtO_2 on Rutile TiO_2 for Pt/TiO_2 Catalysts. *J. Am. Chem. Soc.* **2024**, 146, 3764-3772.

[122] Wang, Y.; Widmann, D.; Behm, R.J. Influence of TiO_2 Bulk Defects on CO Adsorption and CO Oxidation on Au/TiO_2: Electronic Metal-Support Interactions (EMSIs) in Supported Au Catalysts. *ACS Catal.* **2017**, 7, 2339-2345.

[123] Chen, B.H.; White, J.M. Properties of platinum supported on oxides of titanium. *J. Phys. Chem.* **1982**, 86, 3534-3541.

[124] Schierbaum, K.D.; Fischer, S.; Torquemada, M.C.; de Segovia, J.L.; Román, E.; Martín-Gago, J.A. The interaction of Pt with TiO_2(110) surfaces: a comparative XPS, UPS, ISS, and ESD study. *Surf. Sci.* **1996**, 345, 261-273.

[125] Ebrahimi, P.; Kumar, A.; Khraisheh, M. A Review of CeO_2 Supported Catalysts for CO_2 Reduction to CO through the Reverse Water Gas Shift Reaction. *Catalysts* **2022**, 12, 1101.

[126] Daelman, N.; Capdevila-Cortada, M.; López, N. Dynamic charge and oxidation state of Pt/CeO_2 single-atom catalysts. *Nat. Mater.* **2019**, 18, 1215-+.

[127] Chen, X.; Su, X.; Liang, B.; Yang, X.; Ren, X.; Duan, H.; Huang, Y.; Zhang, T. Identification of relevant active sites and a mechanism study for reverse water gas shift reaction over Pt/CeO_2 catalysts. *J. Energy Chem.* **2016**, 25, 1051-1057.

[128] Yaseen, M.; Jiang, H.; Li, J.; Yu, X.; Ashfaq Ahmad, M.; Nauman Ali, R.; Wang, L.; Yang, J.; Liu, Q. Synergistic effect of Z-scheme and oxygen vacancy of CeO_2/WO_3 heterojunction for enhanced CO_2 reduction activity. *Appl. Surf. Sci.* **2023**, 631, 157360.

[129] Yu, J.; Qin, X.T.; Yang, Y.S.; Lv, M.X.; Yin, P.; Wang, L.; Ren, Z.; Song, B.Y.; Li, Q.; Zheng, L.R.; Hong, S.; Xing, X.R.; Ma, D.; Wei, M.; Duan, X. Highly Stable Pt/CeO_2 Catalyst with Embedding Structure toward Water-Gas Shift Reaction. *J. Am. Chem. Soc.* **2023**, 146, 1071-1080.

[130] Chen, L.; Kovarik, L.; Szanyi, J. Temperature-Dependent Communication between Pt/Al_2O_3 Catalysts and Anatase TiO_2 Dilutant: the Effects of Metal Migration and Carbon Transfer on the Reverse Water-Gas Shift Reaction. *ACS Catal.* **2021**, 11, 12058-12067.

[131] Zhang, L.L.; Zhou, M.X.; Wang, A.Q.; Zhang, T. Selective Hydrogenation over Supported Metal Catalysts: From Nanoparticles to Single Atoms. *Chem. Rev.* **2020**, 120, 683-733.

[132] Peng, R.; Li, S.; Sun, X.; Ren, Q.; Chen, L.; Fu, M.; Wu, J.; Ye, D. Size effect of Pt nanoparticles on the catalytic oxidation of toluene over Pt/CeO_2 catalysts. *Appl. Catal. B-Environ.* **2018**, 220, 462-470.

[133] Li, Z.; Ji, S.F.; Liu, Y.W.; Cao, X.; Tian, S.B.; Chen, Y.J.; Niu, Z.G.; Li, Y.D. Well-Defined Materials for Heterogeneous Catalysis: From Nanoparticles to Isolated Single-Atom Sites. *Chem. Rev.* **2020**, 120, 623-682.

[134] Lee, S.; Ha, H.; Bae, K.T.; Kim, S.; Choi, H.; Lee, J.; Kim, J.H.; Seo, J.; Choi, J.S.; Jo, Y.-R.; Kim, B.-J.; Yang, Y.; Lee, K.T.; Kim, H.Y.; Jung, W. A measure of active interfaces in supported catalysts for high-temperature reactions. *Chem* **2022**, 8, 815-835.

[135] Zhang, J.Q.; Zhao, Y.F.; Guo, X.; Chen, C.; Dong, C.L.; Liu, R.S.; Han, C.P.; Li, Y.D.; Gogotsi, Y.; Wang, G.X. Single platinum atoms immobilized on an MXene as an efficient catalyst for the hydrogen evolution reaction. *Nat. Catal.* **2018**, 1, 985-992.

[136] Zhang, N.Q.; Zhang, X.X.; Kang, Y.K.; Ye, C.L.; Jin, R.; Yan, H.; Lin, R.; Yang, J.R.; Xu, Q.; Wang, Y.; Zhang, Q.H.; Gu, L.; Liu, L.C.; Song, W.Y.; Liu, J.; Wang, D.S.; Li, Y.D. A Supported Pd_2 Dual-Atom Site Catalyst for Efficient Electrochemical CO_2 Reduction. *Angew. Chem. Int. Edit.* **2021**, 60, 13388-13393.

[137] Chen, Y.J.; Ji, S.F.; Sun, W.M.; Lei, Y.P.; Wang, Q.C.; Li, A.; Chen, W.X.; Zhou, G.; Zhang, Z.D.; Wang, Y.; Zheng, L.R.; Zhang, Q.H.; Gu, L.; Han, X.D.; Wang, D.S.; Li, Y.D. Engineering the Atomic Interface with Single Platinum Atoms for Enhanced Photocatalytic Hydrogen Production. *Angew. Chem. Int. Edit.* **2020**, 59, 1295-1301.

[138] Maurer, F.; Jelic, J.; Wang, J.; Gänzler, A.; Dolcet, P.; Wöll, C.; Wang, Y.; Studt, F.; Casapu, M.; Grunwaldt, J.-D. Tracking the formation, fate and consequence for catalytic activity of Pt single sites on CeO_2. *Nat. Catal.* **2020**, 3, 824-833.

[139] DeRita, L.; Dai, S.; Lopez-Zepeda, K.; Pham, N.; Graham, G.W.; Pan, X.; Christopher, P. Catalyst Architecture for Stable Single Atom Dispersion Enables Site-Specific Spectroscopic and Reactivity Measurements of CO Adsorbed to Pt Atoms, Oxidized Pt Clusters, and Metallic Pt Clusters on TiO_2. *J. Am. Chem. Soc.* **2017**, 139, 14150-14165.

[140] Pan, Y.; Zhang, C.; Liu, Z.; Chen, C.; Li, Y.D. Structural Regulation with Atomic-Level Precision: From Single-Atomic Site to Diatomic and Atomic Interface Catalysis. *Matter* **2020**, 2, 78-110.

[141] Li, S.; Xu, Y.; Chen, Y.; Li, W.; Lin, L.; Li, M.; Deng, Y.; Wang, X.; Ge, B.; Yang, C.; Yao, S.; Xie, J.; Li, Y.; Liu, X.; Ma, D. Tuning the Selectivity of Catalytic Carbon Dioxide Hydrogenation over Iridium/Cerium Oxide Catalysts with a Strong Metal-Support Interaction. *Angew. Chem. Int. Ed.* **2017**, 56, 10761-10765.

[142] Yan, H.; Li, J.; Rao, Z.Q.; Liao, Y.; Li, Y.Q.; Zhou, X.; Meng, F.C.; Li, L.A.; Zhang, B.; Qin, Y.; Zhao, H.; Liu, Y.B.; Chen, X.B.; Feng, X.; Chen, D.; Yang, C.H.; Ma, D. Fully exposed Ptn cluster catalysts enable cascade oxidation of polyol to dicarboxylic acid. *Nat. Commun.* **2025**, 16, 7030.

[143] Si, Y.; Jiao, Y.Y.; Wang, M.L.; Xiang, S.L.; Diao, J.Y.; Chen, X.W.; Chen, J.W.; Wang, Y.; Xiao, D.Q.; Wen, X.D.; Wang, N.; Ma, D.; Liu, H.Y. Fully exposed Pt clusters for efficient catalysis of multi-step hydrogenation reactions. *Nat. Commun.* **2024**, 15, 4887.

[144] Wang, S.W.; Wang, L.G.; Wang, D.S.; Li, Y.D. Recent advances of single-atom catalysts in CO_2 conversion. *Energy Environ. Sci.* **2023**, 16, 2759-2803.

[145] Luo, Y.W.; Wang, D.S. Enhancing Heterogeneous Catalysis by Electronic Property Regulation of Single Atom Catalysts. *Acta Phys.-Chim. Sin.* **2023**, 39, 2212020.

[146] Gan, T.; Wang, D.S. Atomically dispersed materials: Ideal catalysts in atomic era. *Nano Res.* **2024**, 17, 18-38.

[147] Wan, Y.; Li, R.; Su, J.; Yi, W.; Li, Y.; Chu, H.; Shen, Z.; Gao, S.; Hai, X.; Zhong, R.; Zou, R. Single-Atom Supported Catalysts and Beyond. *Adv. Mater.* **2025**, 37, 2504518.

[148] Zhang, L.; Yang, J.; Yang, X.; Wang, A.; Zhang, T. Structural evolution of single-atom catalysts. *Chem Catal.* **2023**, 3, 100560.

[149] Wang, Y.; Wang, D.S.; Li, Y.D. Rational Design of Single-Atom Site Electrocatalysts: From Theoretical Understandings to Practical Applications. *Adv. Mater.* **2021**, 33, 2008151.

[150] Yang, J.R.; Li, W.H.; Wang, D.S.; Li, Y.D. Electronic Metal-Support Interaction of Single-Atom Catalysts and Applications in Electrocatalysis. *Adv. Mater.* **2020**, 32, 2003300.

[151] Wang, A.Q.; Li, J.; Zhang, T. Heterogeneous single-atom catalysis. *Nat. Rev. Chem.* **2018**, 2, 65-81.

[152] Dang, Y.; Düngen, P.; Hao, J.; Zeng, D.; Liang, C.; Huang, X.; Sun, X.; Schlögl, R.; Xia, C.; Ding, Y.; Heumann, S. Insights into Single-Atom Catalysts on Oxygen Functionalized Carbon Nanotubes. *Green Carbon* **2026**.

[153] Chen, L.; Unocic, R.R.; Hoffman, A.S.; Hong, J.; Braga, A.H.; Bao, Z.; Bare, S.R.; Szanyi, J. Unlocking the Catalytic Potential of TiO_2-Supported Pt Single Atoms for the Reverse Water-Gas Shift Reaction by Altering Their Chemical Environment. *JACS Au* **2021**, 1, 977-986.

[154] DeRita, L.; Resasco, J.; Dai, S.; Boubnov, A.; Thang, H.V.; Hoffman, A.S.; Ro, I.; Graham, G.W.; Bare, S.R.; Pacchioni, G.; Pan, X.; Christopher, P. Structural evolution of atomically dispersed Pt catalysts dictates reactivity. *Nat. Mater.* **2019**, 18, 746-751.

[155] Hvolbæk, B.; Janssens, T.V.W.; Clausen, B.S.; Falsig, H.; Christensen, C.H.; Nørskov, J.K. Catalytic activity of Au nanoparticles. *Nano Today* **2007**, 2, 14-18.

[156] Wei, S.J.; Li, A.; Liu, J.C.; Li, Z.; Chen, W.X.; Gong, Y.; Zhang, Q.H.; Cheong, W.C.; Wang, Y.; Zheng, L.R.; Xiao, H.; Chen, C.;

Wang, D.S.; Peng, Q.; Gu, L.; Han, X.D.; Li, J.; Li, Y.D. Direct observation of noble metal nanoparticles transforming to thermally stable single atoms. *Nat. Nanotechnol.* **2018**, 13, 856-+.

[157] Liu, H.-X.; Li, S.-Q.; Wang, W.-W.; Yu, W.-Z.; Zhang, W.-J.; Ma, C.; Jia, C.-J. Partially sintered copper-ceria as excellent catalyst for the high-temperature reverse water gas shift reaction. *Nat. Commun.* **2022**, 13, 867.

[158] Liu, K.P.; Zhao, X.T.; Ren, G.Q.; Yang, T.; Ren, Y.J.; Lee, A.F.; Su, Y.; Pan, X.L.; Zhang, J.C.; Chen, Z.Q.; Yang, J.Y.; Liu, X.Y.; Zhou, T.; Xi, W.; Luo, J.; Zeng, C.B.; Matsumoto, H.; Liu, W.; Jiang, Q.K.; Wilson, K.; Wang, A.Q.; Qiao, B.T.; Li, W.Z.; Zhang, T. Strong metal-support interaction promoted scalable production of thermally stable single-atom catalysts. *Nat. Commun.* **2020**, 11, 1263.

[159] Jones, J.; Xiong, H.; DeLaRiva, A.T.; Peterson, E.J.; Pham, H.; Challa, S.R.; Qi, G.; Oh, S.; Wiebenga, M.H.; Pereira Hernández, X.I.; Wang, Y.; Datye, A.K. Thermally stable single-atom platinum-on-ceria catalysts via atom trapping. *Science* **2016**, 353, 150-154.

[160] Lang, R.; Xi, W.; Liu, J.-C.; Cui, Y.-T.; Li, T.; Lee, A.F.; Chen, F.; Chen, Y.; Li, L.; Li, L.; Lin, J.; Miao, S.; Liu, X.; Wang, A.-Q.; Wang, X.; Luo, J.; Qiao, B.; Li, J.; Zhang, T. Non defect-stabilized thermally stable single-atom catalyst. *Nat. Commun.* **2019**, 10, 234.

[161] Liu, Y.; Cheng, Q.; Lyu, S.; Li, X.; Song, S.; Ding, T.; Tian, Y.; Li, X. Strategic assembly of active phases on Co-Fe bimetallic catalysts for efficient Fischer-Tropsch synthesis. *Chem. Eng. J.* **2024**, 494, 152936.

[162] Han, A.; Wang, X.J.; Tang, K.; Zhang, Z.D.; Ye, C.L.; Kong, K.J.; Hu, H.B.; Zheng, L.R.; Jiang, P.; Zhao, C.X.; Zhang, Q.; Wang, D.S.; Li, Y.D. An Adjacent Atomic Platinum Site Enables Single-Atom Iron with High Oxygen Reduction Reaction Performance. *Angew. Chem. Int. Edit.* **2021**, 60, 19262-19271.

[163] Tian, S.B.; Wang, B.X.; Gong, W.B.; He, Z.Z.; Xu, Q.; Chen, W.X.; Zhang, Q.H.; Zhu, Y.Q.; Yang, J.R.; Fu, Q.; Chen, C.; Bu, Y.X.; Gu, L.; Sun, X.M.; Zhao, H.J.; Wang, D.S.; Li, Y.D. Dual-atom Pt heterogeneous catalyst with excellent catalytic performances for the selective hydrogenation and epoxidation. *Nat. Commun.* **2021**, 12, 3181.

[164] Wu, Y.; Wang, D.; Niu, Z.; Chen, P.; Zhou, G.; Li, Y. A Strategy for Designing a Concave Pt–Ni Alloy through Controllable Chemical Etching. *Angew. Chem. Int. Edit.* **2012**, 51, 12524-12528.

[165] Zhou, X.; Hansen, C.; Isler, D.; Zhou, W.; Paterson, J.; Southouse, J.; Copéret, C. Tellurium-Induced Noble-Metal Reactivity in CO_2 Hydrogenation Catalysts. *J. Am. Chem. Soc.* **2025**, 147, 22309-22313.

[166] Mao, J.J.; Chen, Y.J.; Pei, J.J.; Wang, D.S.; Li, Y.D. Pt-M (M = Cu, Fe, Zn, etc.) bimetallic nanomaterials with abundant surface defects and robust catalytic properties. *Chem. Commun.* **2016**, 52, 5985-5988.

[167] Kattel, S.; Yu, W.; Yang, X.; Yan, B.; Huang, Y.; Wan, W.; Liu, P.; Chen, J.G. CO_2 Hydrogenation over Oxide-Supported PtCo Catalysts: The Role of the Oxide Support in Determining the Product Selectivity. *Angew. Chem. Int. Edit.* **2016**, 55, 7968-7973.

[168] Zhai, P.; Xu, C.; Gao, R.; Liu, X.; Li, M.Z.; Li, W.Z.; Fu, X.P.; Jia, C.J.; Xie, J.L.; Zhao, M.; Wang, X.P.; Li, Y.W.; Zhang, Q.W.; Wen, X.D.; Ma, D. Highly Tunable Selectivity for Syngas-Derived Alkenes over Zinc and Sodium-Modulated Fe_5C_2 Catalyst. *Angew. Chem. Int. Edit.* **2016**, 55, 9902-9907.

[169] Gu, M.W.; Dai, S.; Qiu, R.F.; Ford, M.E.; Cao, C.X.; Wachs, I.E.; Zhu, M.H. Structure-Activity Relationships of Copper- and Potassium-Modified Iron Oxide Catalysts during Reverse Water-Gas Shift Reaction. *ACS Catal.* **2021**, 11, 12609-12619.

[170] Yu, J.; Sun, X.; Tong, X.; Zhang, J.; Li, J.; Li, S.; Liu, Y.; Tsubaki, N.; Abe, T.; Sun, J. Ultra-high thermal stability of sputtering reconstructed Cu-based catalysts. *Nat. Commun.* **2021**, 12, 7209.

[171] Gan, T.; Tao, L.; Zhang, Z.D.; Zhou, A.; Chen, Y.; Li, J.; Zhang, S.; Du, S.X.; Li, Y.D. Defect-Engineered $LaFeO_3$ Stabilizing Oxidized Pt Single-Atom Sites for Low-Temperature CO Oxidation. *J. Am. Chem. Soc.* **2025**, 147, 32729-32736.

[172] Liang, X.; Gao, Z.R.; Peng, X.J.; Wang, M.L.; Xu, Y.; Zhang, J.; Tian, S.H.; Li, C.Y.; Qin, X.T.; Mi, R.L.; Wang, Z.H.; Zhou, W.; Wang, M.; Ma, D. Efficient Hydrogen Production from Ethylene Glycol Steam Reforming Catalyzed by Na-Promoted Pt/γ-Mo_2N. *J. Am. Chem. Soc.* **2025**, 147, 33395-33402.

[173] Liu, W.; Zhang, R.Q.; Li, C.Y.; Liu, X.W.; Tian, S.H.; Ren, X.; Ma, D. Stabilizing High-Valence Ni/Fe Through Li Vacancy Engineering in $Li_{(1-x)}NiFeO_2$/NiFeOOH Heterostructures for Enhanced Oxygen Evolution Reaction. *ACS Catal.* **2025**, 15, 11886-11895.

[174] Rong, H.P.; Ji, S.F.; Zhang, J.T.; Wang, D.S.; Li, Y.D. Synthetic strategies of supported atomic clusters for heterogeneous catalysis. *Nat. Commun.* **2020**, 11, 5884.

[175] Ze, H.; Yang, Z.-L.; Li, M.-L.; Zhang, X.-G.; A, Y.-L.; Zheng, Q.-N.; Wang, Y.-H.; Tian, J.-H.; Zhang, Y.-J.; Li, J.-F. In Situ Probing the Structure Change and Interaction of Interfacial Water and Hydroxyl Intermediates on $Ni(OH)_2$ Surface over Water Splitting. *J. Am. Chem. Soc.* **2024**, 146, 12538-12546.

[176] Yang, F.; Li, C.; Wang, M.; Yu, S.; Zhao, J.; Xu, Y.; Zhou, W.; Yi, X.; Ma, D. Inverse decoration of TiO_x to NiSn alloy nanoparticles for efficient hydrodeoxygenation of m-cresol. *Nat. Commun.* **2025**, 17, 902.

[177] Wang, Y.; Feng, S.; Leong, P.; Shi, X.; Zhu, G.; Tang, C. MnO_x-encapsulated $LaMnO_3$ core-shell structures with Au interactions for enhanced CO oxidation catalysis. *Appl. Catal. B-Environ.* **2025**, 366, 125018.

[178] Lin, W.; Stocker, K.M.; Schatz, G.C. Mechanisms of Hydrogen-Assisted CO_2 Reduction on Nickel. *J. Am. Chem. Soc.* **2017**, 139, 4663-4666.

[179] Yang, H.C.; Duan, P.F.; Zhuang, Z.C.; Luo, Y.W.; Shen, J.; Xiong, Y.L.; Liu, X.W.; Wang, D.S. Understanding the Dynamic Evolution of Active Sites among Single Atoms, Clusters, and Nanoparticles. *Adv. Mater.* **2025**, 37, 2415265.

[180] Zhang, M.T.; Zhu, Y.C.; Yan, J.; Xie, J.Z.; Yu, T.; Peng, M.; Zhao, J.Y.; Xu, Y.; Li, A.W.; Jia, C.J.; He, L.; Wang, M.; Zhou, W.; Wang, R.M.; Jiang, H.; Shi, C.; Rodriguez, J.; Ma, D. A Highly Active Molybdenum Carbide Catalyst with Dynamic Carbon Flux for Reverse Water-Gas Shift Reaction. *Angew. Chem. Int. Edit.* **2025**, 64, e202418645.

[181] Roldán Cuenya, B.; Bañares, M.A. Introduction: Operando and In Situ Studies in Catalysis and Electrocatalysis. *Chem. Rev.* **2024**, 124, 8011-8013.

[182] Chen, X.; Lee, Y.; Hong, S.; Schroeder, E.K.; Gericke, S.M.; Barber, G.D.; Chen, Z.; Hesse, S.A.; Tassone, C.J.; Rioux, R.M.; Christopher, P.; Bare, S.R.; Li, M.; Zakharov, D.N.; Alexandrova, A.N.; Head, A.R.; Zhou, G.; Yang, J.C. Defect-Driven Redox Interplay on Anatase TiO_2: Surface-Structure Dependent Activation for CO_2 Hydrogenation Catalysis. *J. Am. Chem. Soc.* **2025**, 147, 43273-43285.

[183] Bamonte, S.; Khanna, H.S.; Perera, I.; Li, M.; Posada, L.F.; March, S.; Eddy, N.A.; Shimogawa, R.; Figueroa, A.; Li, C.; Shuster, S.; Tan, H.; Marinkovic, N.; Head, A.R.; Zakharov, D.N.; Ma, L.; Gao, P.-X.; Frenkel, A.I.; Suib, S.L. In-situ monitoring of atomically dispersed Pt sites supported on OMS-2 during CO_2 activation. *Appl. Catal. B Environ.* **2026**, 383, 126016.

[184] Keturakis, C.J.; Zhu, M.; Gibson, E.K.; Daturi, M.; Tao, F.; Frenkel, A.I.; Wachs, I.E. Dynamics of CrO_3-Fe_2O_3 Catalysts during the High-Temperature Water-Gas Shift Reaction: Molecular Structures and Reactivity. *ACS Catal.* **2016**, 6, 4786-4798.

[185] Ahmadi Khoshooei, M.; Wang, X.; Vitale, G.; Formalik, F.; Kirlikovali, K.O.; Snurr, R.Q.; Pereira-Almao, P.; Farha, O.K. An active, stable cubic molybdenum carbide catalyst for the high-temperature reverse water-gas shift reaction. *Science* **2024**, 384, 540-546.

[186] Qiu, C.; Sun, J.; Li, M.; Mao, C.; Song, R.; Zhang, Z.; Perovic, D.D.; Howe, J.Y.; Wang, L.; Ozin, G.A. Irreversible Lattice Expansion Effects in Nanoscale Indium Oxide for CO_2 Hydrogenation Catalysis. *J. Am. Chem. Soc.* **2024**, 146, 33997-34007.

[187] Phongprueksathat, N.; Ting, K.W.; Mine, S.; Jing, Y.; Toyoshima, R.; Kondoh, H.; Shimizu, K.-i.; Toyao, T.; Urakawa, A. Bifunctionality of Re Supported on TiO_2 in Driving Methanol Formation in Low-Temperature CO_2 Hydrogenation. *ACS Catal.* **2023**, 13, 10734-10750.

[188] Wang, D.-J.; Sun, X.-C.; Yin, H.-J.; Dong, H.; Liu, H.; Zhang, Y.-W. Tuning Selectivity of CO_2 Hydrogenation via Support Composition Modification Adjusted the Activity Reduction of H Species over $Ce_{1-x}Pr_xO^{2-\delta}$-Supported Metal (Ru, Rh) Nanoclusters. *ACS Catal.* **2024**, 14, 10060-10076.

[189] Rao, K.R.; Pace, R.B.; Suarez, H.; Santillan-Jimenez, E.; Risko, C. Carboxylic Acid Decarbonylation on Nickel: The Critical Role

of the Acid Binding Geometry. *ACS Catal.* **2023**, 13, 9102-9112.

[190] Zhang, X.; Zhang, M.; Deng, Y.; Xu, M.; Artiglia, L.; Wen, W.; Gao, R.; Chen, B.; Yao, S.; Zhang, X.; Peng, M.; Yan, J.; Li, A.; Jiang, Z.; Gao, X.; Cao, S.; Yang, C.; Kropf, A.J.; Shi, J.; Xie, J.; Bi, M.; van Bokhoven, J.A.; Li, Y.-W.; Wen, X.; Flytzani-Stephanopoulos, M.; Shi, C.; Zhou, W.; Ma, D. A stable low-temperature H_2-production catalyst by crowding Pt on α-MoC. *Nature* **2021**, 589, 396-401.

[191] Wang, Y.; Xue, F.; Zhang, W.; Cao, D.; Zhang, M.; Li, Z.; Zhan, C.; Kuang, Q.; Xie, Z. Overcoming Copper Instability via Nickel Alloying for Efficient Plasmon-Catalytic CO_2 Hydrogenation. *Angew. Chem. Int. Ed.* **2026**, n/a, e21576.

[192] Choi, Y.; An, B.-S.; Sim, G.D.; Jung, U.; Park, Y.; Koo, K.Y. Synthesis of CuO_x catalysts supported on Fe-modified mixed oxides with high CO formation rates in low-temperature CO_2 hydrogenation. *Appl. Catal. B-Environ.* **2025**, 377, 125475.

[193] Kim, K.Y.; Jang, W.; Byun, W.J.; Lee, J.Y.; Kim, M.; Lee, J.H.; Rhim, G.B.; Youn, M.H.; Chun, D.H.; Kim, S.K.; Cho, S.; Lee, J.S. Highly Efficient Layered Double Hydroxide-Derived Bimetallic Cu-Co Alloy Catalysts for the Reverse Water-Gas Shift Reaction. *ACS Catal.* **2024**, 14, 7020-7031.

[194] Zhou, W.; Brack, E.; Ehinger, C.; Paterson, J.; Southouse, J.; Copéret, C. Reactivity Switch of Platinum with Gallium: From Reverse Water Gas Shift to Methanol Synthesis. *J. Am. Chem. Soc.* **2024**, 146, 10806-10811.

[195] Chen, Z.M.; Wang, C.F.; Zhang, B.N.; Li, J.N.; Wang, D.C.; Xu, G.Y.; Zhang, J.J.; Peng, M.; Ma, D.; Zhang, Y. Interface Modification of Single Atom-Nanocluster Synergistic Sites to Break the Activity-Selectivity-Stability Trade-Off in Selective Hydrogenations. *Adv. Mater.* **2025**, 37, 2503841.

[196] Zhou, B.; Xie, Y.; Wang, C.; Li, K.; Bao, S.; Sun, X.; Huang, X.; Ning, P.; Li, K.; Shi, L.; Wang, F. The key role of catalyst structure adjustment and optimization in the Reverse Water-Gas Shift Reaction. *Green Carbon* **2026**.

[197] Ou, Z.; Qin, C.; Niu, J.; Zhang, L.; Ran, J. A comprehensive DFT study of CO_2 catalytic conversion by H_2 over Pt-doped Ni catalysts. *Int. J. Hydrogen Energ.* **2019**, 44, 819-834.

[198] Lin, L.; Zhou, W.; Gao, R.; Yao, S.; Zhang, X.; Xu, W.; Zheng, S.; Jiang, Z.; Yu, Q.; Li, Y.-W.; Shi, C.; Wen, X.-D.; Ma, D. Low-temperature hydrogen production from water and methanol using Pt/α-MoC catalysts. *Nature* **2017**, 544, 80-83.

[199] Sun, X.; Yu, J.; Zada, H.; Han, Y.; Zhang, L.; Chen, H.; Yin, W.; Sun, J. Reaction-induced unsaturated Mo oxycarbides afford highly active CO_2 conversion catalysts. *Nat. Chem.* **2024**, 16, 2044-2053.

[200] Christopher, P. Single-Atom Catalysts: Are All Sites Created Equal? *ACS Energy Lett.* **2019**, 4, 2249-2250.

[201] Szenti, I.; Efremova, A.; Kiss, J.; Sápi, A.; Óvári, L.; Halasi, G.; Haselmann, U.; Zhang, Z.; Morales-Vidal, J.; Baán, K.; Kukovecz, Á.; López, N.; Kónya, Z. Pt/MnO Interface Induced Defects for High Reverse Water Gas Shift Activity. *Angew. Chem. Int. Ed.* **2024**, 63, e202317343.

[202] Zhang, J.; Yu, S.X.; Liu, X.W.; Wang, M.L.; Gao, Z.R.; Qin, X.T.; Xu, Y.; Wang, M.; Ma, D. Interplay Between Metal and Acid Sites Tunes the Catalytic Selectivity Over Pd/Nanodiamond Catalysts. *J. Am. Chem. Soc.* **2024**, 146, 34990-34997.

[203] Yao, L.; Rivera-Cruz, K.E.; Zimmerman, P.M.; Singh, N.; McCrory, C.C.L. Electrochemical CO_2 Reduction to Methanol by Cobalt Phthalocyanine: Quantifying CO_2 and CO Binding Strengths and Their Influence on Methanol Production. *ACS Catal.* **2024**, 14, 366-372.

[204] Liu, J.; Lucci, F.R.; Yang, M.; Lee, S.; Marcinkowski, M.D.; Therrien, A.J.; Williams, C.T.; Sykes, E.C.H.; Flytzani-Stephanopoulos, M. Tackling CO Poisoning with Single-Atom Alloy Catalysts. *J. Am. Chem. Soc.* **2016**, 138, 6396-6399.

[205] Kim, D.-H.; Kim, H.-J.; Kang, E.; Gwon, Y.; Ku, B.-J.; Park, S.; Yi, K.B.; Reboul, J.; Kim, H.Y.; Lee, K. Exsolution-Driven Spinel Ni–Cu Bimetallic Catalysts for RWGS Reaction: Compositional Tuning for Enhanced Stability and CO Selectivity. *ChemCatChem* **2026**, 18, e01799.

[206] Feng, L.; Liu, J.-X. Identification of Active Sites for Reverse Water–Gas Shift Reactions on Pt/TiO_2 Cluster Catalysts. *Precision Chemistry* **2025**, 3, 380-388.

[207] Ammal, S.C.; Heyden, A. Understanding the Nature and Activity of Supported Platinum Catalysts for the Water–Gas Shift Reaction: From Metallic Nanoclusters to Alkali-Stabilized Single-Atom Cations. *ACS Catal.* **2019**, 9, 7721-7740.

[208] Qi, Y.; Zhu, Y.-A.; Chen, D. Mechanism investigation and catalyst screening of high-temperature reverse water gas shift reaction. *GreenChE* **2020**, 1, 131-139.

[209] Tesvara, C.; Yousuf, M.R.; Albrahim, M.; Troya, D.; Shrotri, A.; Stavitski, E.; Karim, A.M.; Sautet, P. Unraveling the CO Oxidation Mechanism over Highly Dispersed Pt Single Atom on Anatase TiO_2(101). *ACS Catal.* **2024**, 14, 7562-7575.

[210] Zhang, K.-X.; Liu, Z.-P. In Situ Surfaced Mn-Mn Dimeric Sites Dictate CO Hydrogenation Activity and C_2 Selectivity over MnRh Binary Catalysts. *J. Am. Chem. Soc.* **2024**, 146, 27138-27151.

[211] Dong, F.; Liang, X.; Zhang, Z.D.; Yin, H.B.; Wang, D.S.; Li, J.H.; Li, Y.D. Atomic Pt Sites Anchored in the Interface between Grains on Vacancy-Enriched CeO_2 Nanosheets: One-Step Precursor Combustion Synthesis. *Adv. Mater.* **2024**, 36, 2401055.

[212] Gai, Y.; Li, S.; Wang, H.; Pu, M.; Lei, M. The First-Principles Study on the Mechanism of the RWGS Reaction Catalyzed by $Pt_1@CeO_{2-x}$(110) Single-Atom Catalyst. *ChemCatChem* **2025**, 17, e202500027.

[213] Yan, X.; Duan, C.; Yu, S.; Dai, B.; Sun, C.; Chu, H. Recent advances on CO_2 reduction reactions using single-atom catalysts. *Renew. Sust. Energ. Rev.* **2024**, 190, 114086.

[214] Prats, H.; Stamatakis, M. First-Principles Kinetic Monte Carlo Simulations for Single-Cluster Catalysis: Study of CO_2 and CH_4 Conversion on Pt/HfC. *ACS Catal.* **2025**, 15, 2904-2915.

[215] Wang, L.G.; Wu, J.B.; Wang, S.W.; Liu, H.; Wang, Y.; Wang, D.S. The reformation of catalyst: From a trial-and-error synthesis to rational design. *Nano Res.* **2024**, 17, 3261-3301.